12-2017

Geological Characterization of Precambrian Nonconformities: Implications for Injection-Induced Seismicity in the Midcontinent United States

Laura Cuccio
Utah State University

GEOLOGICAL CHARACTERIZATION OF PRECAMBRIAN NONCONFORMITIES: IMPLICATIONS FOR INJECTION-INDUCED SEISMICITY IN THE MIDCONTINENT UNITED STATES

by

Laura Cuccio

A thesis submitted in partial fulfillment
of the requirements for the

of

MASTER OF SCIENCE

in

Geology

Approved:

_____	_____
James P. Evans, Ph.D. Major Professor	Kelly K. Bradbury, Ph.D. Committee Member
_____	_____
Peter S. Mozley, Ph.D. Committee Member	Mark R. McLellan, Ph.D. Vice President for Research and Dean of the School of Graduate Studies

UTAH STATE UNIVERSITY
Logan, Utah

2017

ABSTRACT

Geological Characterization of Precambrian Nonconformities: Implications for Induced Seismicity in the Midcontinent United States

by

Laura Cuccio, Master of Science

Utah State University, 2017

Major Professor: James P. Evans
Department: Geology

A rapid increase in seismic activity in the 'tectonically quiet' midcontinent United States has been linked to the injection of wastewater via Class II injection wells completed near the nonconformity between sedimentary rocks and the Precambrian crystalline rocks of the region. The majority of injection-induced earthquakes nucleate on or near deep basement faults due to an increase in pore fluid pressures, indicating that these faults are hydrologically connected to the injection point. We hypothesize that the Precambrian nonconformity is a likely hydrological connection, and that the character of the rock adjacent to the nonconformity plays a role in determining the nature of this connection.

We investigate the range of rock properties and spatial heterogeneity at the Precambrian nonconformity zone, using outcrop and core analogs, and examine how the geology of the nonconformity zone may influence fluid flow. Methods of analyses include mapping of lithologies and deformation structures, petrographic and microstructural analysis, and geochemical analysis of rocks. We infer the nature of fluid flow in the past, and make predictions about fluid flow in the future. In addition, this information is used to inform hydrological models, improving the ability to refine seismic hazard models associated with wastewater injection.

Based on our observations at multiple outcrop localities and several drill cores, we identify three main geological scenarios that are likely to be encountered at the nonconformity. These consist of the presence of: 1) basal conglomerate, 2) weathered/altered horizon, and 3) mineralized contacts. These scenarios, or combinations thereof, may be fractured or faulted, resulting in a variety of hydrological consequences. The permeability of basal conglomerates and weathered horizons at the contact is texturally and mineralogically dependent. Regolith, clast-supported grus or granitic wash, or poorly cemented conglomeratic horizons may act as high permeability conduits, whereas a clay-rich matrix-supported grus or granitic wash, or tightly cemented conglomerate, may act as low permeability barriers. Mineralized contacts may act as low permeability barriers due to a reduction of pore space and/or resistance to weathering. The introduction of modern warm brines of complex or mixed geochemistries during injection may result in mineralization or chemical alteration, dynamically affecting permeability over time and space depending on the mineralogy of the host rock and chemical composition of the injected brine.

(131 pages)

PUBLIC ABSTRACT

Geological Characterization of Precambrian Nonconformities: Implications for Induced Seismicity in the Midcontinent United States

Laura A. Cuccio

The midcontinent United States, a region which typically does not experience many earthquakes, has experienced a significant increase in the number of earthquakes over the last decade. This increase in earthquake activity has been linked to wastewater injection, a process in which large volumes of wastewater from oil and gas extraction are injected into deep (2-3 km), high-permeability sedimentary rocks, near low-permeability Precambrian (>540-million-year-old) crystalline 'basement' rocks. The contact between these two rock types is referred to as the Precambrian nonconformity. Injection-induced earthquakes occur on or near basement-hosted faults due to an increase in pore fluid pressures, which implies that there may be a hydrological connection between the basement-hosted faults and the injection point. We hypothesize that the Precambrian nonconformity greatly influences this hydrological connection.

We investigate the geologic properties of Precambrian nonconformity zone outcrop and core analogs to examine how the geology of the nonconformity zone controls fluid flow. Methods include mapping of geological materials and deformation structures (faults and fractures), mineralogical analysis, and geochemical analysis. These data sets allow us to infer the nature of fluid flow in the past, and make predictions about fluid flow in the future. In addition, this information is used to inform hydrological models, improving the ability to predict earthquakes due to wastewater injection.

We identify three main geological scenarios that are likely to be encountered at the nonconformity. These are: 1) basal conglomerate, 2) weathered/altered horizon, and 3)

mineralized contacts. These scenarios, or combinations of these scenarios, may be fractured or faulted, resulting in a variety of hydrological implications. The permeability of basal conglomerates and weathered horizons at the contact depends on the textures and minerals that are present. Regolith, clast-supported granitic wash, or poorly cemented conglomeratic horizons, may act as high permeability conduits, whereas a clay-rich grus or granitic wash, or tightly cemented conglomerate, may act as low permeability barriers. Mineralized contacts may act as low permeability barriers due to a reduction of pore space. The mineralized contact shows that the introduction of warm brines by modern injection may result in mineralization or chemical weathering, dynamically affecting permeability over time depending on the mineralogy of the host rock and chemical composition of the injected brine.

ACKNOWLEDGMENTS

I would first like to thank my advisor, Jim Evans, for giving me the opportunity to work on this project. Under your guidance I was able to grow tremendously as a scientist, whilst still having the freedom to experience the mountains and deserts of this part of the country, and I will be forever grateful for that. I'd also like to thank my Peter Mozley for serving on my committee, and offering valuable insight and advice throughout the course of this research. Thank you to my other committee member, Kelly Bradbury, for being an incredible resource in the field and in the lab, as well as an excellent eating, drinking, and hiking buddy!

I would also like to acknowledge Andrew Lonero and Dennis Newell for helping me with my isotope data, or any other lab-related tasks I took on. I'd also like to thank my field assistant, Mike Ferraro, for helping me with my Wind River field work. We forded streams, navigated talus and deadfall, and braved high winds, rain, and hail, all in the name of science!

A big thank you to my family back east, for not freaking out when I decided to move across the country, for their support and encouragement, and for providing me with all of the opportunities that led me to this degree. And to Tom, for his constant love and encouragement, and for teaching me to always save time for adventure, even when life gets hectic. And lastly, thank you to my squad, for the many adventures, baking excursions, late nights, emotional support, and all around comradery. This journey would not have been the same without you guys!

This research was largely supported by the U. S. Geological Survey NEHRP Grant #2015-0137 to James Evans. Support for this work also came from the GDL Foundation, Utah State University's Graduate Research and Collaborative Opportunities Program, the Geological Society of America student research grant, the Tobacco Root Geological Society student research grant, the Institute on Lake Superior Geology student research grant, and the Utah State University Geology Department.

CONTENTS

Page

LIST OF TABLES

LIST OF FIGURES

1. Introduction

1.1 Problem Background

The extraction of oil and gas in the United States produces billions of gallons of wastewater fluids annually. The chemical composition of these brines, typically termed formation water, oil field brine, or produced water, is variable, and the large volumes make them costly to treat. The produced waters often cannot be disposed of in any fresh water aquifer or ecosystem due to the chemical contaminants and high concentrations of total dissolved solids, therefore, they are primarily disposed of via Class II injection wells (Tyrrell et al., 2013). Class II wells are completed into a range of depths insuring isolation from shallow aquifers (EPA and UIC, 2015). In most states, and some tribal lands and reservation lands, Class II injectors are regulated by state agencies, whose regulatory framework includes traditional geomechanical analyses of wellbore integrity (National Technical Workgroup and Underground Injection Control, 2014). Injector wells are typically repurposed oil and gas production wells, or dedicated brine disposal wells, completed into porous and permeable units.

Although wastewater injection helps prevent the contamination of water resources at the Earth's surface and in the unsaturated zone, injecting large volumes of fluids into the deep subsurface may come with a price. One possible side effect is *injection induced seismicity*. Over the past 20 years, the central United States has experienced a large increase in the rate of seismic activity (Figure 1). The central United States is thought to be a 'tectonically quiet' region, in which intraplate strain rates are low ($<10^{-17}$ sec^{-1}) (Calais et al., 2006; Dixon et al., 1996), fault slip rates are slow (<<1 mm/yr) (Harrison et al., 1999), recurrence intervals of intraplate earthquakes are long (10^4-10^5 yrs.) (Crone et al., 2003), and fault slip may occur on ancient 'hidden' faults not seen in historic seismic records. The high rates of current seismic activity have motivated numerous studies investigating the causes for these earthquakes. Determining whether

the increased seismic activity in the midcontinent U.S. is a product of deep wastewater injection, or natural tectonic activity, requires an understanding of the subsurface geology and any possible fluid-pressure pathways that may exist near injection sites. Numerous multidisciplinary studies explore a range of questions surrounding injection-related seismicity to better understand the processes involved in induced seismicity via deep wastewater injection. Recent observations suggest that deep wastewater injection is the culprit (Ellsworth, 2013; Keranen et al., 2014; Weingarten et al., 2015; Yeck et al., 2016; Walsh and Zoback, 2015; Zhang et al., 2013).

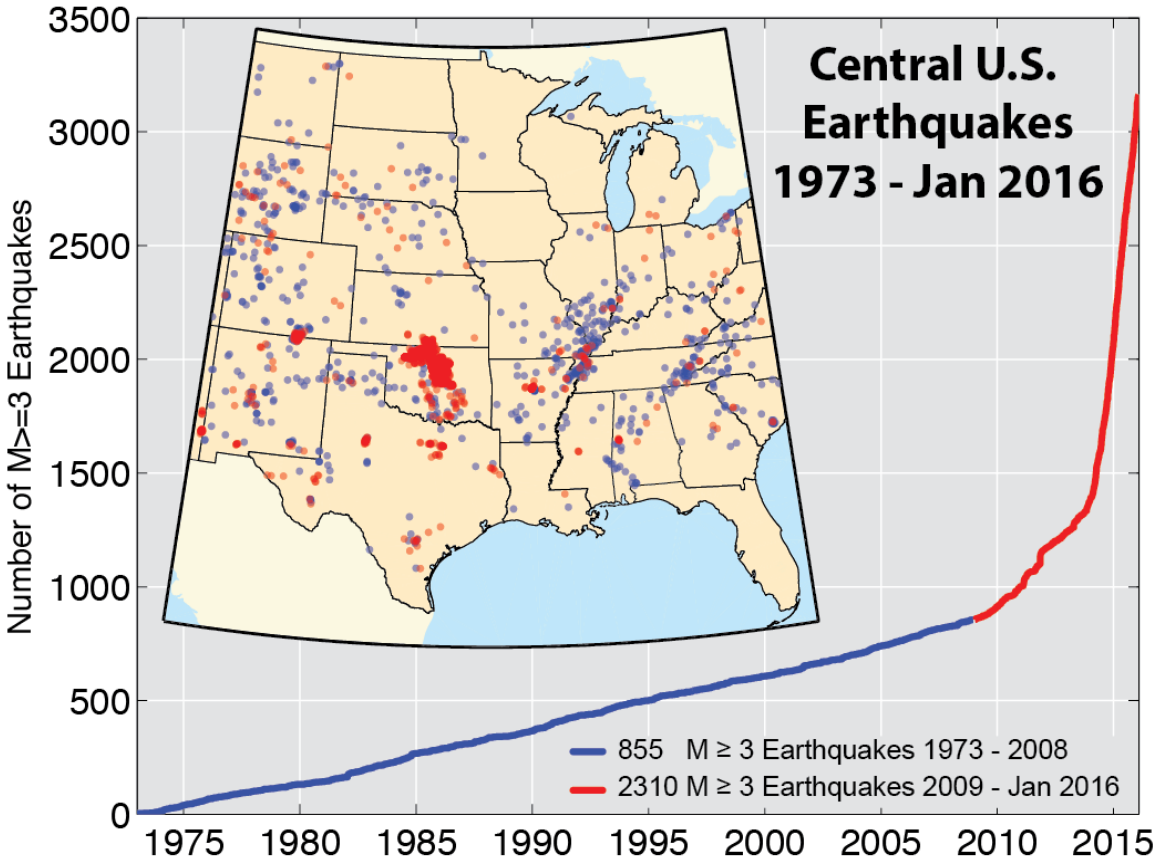

Figure 1: The midcontinent United States has seen a rapid increase in the number of M 3+ earthquakes over the past decade. This rapid increase in seismic activity rate began around 2009, and has been attributed to the wastewater disposal via Class II injection wells. From the U.S. Geological Survey Earthquake Hazards Program webpage (accessed in June, 2017).

1.2 Nature of Brine Injection in the Midcontinent United States

The total number of Class II wells in the United States is reported to be between 140,000 and 160,000 as of 2013 (Evans et al., 2013). Approximately 16,000 of these wells are active brine disposal wells, 3,400 of which inject fluids at depths of >1.8 km, where most M>3.0 midcontinent earthquakes occur (Evans et al., 2013). Injection of wastewater occurs on a large scale, with the volume of brine disposed in Oklahoma alone in 2015 totaling 2,731,203 barrel per day (Murray, 2016). Rates of injection in individual wells range between ~100 barrels per month (bbl/month) to up to 2 million bbl/month (Weingarten et al., 2015). The majority of these active brine disposal wells are located in major oil and gas basins in Oklahoma, Texas, Kansas, and Wyoming (Weingarten et al., 2015). Weingarten et al. (2015) shows that only 8% of all active injection wells are in Oklahoma, however, Oklahoma contains 40% of all seismically associated active wells (Figure 2).

Other regions experiencing high rates of induced seismicity include west Texas, southeastern Colorado, central Arkansas, southern Illinois, and northern New Mexico. Previously, northeastern Ohio experienced seismicity due to injection into sandstone intervals in the Knox Dolomite and in the Mt. Simon Sandstone (Kim, 2013), however, deep injection has since ceased due to successful mitigation efforts by the state following a M 4.0 earthquake in December, 2011. Mitigation efforts included: 1) shutting down the well associated with seismicity and the surrounding wells, 2) prohibiting the drilling of Class II injection wells into Precambrian basement rock, 3) changing the volumes of injection in a well, and 4) increasing supplemental site assessment documents required to obtain a permit (National Technical Workgroup and Underground Injection Control, 2014). Several areas with large numbers of brine disposal wells (i.e., North Dakota, the Michigan Basin, large areas of Texas and Louisiana Gulf Coast) are not affected by induced seismicity, indicating that region-specific subsurface geology and in-situ stress states may be a controlling factor in the seismic outcome of brine disposal.

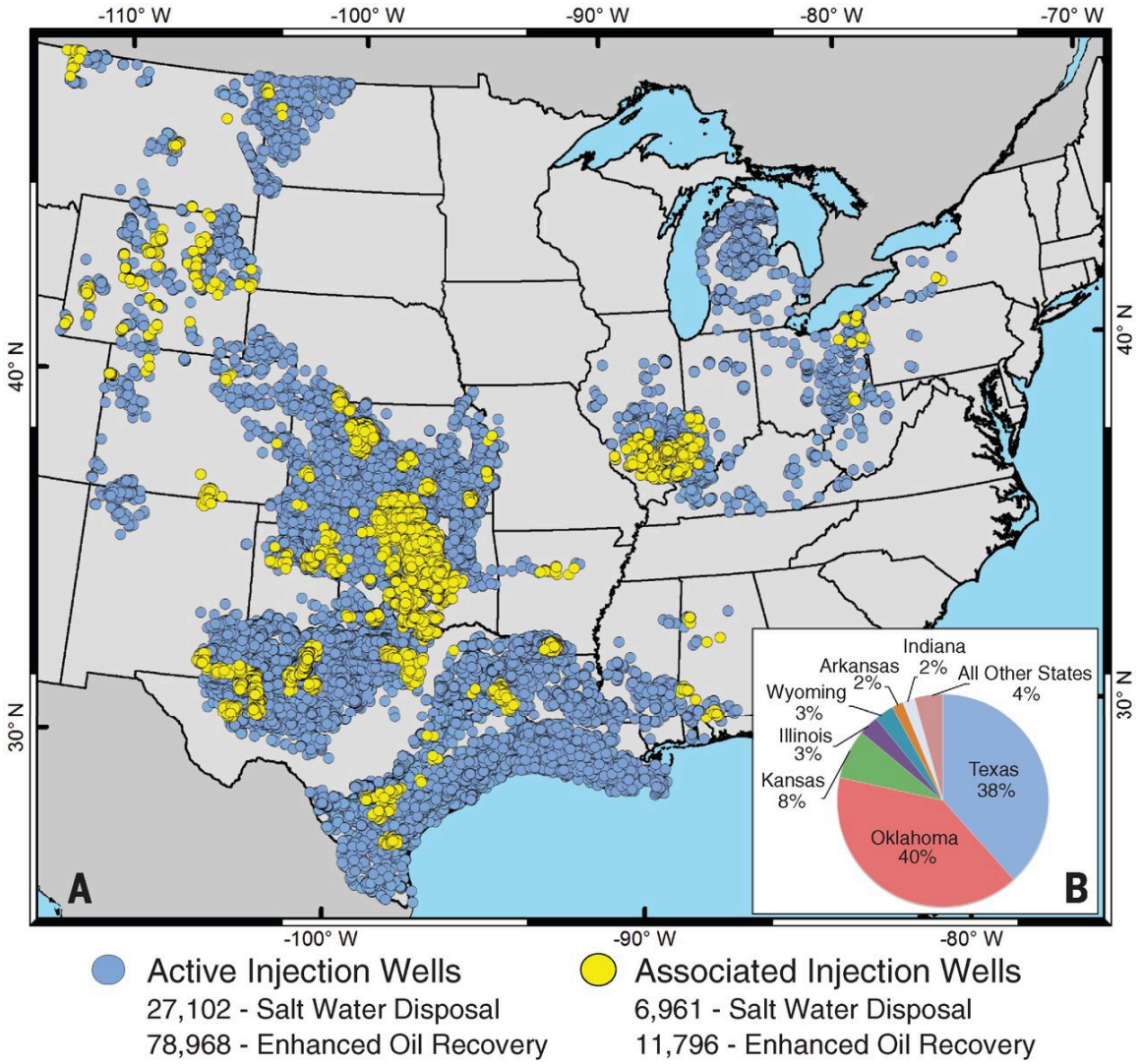

Figure 2: (A) Map showing the location of active class II injection wells in the central eastern United States (CEUS). Active injection wells from the database are shown as blue circles. Spatiotemporally associated injection wells, defined as those within a 15-km radius and active at the time of an earthquake, are shown as yellow circles. The CEUS region comprises all states intersected by 109°W longitude and eastward. The total number of wells, including inactive or abandoned wells in the CEUS, is 188,570. Of the 18,757 associated injection wells, >77% are currently active. (B) The inset pie diagram shows spatiotemporally associated injection wells by state. Only 8% of all injection wells are located in Oklahoma, but 40% of the associated injection wells in the CEUS are located in Oklahoma. From Weingarten et al., (2015).

1.3 Geologic and Hydrologic Setting of Midcontinent Brine Injection

Many brine disposal wells are completed into basal (Cambro-Ordovician) sedimentary reservoirs near Precambrian crystalline basement rock (Murray, 2015). The Cambro-Ordovician Arbuckle Formation is the predominant target disposal zone for ~50% of injection wells in Oklahoma and Kansas (Murray, 2015). Other target formations for wastewater disposal in the midcontinent region include the Cambrian Mt. Simon Sandstone, the Cambro-Ordovician Knox Group, and the lower Ordovician Ellenberger Group. Basement rocks in the midcontinent primarily consist of granite, rhyolite, and varying grades of metamorphic rocks (Denison et al., 1984). The contact between the sedimentary rocks and crystalline igneous and metamorphic rocks in the central United States forms the subsurface nonconformity contact of the region (Sloss, 1963).

Fault zones in the midcontinent are not commonly exposed at the surface, and typically penetrate basement, dip steeply, and follow two dominant trends: east-west to northwest-southeast, and north-south to northeast-southwest (Marshak and Paulsen, 1996) (Figure 3). The surface of the nonconformity in the midcontinent has a structural relief of 1 to 5 km, and lies between 0.5 to ~8 kilometers below sea level (Marshak and Paulsen, 1996) (Figure 3).

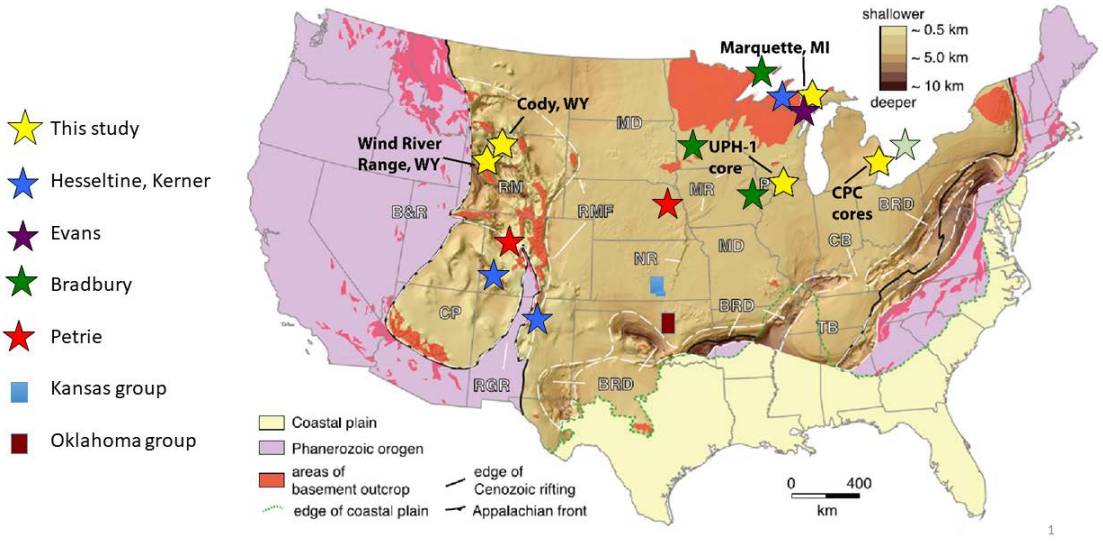

Figure 3: Digital elevation model of the Great Unconformity (United States), in shaded relief. Brown areas represent cratonic platform crust of the continent. The map shows the locations of major faults and folds, as well as the locations of nonconformity analogs examined as part of this study (yellow stars) and other studies. Modified from Domrois et al., 2015 and Marshak et al., (2017).

Earthquakes that have been associated with deep wastewater injection are typically small magnitude events occurring at depths of >1.8 km, primarily nucleating along basement-hosted faults up to 20 km away from the injection point, near the nonconformity between injection points and basement faults (Keranen et al., 2014; Zhang et al., 2013, 2016). Although most earthquakes are small, induced seismic events have potential to be damaging (Evans et al., 2013). Many notable (M 3+) events have occurred over the past decade, such as the 2011 M 5.7 Prague, OK earthquake; the 2014 Guthrie, OK earthquakes (33 M3+ events); the 2014 M 4.9 Milan, KS earthquake; the 2011 M 5.3 Trinidad, CO earthquake; the 2011 M 4.8 Fashing, TX earthquake; the 2011 M 4.7 Guy, AR earthquake; the 2011 M 3.9 Youngstown, OH earthquake; among others (Kim, 2013). Recently, Oklahoma has experienced a total of 623 M3+ earthquakes in 2016, including one M 5.8 event near Pawnee, OK (Earthquake Top Ten and Yearly Summaries, http://www.ou.edu/content/ogs/research/earthquakes/Information.html).

The mechanics of injection related to seismicity is related to the increased pore fluid pressures that occur when fluids are injected into the subsurface (National Research Council, 2013). Injection-related seismicity nucleates on deep basement faults that may be up to 15 km or more from the injection point (Keranen et al., 2014; Zhang et al., 2016). Seismic events may occur months to a few years after injection, indicating that fluid pressure must be traveling along relatively fast hydrological pathways between the injection point and the faults that slip. The propagation of pore fluid pressure from the injection point to basement-hosted faults can modify the stress state of the fault, causing failure, ultimately resulting in seismic activity (National Research Council, 2013). Geologically reasonable fast paths include connected fracture and fault networks or the Precambrian nonconformity zone, which lies in proximity to most injection points (Figure 4). The Precambrian nonconformity, commonly known as The Great Unconformity, is a globally occurring stratigraphic surface that represents a gap in time of 0.7 to > 2.0 Ga, a time during which exposed crystalline rock may have become deeply weathered, or partially eroded (Dutton, 1882). The subsequent basal Cambrian transgression may have acted as a ‘wave-based razor’, removing the deeply weathered surface of the exposed crystalline rock, exposing fresh crystalline rock that was subjected to rapid weathering rates during the early Cambrian (Peters and Gaines, 2012).

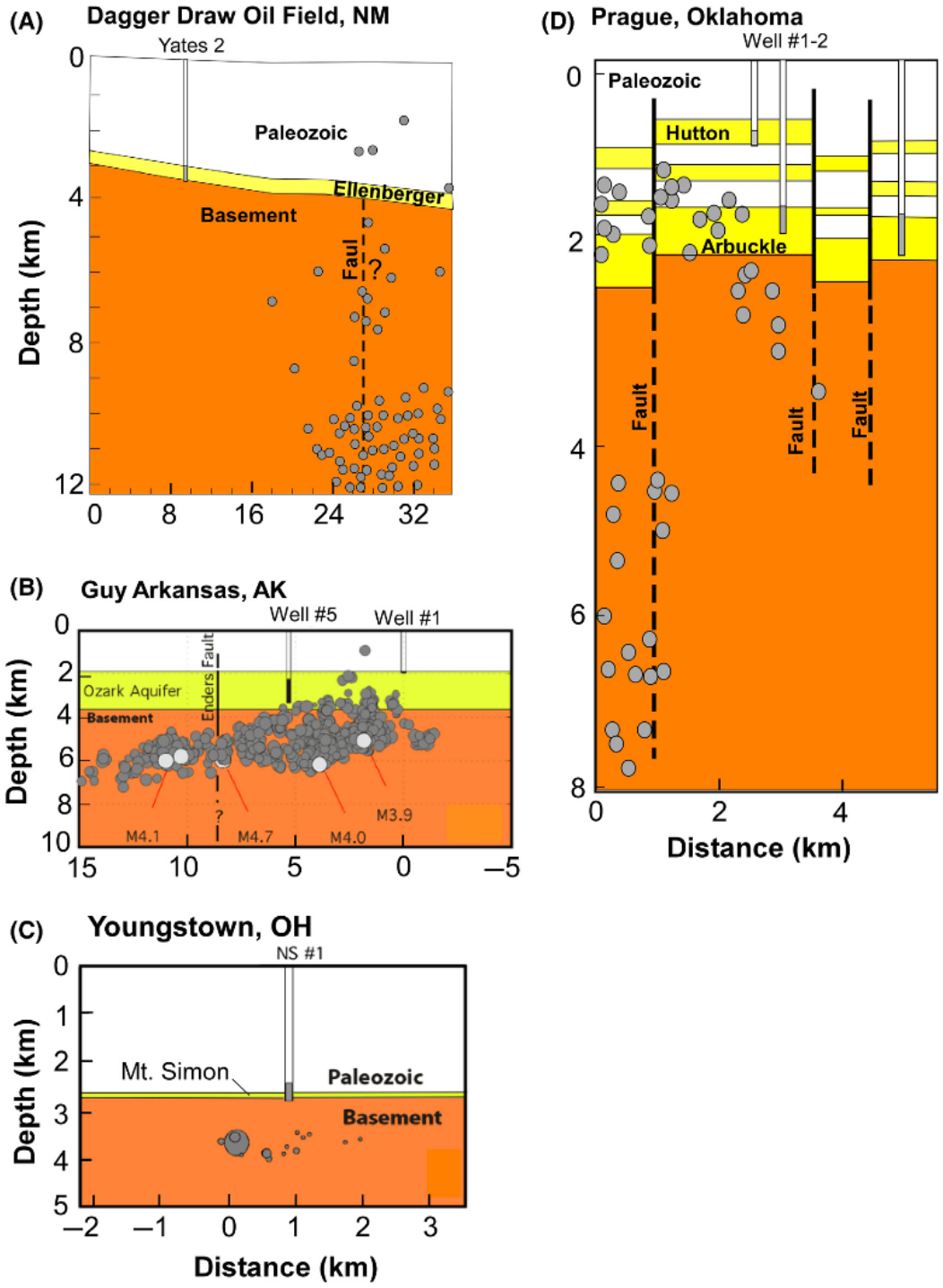

Figure 4: Generalized geologic cross sections showing locations of oil-field brine reinjection wells and associated seismicity within the crystalline basement in New Mexico (A, Edel et al. 2016); Arkansas (B, Horton 2012); Ohio (C, Kim 2013); and Oklahoma (D, Keranen et al. 2013). Original figure from Zhang et al., (2016).

1.4 Project Objectives

Hydrologic modelling of deep injection is an important component to understanding the processes behind induced seismicity(Zhang et al., 2016; Ortiz, 2017), however, specific geologic data on the rock properties of the nonconformity zone are needed to improve the accuracy of these models. The goal of this research project is to examine the composition and structure of the Precambrian nonconformity zone in order to provide a representative range of rock properties for input into hydrologic models, with the ultimate goal of mitigating induced seismicity related to deep wastewater injection. We investigate the unique structure, mineralogy, and geochemistry of the rocks at and near the Precambrian nonconformity in order to understand how the Precambrian nonconformity 'contact zone' may act as a hydrological pathway. We document evidence for past fluid flow in the nonconformity zone, which can be used as a proxy for fluid flow in the future. We characterize the geology of examples of faulted and un-faulted contact zones with the goal of better predicting how the introduction of brines may alter the surrounding rock. This work was performed in conjunction with modeling work by Ortiz (2017), who incorporated basic geometries and properties of nonconformities and faults presented here, and in Hesseltine (2016; in prep), to constrain the seismic effects of injecting wastewater through a range of hydrological and geological scenarios.

The objectives of this work are to examine core and outcrops that represent analogs of the nonconformity zone in order to investigate the range of rock properties and spatial heterogeneity that may exist. Core studies contribute to our understanding of the nonconformity zone at depth, where the influence of uplift and surface alteration is minimized, and are a proxy for the rocks into which fluids are presently being injected. Field studies allow us to examine the nonconformity zone on the mesoscale, laterally and vertically. Outcrop exposures of the nonconformity have been exposed to surface weathering processes, therefore they serve as a proxy for what the geology of the contact may be after a high degree of weathering and/or

alteration has taken place (i.e. prolonged injection at high pressures). We examined sites that sample a range of geological properties that may exist at the contact, enabling us to document end-member geological scenarios (Figure 5). Exposures of the nonconformity in the areas affected by induced seismicity are rare, and core capturing the nonconformity zone is not widely available, therefore, we look to other parts of the country for workable sites where the nonconformity is exposed at the surface, and drill holes to depths of ~2-3 km sample the nonconformity. We examine 2 drill cores from the Michigan Basin which sample the contact between the Cambrian Mt. Simon Sandstone and Precambrian gneiss, and one drill core from northern Illinois which encompasses the contact between the Cambrian Mt. Simon Sandstone and Precambrian granite. We examine field sites with 3 types of basement lithologies and 2 different sedimentary units. One site in Cody, WY exposes the contact between the Cambrian Flathead Sandstone and Precambrian alkali granite. The other field area, near Marquette, MI, contains exposures of the Neoproterozoic Jacobsville Sandstone in contact with Archean altered ultramafic rocks and granitoid gneiss. In addition to these outcrops, field mapping and image analysis of a ~10 km^2 area in the northeastern Wind River Range, WY was examined to allow us to evaluate how fracture and fault networks might be manifested at the m's to km's scale.

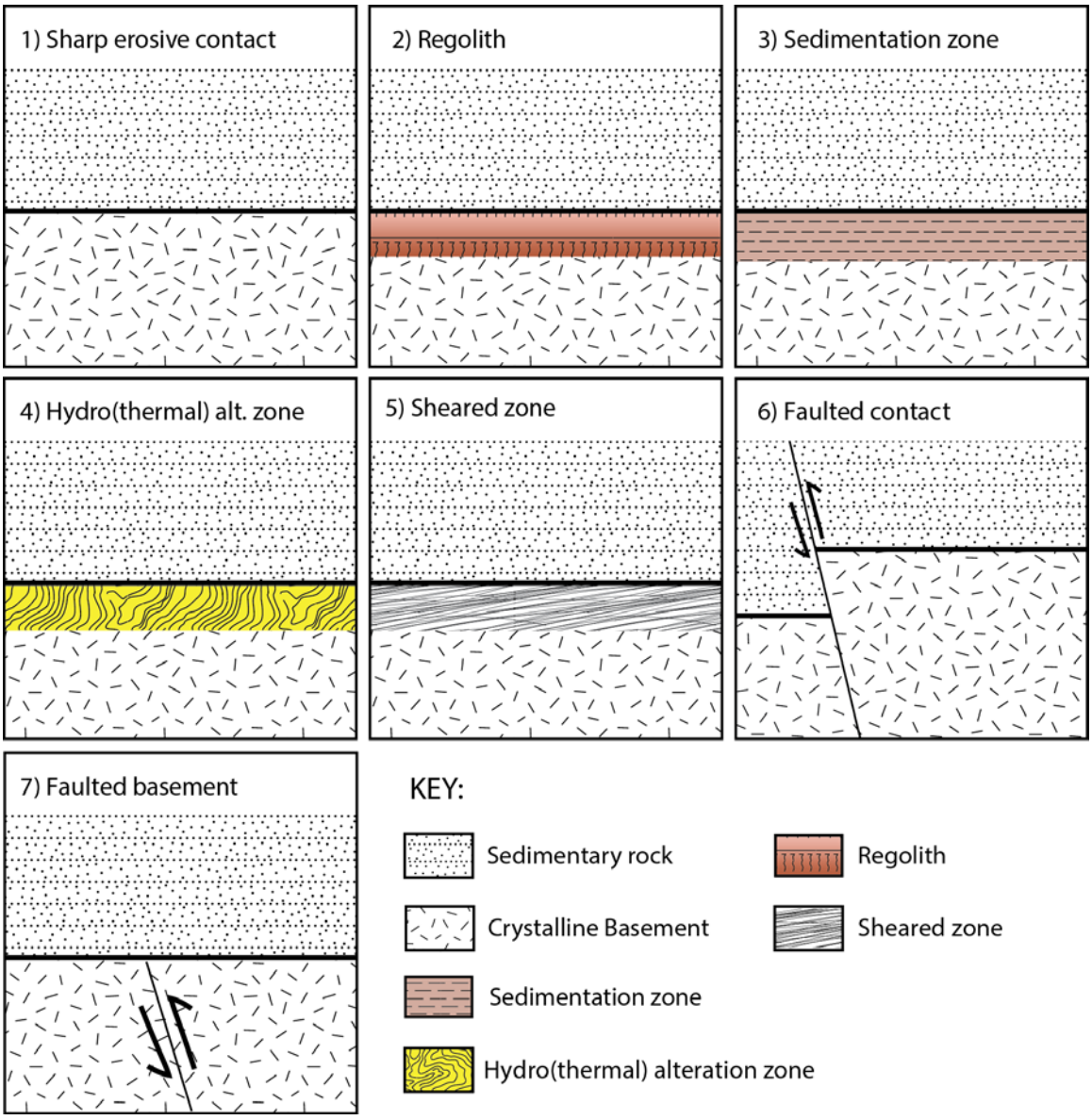

Figure 5: Conceptual models showing a range of geological scenarios that may exist at the contact at depth. Models 1, 6, and 7 represent the standard depictions of the contact in most hydrological models of deep injection. The basis of this work is that we predict that the contact is a geologically complex zone, and may exhibit one or more of the scenarios presented here. The characteristics exhibited at the contact may have implications for relative porosity and permeability parameters, therefore may play an important role in fluid migration and pore fluid pressure transmission.

2. Geologic Background of Core and Outcrop Study Sites

2.1 Core Analogs: CPC BD-139, CPC BD-151

The CPC-BD-139 and CPC BD-151 cores were sampled from selected intervals of brine disposal wells drilled for the Consumers Power Company in 1964. The drill holes are located in St. Clair County, Michigan, at the southeastern edge of the Michigan basin. CPC BD-139 is located at approximately 359437 E, 4732092 N (UTM Grid 17T), and CPC BD-151 is located at approximately 359024 E, 4738656 N (UTM Grid 17T) (Figure 6). The cores are stored at the Michigan Geological Repository for Research and Education (MGRRE), in Kalamazoo, Michigan, and were logged and sampled by James Evans in June 2015. The majority of work for this project was done on the CPC BD-139 core. Billet samples for CPC BD-139 were requested and sub-sampled by members of the MGRRE staff.

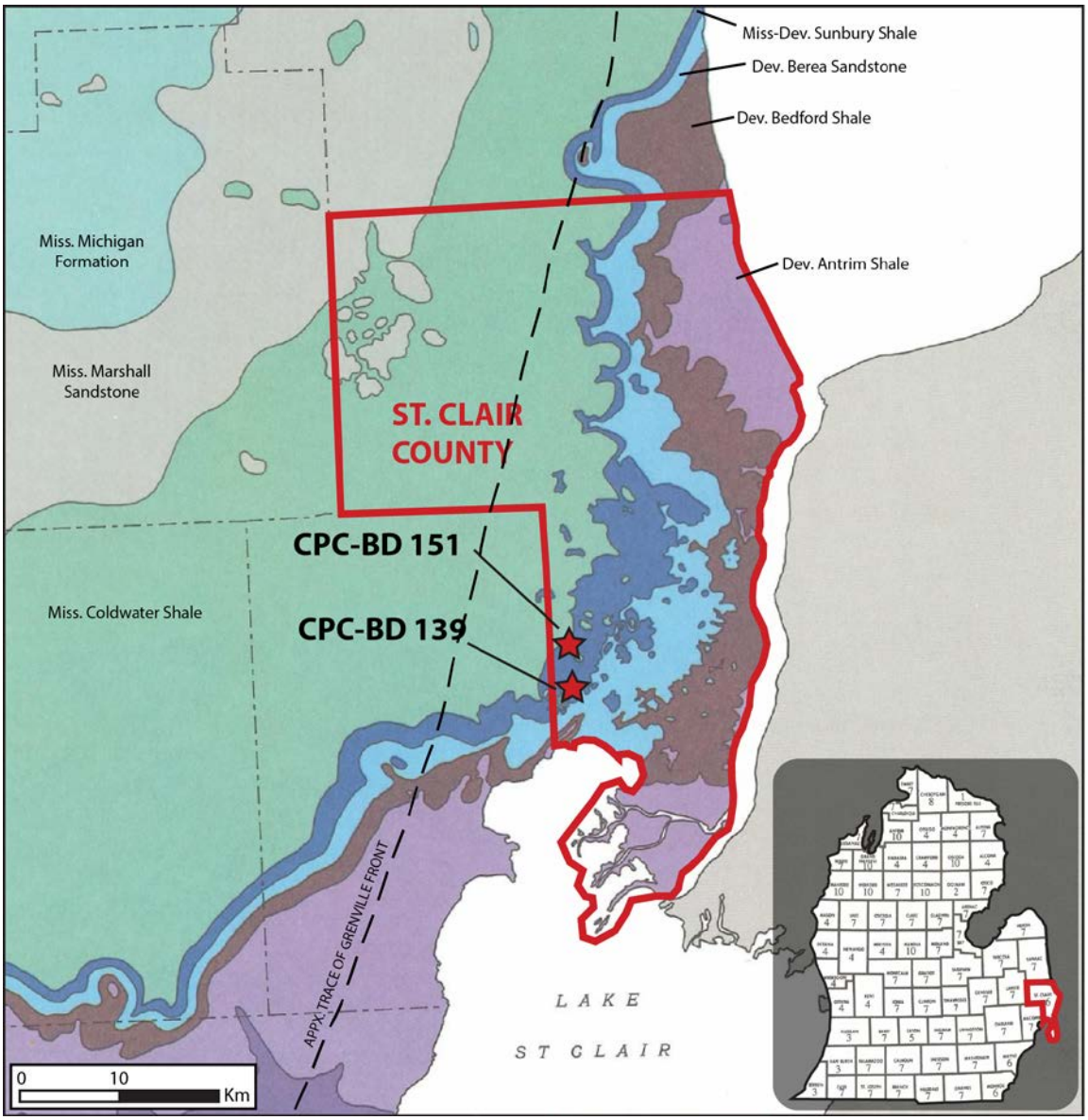

Figure 6: Geologic map showing the locations of the CPC BD-139 and CPC BD-151 drill holes, St. Clair County, Michigan. Modified from Milstein, (1987).

The CPC BD-139 core reaches a total depth of 1412 meters, and contains the section of rock that lies between the Mississippian Sunbury Formation through Precambrian gneiss. We examine the section of core between 1404.5-1412 m depth, which captures the contact between the Mt. Simon Sandstone and Precambrian gneiss. The ~10 meters of the CPC BD-151 core that

was examined also captures the contact between the Mt. Simon Sandstone and Precambrian gneiss, however, the depths indicated on the core boxes are unclear.

The Cambrian Mt. Simon Sandstone in the Michigan Basin is characterized as a porous (5-15% pore space) arenite to sub-arkosic sandstone (Leeper et al., 2012). Permeability in the basal Mt. Simon Sandstone is reported to be between $1x10^{-16}$ m^2 to $1x10^{-12}$ m^2 (Frailey et al., 2011). The Precambrian gneiss captured in this core correlates to the Grenville Front Tectonic Zone, and is characterized as granitic to tonalitic gneiss (Easton and Carter, 1995). The permeability of a typical crystalline basement rock (unfractured) is between $1x10^{-18}$ m^2 to $1x10^{-13}$ m^2 (Brace, 1984).

The Michigan Basin is a thermally complex intracratonic basin situated over the lower peninsula of Michigan. Unexpectedly high levels of thermal maturity in the Paleozoic strata of the basin is thought to be attributed to elevated basal heat flow occurring up until Silurian time, as well as the prior existence of ~2 km of Pennsylvanian and Permian strata that has since been eroded (Everham and Huntoon, 1999).

2.2 Core Analog: UPH-1

The UPH-1 core is one of three engineering test holes drilled in the late 1970's by Commonwealth Edison as part of the Illinois Deep Hole Project (Vitaliano et al., 1986). The project was part of a feasibility study for an underground pumped hydroelectric (UPH) storage plant. UPH-1 is located at approximately 264394 E, 4709549 N (UTM Grid 16T), in Stephenson County, and reaches a total depth of 639 meters (Figure 7). The core is housed at the Wisconsin Geological & Natural History Survey Research Collections and Education Center, in Mount Horeb, Wisconsin, and was logged and sampled by Laura Cuccio in June 2016.

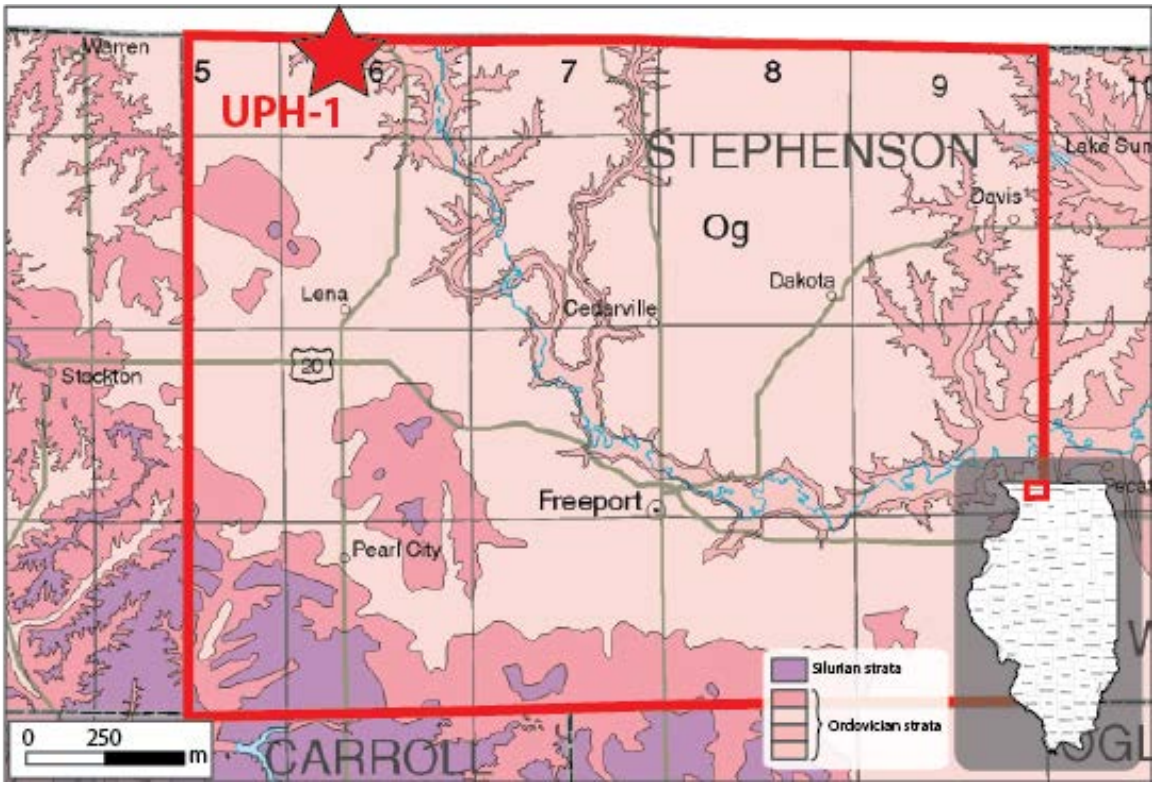

Figure 7: Geologic map of Stephenson County, Illinois, and location of the UPH-1 drill hole. Modified from Kolata, 2005.

We examine the section of core between 593-616 meters depth, which captures the contact between the Cambrian Mt. Simon Sandstone and Precambrian granite, and penetrates into 31 meters of Precambrian basement (Coates et al., 1983; Vitaliano et al., 1986).

The Mt. Simon Sandstone in this area is predominantly characterized as a medium and coarse-grained, arenitic to sub-arkosic sandstone. Grains are typically sub- to well-rounded and moderately to well sorted. Permeability in the basal Mt. Simon Sandstone is reported to be between $1x10^{-16}$ m^2 to $1x10^{-12}$ m^2 (Frailey et al., 2011). The Mt. Simon Formation may also include mudstones and fine-grained sandstones, and conglomeritic sandstones (Duffin, 1989; Bowen et al., 2011).

The Precambrian basement rocks in northern Illinois are part of a vast felsic igneous terrane which spans across much of the midcontinent. The basement rocks sampled by the UPH

cores correlate to the Wisconsin Arch, and are characterized as alkali granites of the Mazatal Province (Whitmeyer and Karlstrom, 2007) (Figure 8). The permeability of a typical crystalline basement rock (unfractured) is between $1x10^{-18}$ m^2 to $1x10^{-13}$ m^2 (Brace, 1984). Geochronological studies on the UPH core basement rock samples indicate an age range of 1450-1500 My (Coates et al., 1983).

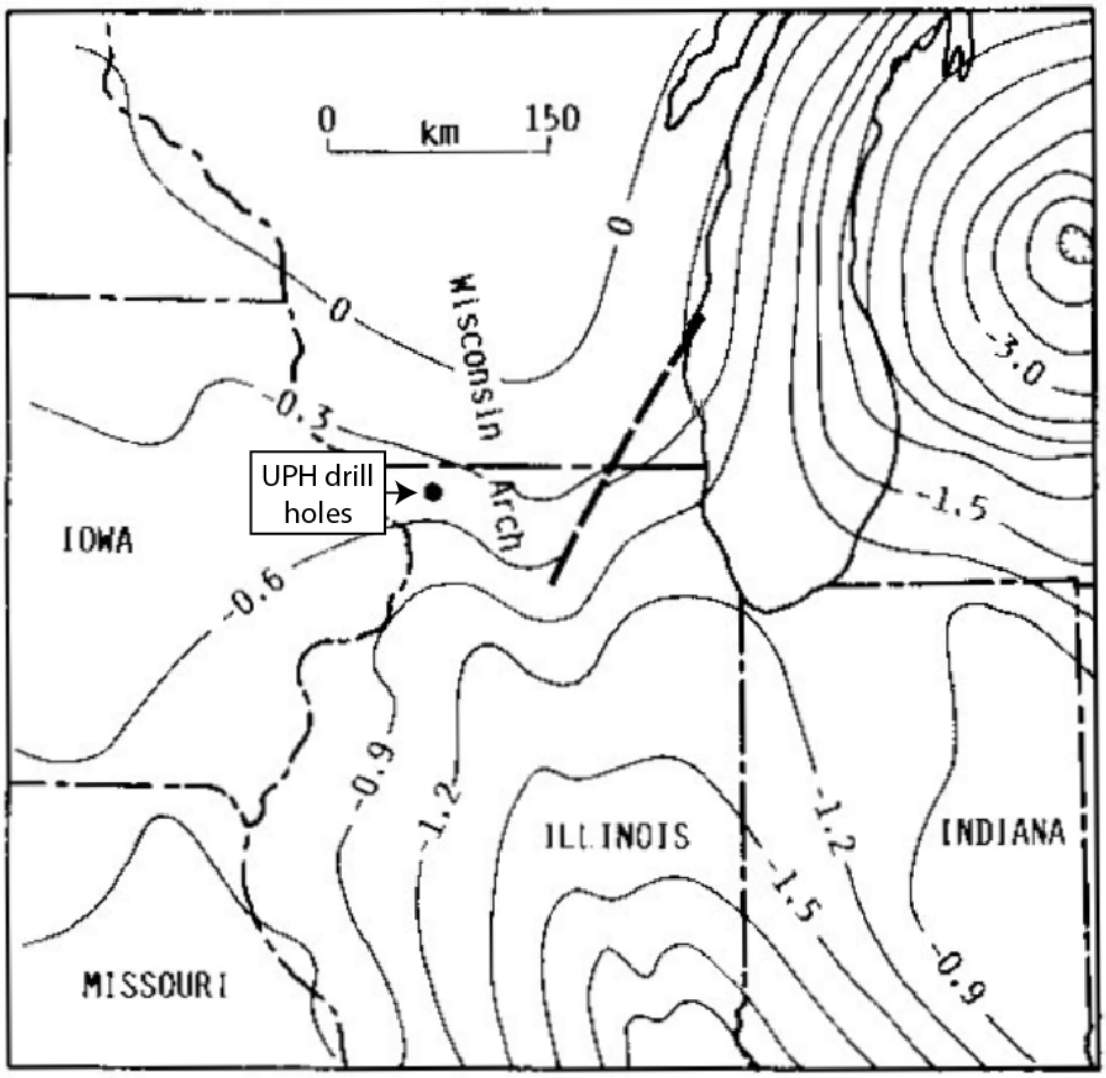

Figure 8: Approximate topography of top of Precambrian basement for region around Commonwealth Edison drill holes. Numbers give elevation in kilometers relative to sea level. Circle in NW Illinois gives approximate location of UPH-1 and other engineering test holes. Near the drill holes the top of the basement is approximately 0.6 km deep. Adopted from Coates et al., 1983.

During our visit to Wisconsin to log the UPH-1 core, we also examined exposures at Devil's Lake State Park and Parfrey's Glen State Natural Area, located near Merrimack, Wisconsin. The sites contain excellent exposures of the contact between the Cambrian Parfrey's Glen Formation (sandstone, conglomeritic sandstone) and the Precambrian Baraboo Formation (quartzite) (Clayton and Attig, 1990). The basal Parfrey's Glen Formation, exposed at the Parfrey's Glen State Natural Area, consists mainly of interbedded conglomerate layers (about <50 cm thick) in a very incohesive sandstone host. The conglomerate contains sub-angular to rounded pebble- to cobble-sized quartzite clasts. Outcrops in Devil's Lake State Park expose the Parfrey's Glen Formation basal conglomerate in contact with the Baraboo Quartzite. Here the basal conglomerate consists of pebble- to boulder-sized rounded quartzite clasts. Many of the boulders are approximately 1-2 meters in diameter.

2.3 Outcrop Analogs: Marquette, Michigan

The southern shoreline of Lake Superior in the greater Marquette area of Michigan's Upper Peninsula exposes the Precambrian nonconformity in several areas (Figure 9). We examine outcrops along the western shore of Presque Isle, located about 4.5 kilometers north of the town of Marquette, MI, and at Hidden Beach and Little Presque Isle, accessed from Wetmore Landing (approximately 464253E, 5163278N, UTM Grid 16T) (Figure 9). The contact between the late Proterozoic (~1.1 Ga) Jacobsville Sandstone and Archean serpentinized peridotites is exposed along the entire western shore of Presque Isle. The contact between the Jacobsville Sandstone and the Archean Compeau Creek Gneiss of the Superior Province is marginally exposed at Hidden Beach (Figure 9).

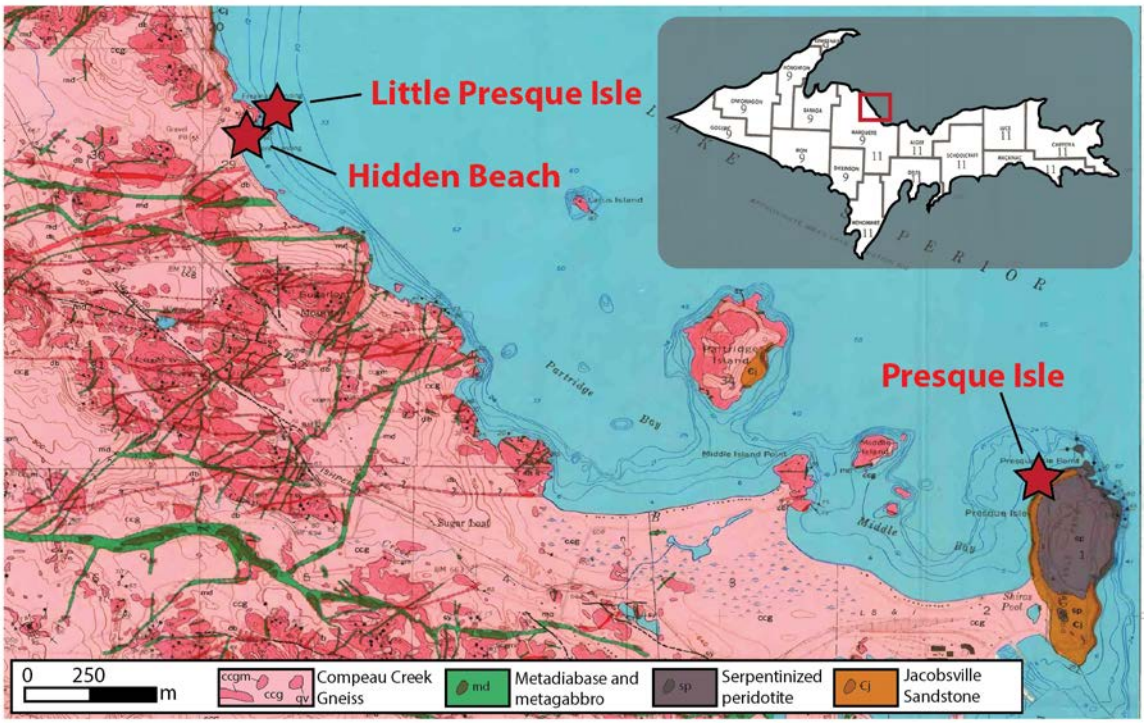

Figure 9: Geologic map of the Marquette, Michigan field area, showing locations of Hidden Beach and Presque Isle. Modified from Gair and Thaden, 1968.

The Jacobsville Sandstone is a red to reddish-brown fine-medium grained subarkosic sandstone, becoming more arkosic near the contact with Archean basement rocks. The reddish color is attributed to the presence of magnetite, ilmenite, and hematite, which compose 50-80% of the heavy minerals in the Jacobsville Sandstone. Grains are cemented by fine quartz mixed with clays, iron oxide, authigenic quartz, and calcite (Hamblin, 1958). Bleaching patterns occur along sub-vertical fractures and bedding planes, or other areas of increased permeability (Gair and Thaden, 1968a). The average permeability for the Jacobsville Sandstone is ~$8x10^{-9}$ m^2 (Heinrich, 2001).

The Archean serpentinized peridotite exposed at Presque Isle is a dark green rock which commonly weathers to black, light green, reddish-brown, or yellowish brown. The rock commonly exhibits blocky jointing patterns, as well as a network of stockwork quartz and

carbonate veinlets in varying abundances (Gair and Thaden, 1968a). Permeability measurements are not available for the Presque Isle serpentinized peridotite, however, the permeability of serpentinite is estimated to be between $1x10^{-22}$ m^2 to $1x10^{-19}$ m^2 (Kawano et al., 2011).

The geologic history of the Presque Isle serpentinized peridotite is not well constrained. Early research by Wadsworth (1884) believed that the peridotite intruded into Paleozoic sandstone, however, fragments of oxidized peridotite within the Jacobsville sandstone were reported by Van Hise and Bayley in 1897 (Gair and Thaden, 1968a). The most recent consensus is that the Presque Isle peridotite intruded after post-Animikie, pre-Keweenawan metamorphism (between 1.8-1.1 Gya), and was partially serpentinized at the time (Gair and Thaden, 1968a). Three metasomatic events have altered the original peridotite. The first phase of alteration is extensive serpentinization of the peridotite. Quenching of a peridotite transforms olivine and pyroxene to serpentine-group minerals and ferrous and ferric iron minerals. Volume change associated with serpentinization forms fracture networks resulting in stockwork serpentine veining (O'Hanley, 1992). The second phase of alteration is the calcium carbon dioxide metasomatism of serpentine veins, resulting in the replacement of serpentine-group minerals with dolomite, calcite, and quartz. Lastly, the interaction of surface waters and the dolomitized serpentinized peridotite resulted in dissolution and removal of carbonate minerals, leaving behind a quartz-rich regolith (Lewan, 1972).

The Archean Compeau Creek Gneiss is characterized as light-colored tonalite and granodiorite gneiss, including dark chloritic, biotitic, amphibolitic, and hornblendic varieties. It is described as largely foliated, however, rarely folded (Gair and Thaden, 1968a). The permeability of a typical crystalline basement rock (unfractured) is between $1x10^{-18}$ m^2 to $1x10^{-13}$ m^2 (Brace, 1984).

2.4 Outcrop Analog: Cody, Wyoming

The contact between Precambrian granite and the Cambrian Flathead Sandstone is exposed in outcrops located 10 km west of Cody, WY on US-20, at approximately 645326 E, 4930046 N (Figure 10). The exposures lie in the hanging wall block of Rattlesnake Mountain, located in the western part of the Bighorn Basin, in the Sevier-Laramide foreland (Beaudoin et al., 2012). The immediate area is structurally characterized by steeply dipping NW-striking basement faults and moderately dipping secondary reverse faults that localize deformation in the basement rocks (Beaudoin et al., 2012) (Figure 10).

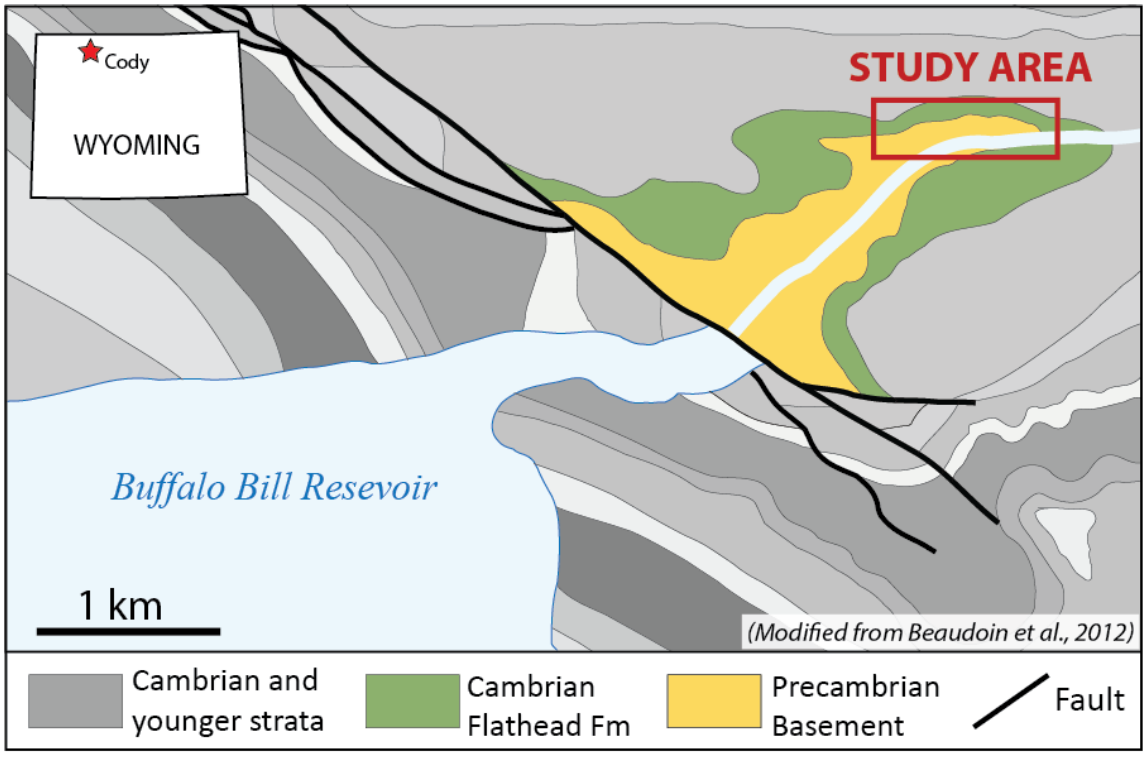

Figure 10: Generalized geologic map of the Cody, Wyoming field area. Modified from Beaudoin et al., (2012).

The basal Cambrian Flathead Sandstone is characterized by cross-stratified, medium-grained, texturally mature orthoquartzite sandstone, often cut by channels. Local variation of this

lower unit includes shaley or conglomeritic characteristics at the base, occasionally transitioning to a highly weathered zone at the top of the Precambrian (Bell and Middleton, 1978). Permeability measurements for the Flathead Sandstone are not publicly available, however, the Flathead Sandstone is commonly known to be a highly permeable, productive formation (Cooley, 1986). The Precambrian basement in this area is predominantly characterized as a coarse-grained alkali granite with mafic intrusions. The permeability of a typical crystalline basement rock (unfractured) is between $1x10^{-18}$ m^2 to $1x10^{-13}$ m^2 (Brace, 1984).

2.5 Outcrop Analog: Ross Lake Area, Wind River Range, Wyoming

The Wind River Range is a NW-SE plunging, overturned anticline that formed during Laramide uplift. The anticline is cored by Archean igneous and high-grade metamorphic rocks, and is flanked by Paleozoic and Mesozoic sedimentary rocks. Due to heavy Pleistocene glaciation, the Wind River Range represents some of the best exposures of Archean crust in the United States, making it a prime location for studying the extent of Laramide deformation structures in basement rocks (Stuckless, 1989). We examine the late Archean granitic gneiss exposed approximately 14 kilometers south of Dubois, WY (Figure 11).

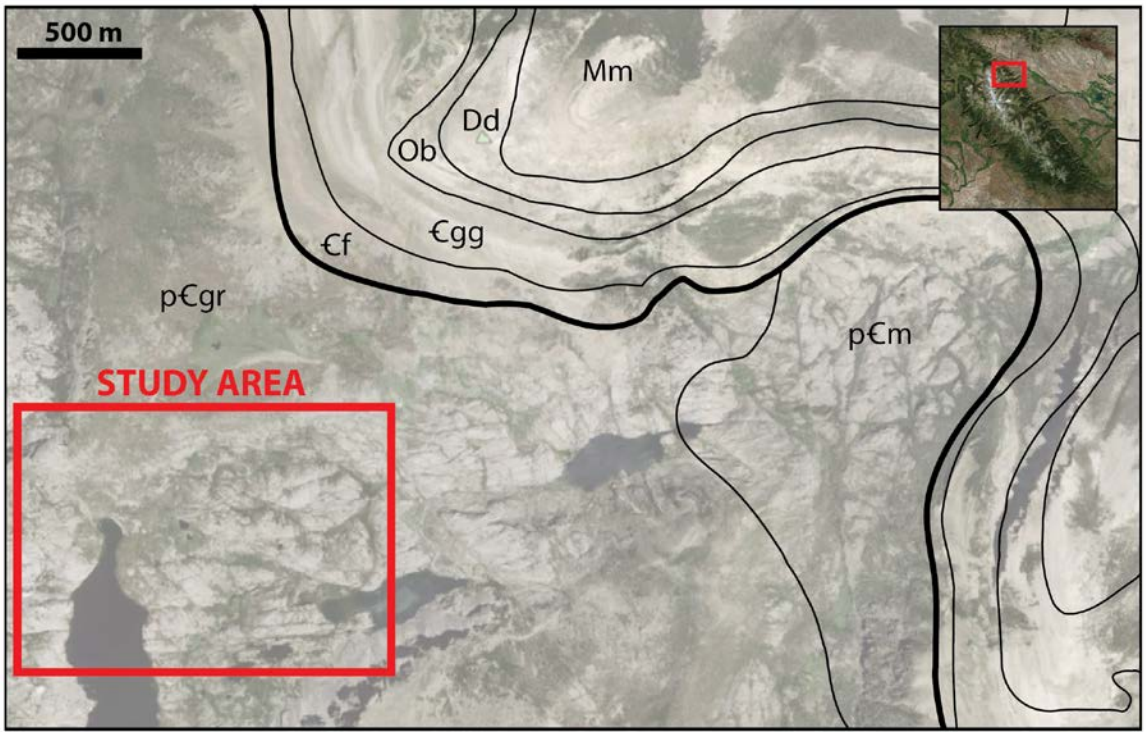

Figure 11: Generalized geologic map of the Ross Lake field area, northeastern Wind River Range, Wyoming.

3. Methods

We implement a multi-scaled approach to document variations in the structure and composition and structural and permeability architecture of nonconformity zones. The methods listed below are employed at each site, where applicable.

3.1 Site-Scale Mapping

Mapping of lithologic and brittle deformation features at the map, outcrop, and core scales allows us to document the geometry of the contact, determine the relationship of faults and fractures to the contact, and to examine lithologic variations in relation to the contact and brittle deformation features. We use outcrop-scale cross-sectional mapping (scales of 1:500 to 1:7,000) to determine the sinuosity of the contact, the nature and distribution of the rocks along the nonconformity, and the distribution and nature of fracture and fault networks. The mapping also enables us to locate key samples for further analyses. We create lithologic columns in core and in outcrop to document meter-scale variations in lithology and textures seen vertically through the contact. Fracture transects on the outcrop and map scale reveal the orientations and intensities of fracture sets and how they may relate to faults or fault zones, providing us insight into potential conduit systems in the nonconformity zone.

I examined core from the UPH-1 drill hole (Coates et al., 1983) at the Wisconsin Geological & Natural History Survey Research Collections and Education Center in Mt. Horeb, Wisconsin, in June of 2016. The CPC BD-139 and CPC BD-151 cores were examined and sampled by James P. Evans at the Michigan Geological Repository for Research and Education in Kalamazoo, Michigan, in June of 2015. Core analyses consists of photography, lithologic logging with special attention to weathering and alteration horizons, noting of fractures and faults where applicable, and sampling of host rocks, alteration, fault or fracture surfaces, and contact rocks. In addition to core analyses, we use the legacy data provided by the core repositories, which provide

permeability and porosity measurements. The data for CPC BD-151 and CPC BD-139 were collected in 1971 by Maness Petroleum Laboratories, in Mt. Pleasant, Michigan, using standard laboratory methods at the time.

3.2 Petrographic Analysis

A total of 58 standard uncovered 30 µm thick thin sections from 4 localities were examined. Blue epoxy impregnation was used on select thin sections to highlight porosity. Optical thin-section analysis was done using Leica DM 2700P and Leica Z16 APO petrographic scopes equipped with a Leica MC170 HD camera. Petrographic analysis was used to document sample mineralogy and micro-scale textures and alteration throughout the contact zone and along fault surfaces, and to compare relative porosity between samples.

3.3 Mineralogical Analysis

X-ray diffraction analysis was performed on a total of 100 samples from 4 localities. Sample preparation and analysis was done in house at the Utah State University Geology Department under the direction of Dr. Kelly Bradbury. Samples were broken into chips using a rock hammer, and then milled into a fine powder in a tungsten carbide vessel. Powdered samples were then run using a PANalytical X'Pert Pro X-ray Diffraction Spectrometer (XRD). All samples were run at 45 kV and 40 mA, with a 1 second per 0.02 º step size over a range of 2º to 75 º. Raw data were collected using the PANalytical X'Pert Data Collector, version 5.4.0.90, and interpreted using the PANalytical X'Pert Highscore, version 4.5.0.22741.

3.4 Geochemical Analysis

3.4.1 Whole-rock Geochemistry

A total of 26 samples were analyzed for whole-rock geochemical analysis at the Washington State University GeoAnalytical Lab. Major and trace element analysis was run on a

Thermo-ARL automated X-ray fluorescence spectrometer (XRF). The data were accompanied by loss on ignition (LOI) values for 23 of the 26 samples. XRF analysis was done post-XRD analysis so that analyses could be run on the same powders.

3.4.2 Stable Isotope Analysis

Eight calcite and 7 dolomite samples from veins, slip surfaces, and interstitial carbonaceous cements, were analyzed for carbon and oxygen stable isotope ratios to better determine the source fluid of mineralization within the nonconformity zone at Presque Isle and Hidden Beach, and in the CPC BD-139 core. Analyses were performed at the Utah State University Geology Department Stable Isotope Laboratory. Samples were run on a Thermo Delta V Advantage Isotope Ration Mass Spectrometer (IRMS) and GasBench II with GC PAL auto-sampler, under the direction of Andrew Lonero. ISODAT 3.0 Gas Isotope Ration MS Software® was used to collect data from the mass spectrometer and perform basic data reduction Analysis of all samples followed the established laboratory methods.

3.4.2.1 Calcite Sample Processing

Calcite samples were acidified with phosphoric acid and allowed to equilibrate for 2 hours at 25 ºC. The data were checked for drift and linearity using a Regression Data Analysis in Excel, and were not found to be significant. Oxygen values were calibrated using the NBS-18 and NBS-19 standards, and carbon values were calibrated using the NBS-19 and LSVEC standards. Calibrated data is precise to ±0.01‰.

2.4.4.2 Dolomite Sample Processing

Dolomites were acidified with phosphoric acid and allowed to equilibrate for 24 hours at 50 ºC. The data were checked for drift and linearity using a Regression Data Analysis in Excel, and were not found to be significant. Oxygen values were calibrated using the NBS-18 and NBS-19 standards. Carbon values were calibrated using the NBS-18, NBS-19, and LSVEC standards. In order to account for the temperature dependency of the oxygen-isotope acid fractionation

factor for dolomites, a linear normalization curve constructed from equations 1 and 2, where $\alpha_{CO2(ACID)\text{-}cal}$ is 1.00934 and $\alpha_{CO2(ACID)\text{-}dol}$ is 1.01081, was applied to the calibrated data (Kim et al., 2015). Calibrated data is precise to ±0.01‰.

$$m = \frac{\left[\left(\delta^{18}O_{NBS19,VPDB}+1\right)\frac{\alpha_{CO2(ACID)-cal}}{\alpha_{CO2(ACID)-dol}}-1\right]-\left[\left(\delta^{18}O_{NBS18,VPDB}+1\right)\frac{\alpha_{CO2(ACID)-cal}}{\alpha_{CO2(ACID)-dol}}-1\right]}{\delta^{18}O_{NBS19-CO2(ACID)}-\delta^{18}O_{NBS18-CO2(ACID)}} \quad (1)$$

$$b = \left[\left(\delta^{18}O_{NBS19,VPDB}+1\right)\frac{\alpha_{CO2(ACID)-cal}}{\alpha_{CO2(ACID)-dol}}-1\right]-m\delta^{18}O_{NBS19-CO2(ACID)} \quad (2)$$

4. Results

Results of the analyses of structure, mineralogy, and geochemistry from core and outcrops of the nonconformity zone are presented from the four sites described above. The types of results presented for each site depend of the methods that were able to be performed at that site. Where available I also show permeability and porosity data collected from the borehole at the time of drilling. Key data are shown in the text of this thesis; complete catalogs of core legacy data, thin section microphotographs, X-ray diffraction sample reports, and geochemical raw data files, are compiled in electronic appendices.

In these descriptions, we use the term ‘regolith’ to describe bedrock which has been altered by processes at or near the surface, consistent with Pain (1991). This definition of regolith does not imply lithology. We use the term ‘grus’ to describe a coarse-grained felsic crystalline rock that has been subject to some degree of weathering, resulting in a poorly sorted, relatively incohesive, and typically clay-rich, horizon (Migon and Thomas, 2002). Grus is technically a type of regolith, however, the specific parent rock lithology and associated clay minerals implied by the definition have specific implications for permeability, therefore, we discuss grus and regolith separately. We use the term ‘granitic wash’ to refer to rock that is compositionally approximately the same as the underlying host rock, but has experienced at least a small amount of transport and deposition (Pettijohn et al., 2012). We use the term ‘altered’ to describe rock that varies chemically from the host rock.

4.1 Boreholes CPC BD-139, CPC BD-151

A total of 16 samples over a depth of 7.9 meters were obtained from the CPC BD-139 core. Sample numbers reflect the depth (in feet) at which the samples were taken.

4.1.1 Mesoscopic Description

The logged section of the CPC BD-139 core is comprised of one meter of Mt. Simon Sandstone and 6.7 meters of Precambrian gneiss (Figure 12, Appendix A). The basal meter of the Mt. Simon Sandstone is a cemented, light tan, fine-grained, and laminated quartz arenite (Figure 13a). Visual inspection (J.P. Evans, pers. comm.) of ~15m of Mt. Simon Sandstone above this zone shows that fine-grained quartz arenite continues up-section, where the only difference is that much of the sandstone is massive up-section. A sharp contact separates the Mt. Simon Sandstone and the Precambrian gneiss (Figure 13a), where the uppermost 10 cm of basement rock is a tan, fine-grained, laminated horizon containing fragmented pinkish-white carbonate veins. This horizon grades over >5 cm into a dark green, finely foliated gneiss with pink sub-vertical fractures that continues for about 1.5 meters below the contact (Figure 13a). The finely foliated gneiss gradually grades into a dark gray gneiss with sub-horizontal pinkish-white veins, which extends through the bottom of the logged section (Figure 13b).

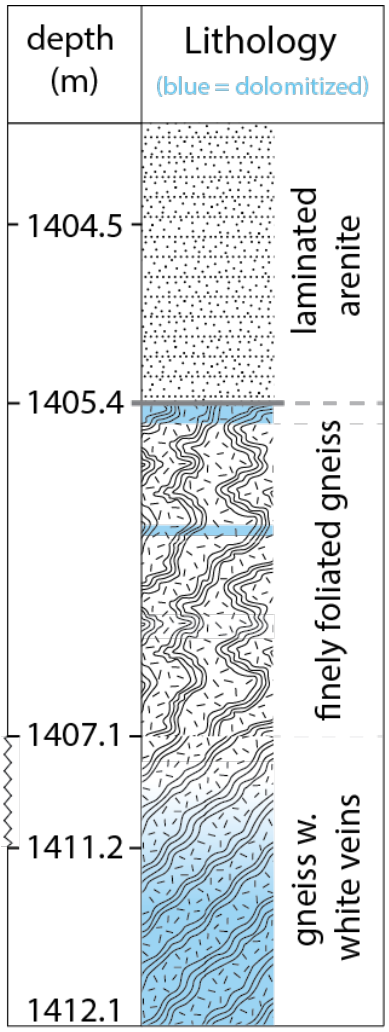

Figure 12: Lithologic core log for the CPC BD-139 core from 1404-1412.1 meters depth, based on observations within that interval. Five main lithologic units were identified, including sandstone, dolomitized and undolomitized finely foliated gneiss, and dolomitized and undolomitized gneiss with sub-horizontal white veins. Blue shading represents dolomitized horizons.

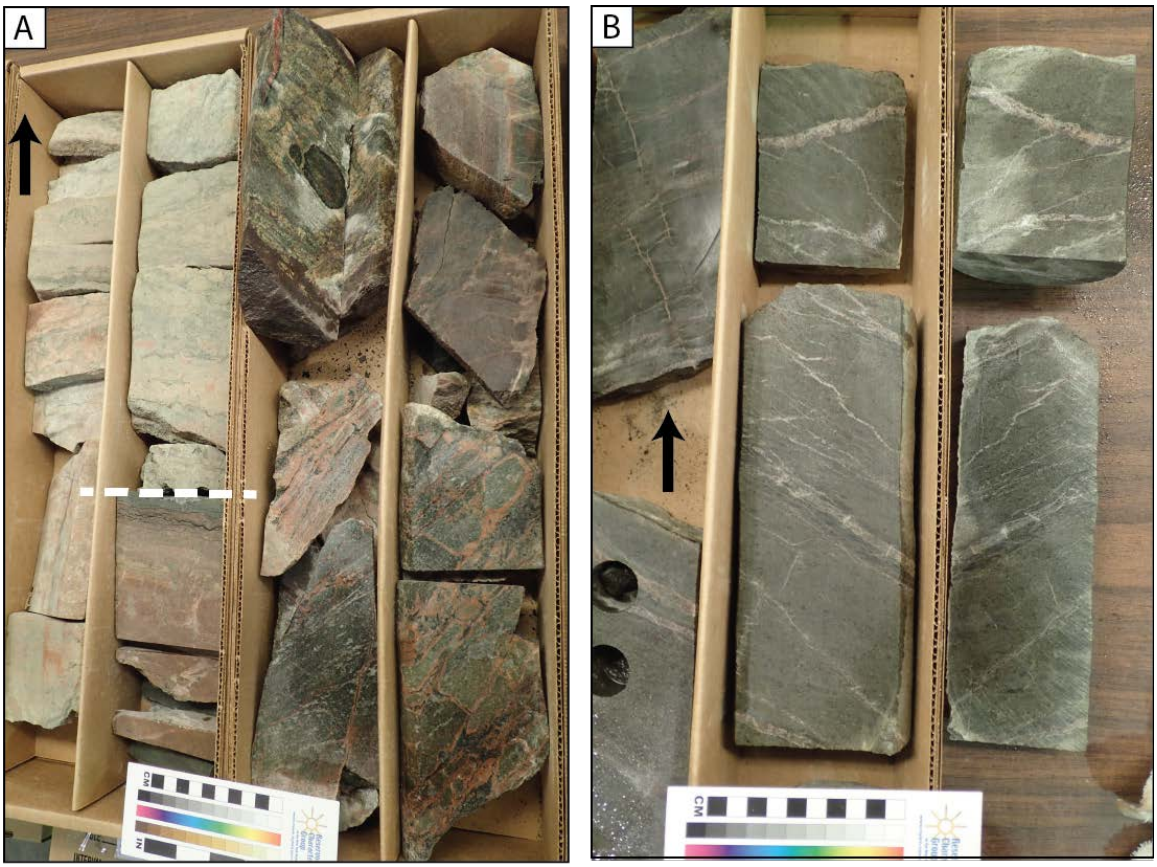

Figure 13: Photographs of the CPC BD-139 core. Black arrows indicate up-direction. (A) Core between ~1404.5-1405.5 meters. The white dashed line marked the contact between the Cambrian Mt. Simon Sandstone (light tan) and the underlying Precambrian gneiss. The gneiss directly at the contact is fine-grained, tan, and dolomitized. This is underlain by green altered gneiss with sub-vertical pink-coated fractures. This lithology grades into a dark gray gneiss with sub-horizontal white veins (B, core between 1411.5-1412.5 meters), which extends through the bottom of the logged section.

4.1.2 Petrographic Analysis

A total of 18 thin sections from 16 samples from the CPC BD-139 core were analyzed (Appendix B). The basal Mt. Simon Sandstone contains rounded to sub-rounded, moderate to well sorted fine to coarse silica-cemented quartz grains. Graded beds (~1 cm thick) are recognizable in one of the two thin sections. Blue epoxy on sample 4607 reveals a porosity of ~5-7% (Figure 14a).

Thin sections of the uppermost 10 cm of basement rock directly at the contact reveal very fine-grained sub-angular quartz grains supported by a tan, very fine-grained, dolomitic matrix (Figure 14b). The concentration of quartz grains is variable, forming patches, laminations, and ptygmatic folds. In sample 4611A, thin (>1mm) calcite veins, and a thicker (3-8mm) carbonate vein, cross-cut the matrix (Figure 14b). The thicker vein appears to be cored by 1-2mm anhedral anhydrite crystals, rimmed by larger (up to 4mm) subhedral to euhedral calcite crystals (Figure 14b).

Thin sections of the green and pink finely foliated gneiss are characterized by elongate polygonal quartz crystals, feldspar grains that exhibit weathered and/or perthitic textures, and fibrous and platy chlorite, biotite, and muscovite (Figure 14c). These feldspar grains appear to account for the pink rimming along fracture boundaries, whereas the green and black groundmass is primarily composed of quartz, micas, and some olivine (Figure 14c). Garnets are fairly common, and are often brecciated.

The dolomitic groundmasses intermittently appear one meter below the contact and increase in density with depth. Dolomite primarily exists as a fine-grained, amorphous matrix and/or fine-grained veins (Figure 14 d, e). The bottom 3 meters of the logged section are dominantly composed of this dolomitic groundmass, and are accompanied by a decrease in grainsize throughout the thin sections and spherulitic recrystallization textures in quartz grains (Figure 14e).

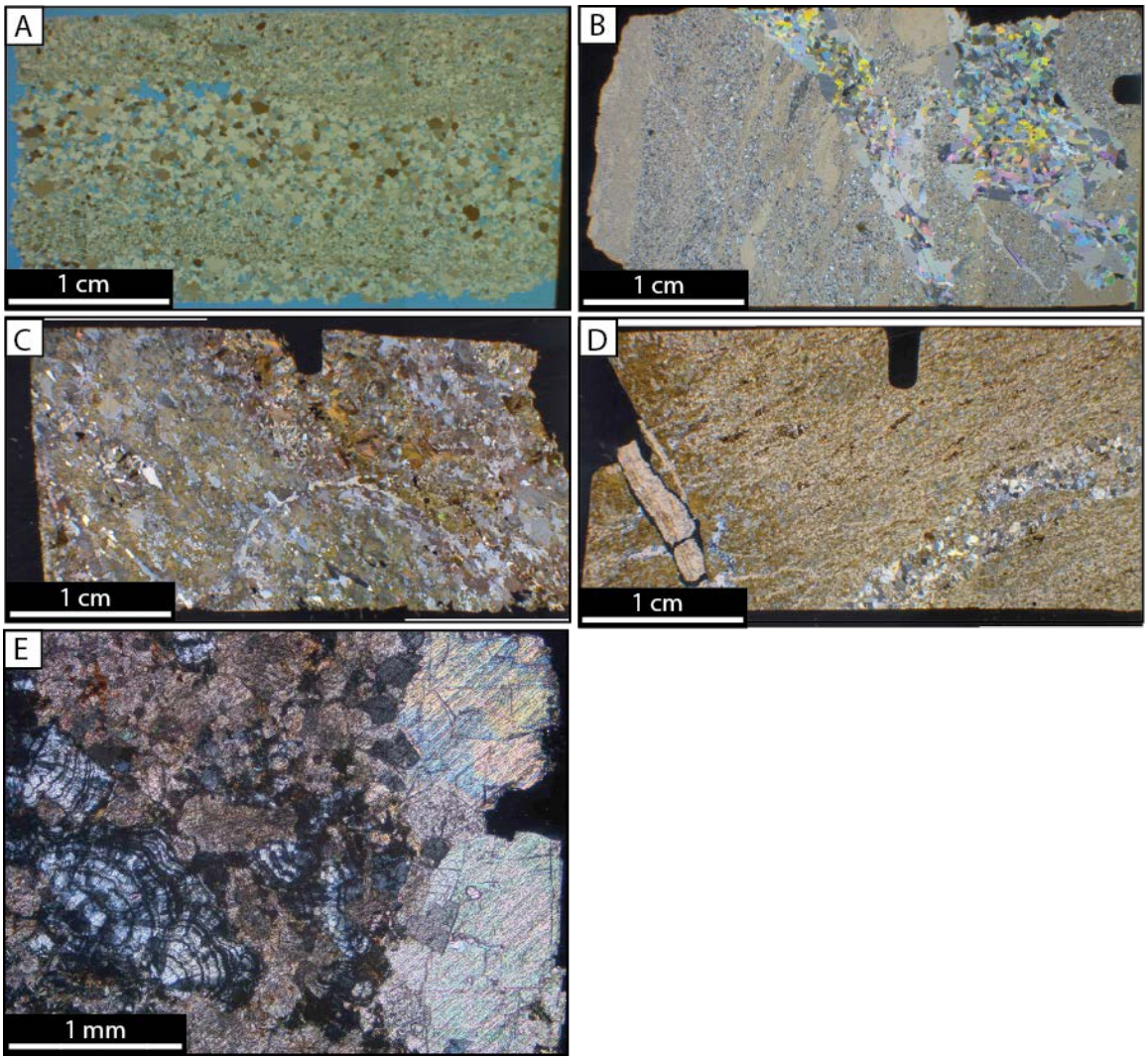

Figure 14: Photomicrographs of thin sections from the CPC BD-139 core, representative of the 5 main lithologies captured by the logged section. (A) Sample 4607, graded bedding in the basal Mt. Simon Sandstone, with blue epoxy to highlight porosity. (B) Sample 4611A, dolomitized gneiss at the contact. The large vein in the top right corner of the thin section is composed of anhydrite at the core, and calcite at the rim. (C) Sample 4613B-1, finely foliated green altered gneiss with sub-vertical pink-coated fractures. (D) Sample 4631.9, dolomitized gneiss at the base of the logged section. Metamorphic fabric is retained in the dolomite matrix. 1-2 mm thick quartz veins are cross-cut by a thicker (3 mm) fine-grained dolomite vein. (E) Sample 4633 under 5x magnification, spherulitic quartz in dolomitic groundmass (left) with coarse-grained crystalline dolomite vein (right).

4.1.3 Mineralogical Analysis

X-ray diffraction (XRD) analysis on 15 of the 16 samples from the CPC BD-139 core (Table 1, Appendix C) reveals that the Mt. Simon Sandstone within a meter of the nonconformity primarily consists of quartz with minor nontronite-rich clay. Quartz and feldspar make up the major phases of the gneissic basement host rock. The uppermost 30 cm of basement rock at the contact is depleted in quartz and feldspar relative to the host rock, and consists primarily of dolomite, with some minor sulfides (Table 1). Dolomite is a major mineral phase in 5 of the 14 analyses run on the basement rocks. Ankerite is also present in varying amounts. Clinochlore is present in trace amounts. Common alteration minerals include clays (primarily nontronite and vermiculite), phlogopite mica, and a variety of zeolites.

Table 1:Interpretation of XRD results for samples from the CPC BD-139 core. Green indicates a major mineral phase (PANalytical X'Pert Highscore score of 0.5 or higher), yellow indicates a minor mineral phase (score of 0.1-0.5), and orange indicates a trace mineral phase (score of <0.1). Abbreviations of mineral name is present where applicable.

LITHOLOGY	SAMPLE ID	qtz	feldspar	micas	clays	carbonates	oxides	hydroxides	sulfides	zeolites
MT. SIMON	4608				nont.					
BASEMENT	4611A					dolo.			CuFeS2	
	4611B									
	4612									
	4613A					dolo.				
	4613B									
	4616.5									gism.
	4620A					ank., dolo.		FeAlphos.		
	4620B				verm.					
	4621			phlogo.			NaMnOx		AgAuS	
	4623					ank.				
	4625.5									
	4630.5				verm.	dolo.		clinochlore		
	4631.9					dolo.	NaMnOx			
	4633					dolo.		clinochlore		

4.1.4 Geochemical Analysis

Major and trace element whole rock analyses were run on 4 samples from the basement rocks in the CPC BD-139 core (Appendix D). The basement rocks at the contact (1405.43 m) are

depleted in SiO_2 (36.16 wt%), with respect to unaltered gneiss (66.44 wt%) (Figure 15). CaO and MgO are enriched at the contact (30.91 wt% CaO, 18.26 wt% MgO) and form a ~1 meter thick zone at the base of the logged section (1412.14 m, 21.40 wt% CaO, 19.45 wt% MgO) with respect to unaltered gneiss (0.3 wt% CaO, 5.58 wt% MgO) (Figure 15). The unaltered gneiss is enriched in K_2O and Al_2O_3 relative to the rocks at the contact and at the base of the logged section. The contact rocks are depleted in FeO with respect to the rest of the core (Figure 15).

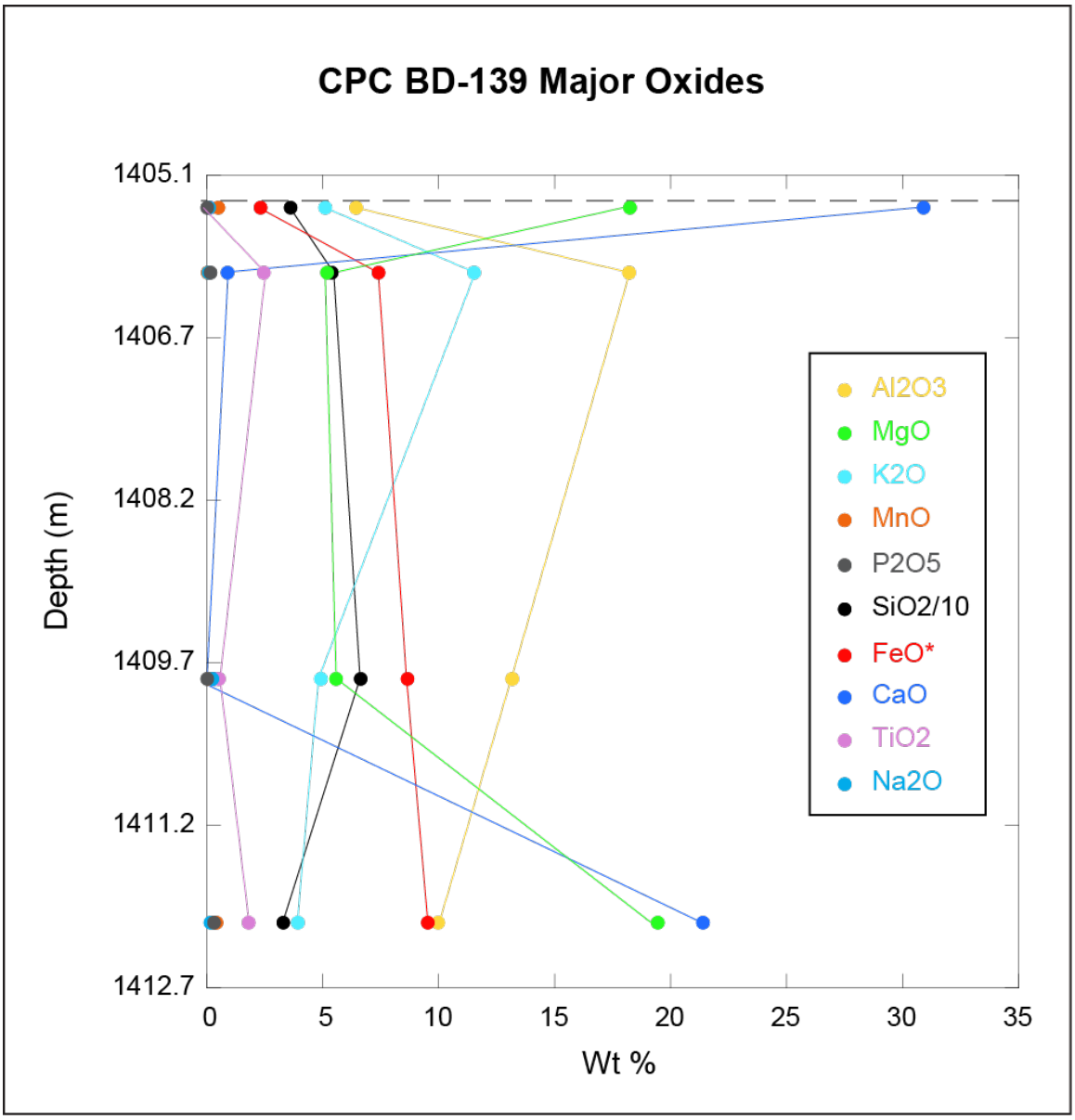

Figure 15: Whole rock geochemical data for all major oxides for basement samples from the CPC BD-139 core. The contact is represented by the gray dashed line. See Appendix D for raw data.

Barium, vanadium, chromium, and zirconium are the primary enriched trace elements constituents in the four analyzed samples (Figure 16, Appendix D). Barium is most concentrated in unaltered gneiss (1409.85 m, 894 ppm), and depleted at the base of the core (123 ppm). The unaltered gneiss is enriched with vanadium (309 ppm) and zirconium (313 ppm) with respect to

the rest of the sampled core. The lowermost sample (1412.14 m) is highly enriched in chromium (2233 ppm) with respect to the rest of the sampled core (Figure 16).

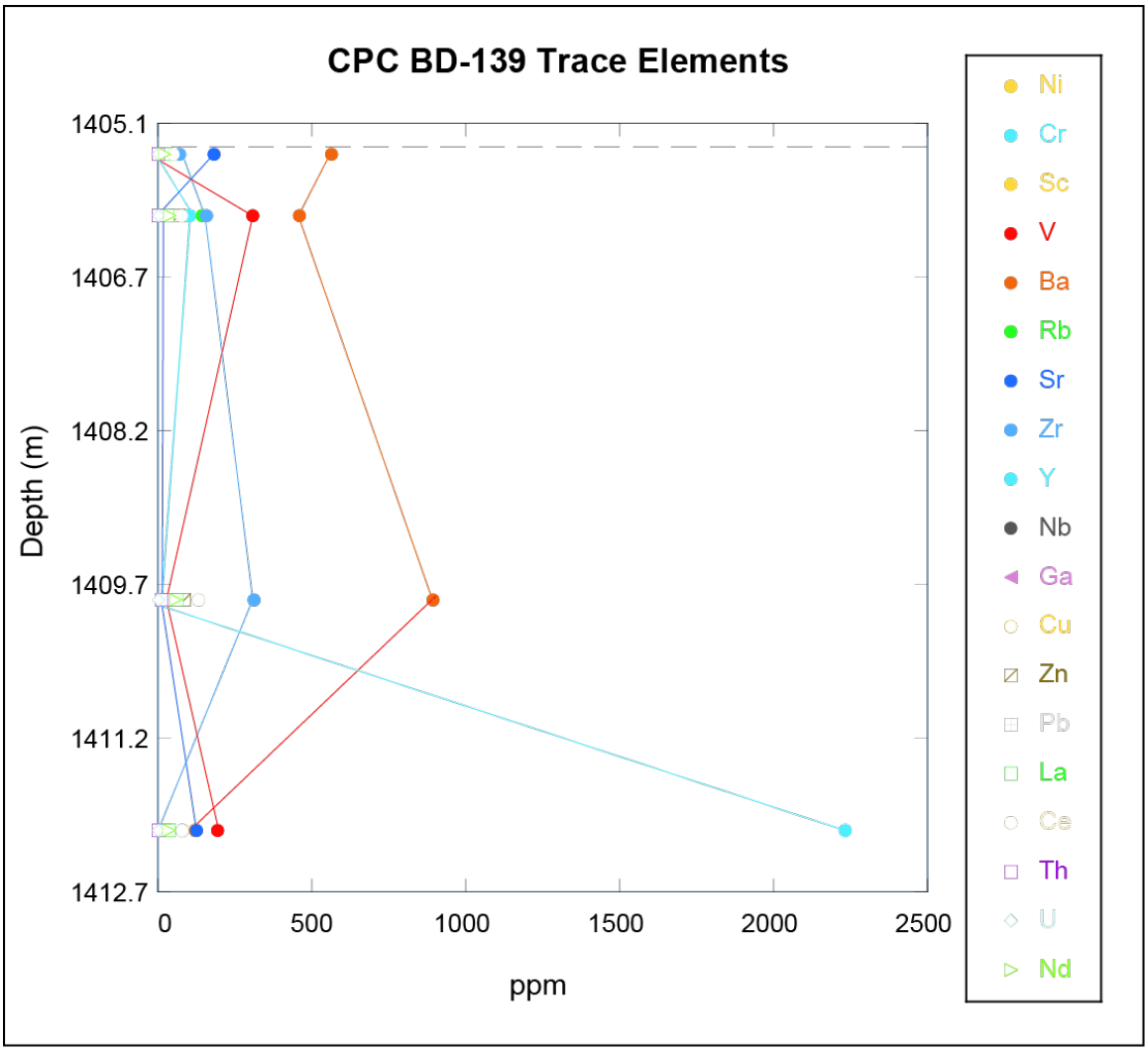

Figure 16: Whole rock geochemical data for all trace element concentrations of the basement samples from the CPC BD-139 core. The depth of the contact is indicated by the gray dashed line. See Appendix D for raw data.

Three calcite veins of sampleable size were identified in thin section and analyzed for oxygen stable isotope values in order to investigate possible source fluids of mineralization using oxygen thermometry. The $\delta^{18}O_{SMOW}$ values for the 3 veins range from 19.23 to 23.93‰ (Table 2).

Table 2: Oxygen stable isotope ratios for vein samples from the CPC BD-139 core. Calibrated data is precise to ±0.01‰.

Sample	**description**	**$\delta^{18}O$‰ (SMOW)**	**$\delta^{18}O$‰ (VPDB)**
CPC-4611A	calcite/anhydrite stringer vein	23.07	-7.60
CPC-4623	rimmed calcite vein	19.23	-11.33
CPC-4630.5	calcite vein perpendicular to fabric	23.93	-6.77

4.1.5 CPC BD-151

A mesoscopic description of the CPC BD-151 core was provided by James P. Evans (Figure 17, Appendix A). The basal meter of the Mt. Simon Sandstone is a very tight, pinkish-tan sandstone with fine-scale laminae, possibly carbonate-cemented, with possible evidence for bioturbation or soft sediment deformation. This gives way to sub-horizontally laminated gneiss that is especially weathered at the contact (~1434.39 m depth) (Figure 17). The weathered gneiss at the contact is a 7-10 cm thick, tightly layered green gneiss. Below this lies about 3 meters of weathered pink and green gneiss with a granulite texture. A sub vertical alteration zone cross-cuts the older gneissic fabric at 1437.44 m depth. This lithology gives way to a hornblende-feldspar-quartz gneiss with 0.5-2 cm banding and horizontal to sub-horizontal mineralized and partly mineralized fractures, which continues through the bottom of the logged section (Figure 17).

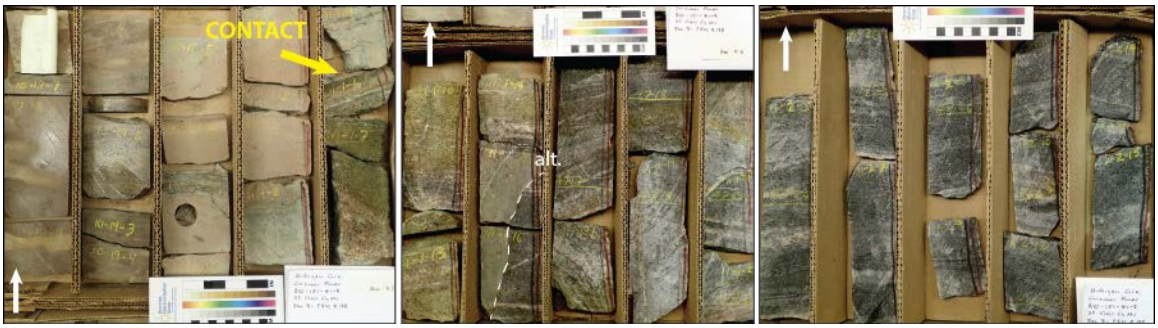

Figure 17: Core photos of the CPC BD-151 core. The contact is at ~1434.39 meters depth, and is indicated by the yellow arrow. White arrows indicate up direction. Note sub-vertical alteration cross-cutting gneissic fabric. Core is 7.6 cm in diameter.

Legacy data acquired by Maness Petroleum Laboratories and stored in well files at the Michigan repository provided brine injection step permeability tests for 2 depths, and borehole porosity and permeability data for the CPC BD-151 core (Appendix A). Permeability and porosity data extends through the basal Mt. Simon Sandstone, truncating at the contact. Porosity in the sandstone fluctuates between about 2-5%, with high (10-15%) porosity zones at 1400 and 1418 meters. Porosity spikes to about 18% at the contact (1434 m), before dropping to about 4% directly below, however, data ends at 1435 meters (Figure 18). Permeability consistently fluctuates between $<10^{-17}$ to 10^{-13} m^{-2} for the ~36 meters of data we were provided, however, permeability peaks appear to be more frequent above 1420 meters (Figure 19). High permeability zones exist at ~1412 m, 1420 m, 1425 m, 1429 m, and at the contact (1434 m) (Figure 19). Values below 10^{-17} m^{-2} were likely not registered by the measuring device at the time of data collection, therefore data points that register at 10^{-17} m^{-2} may have the potential to be even lower. Step permeability tests were done at 1428.90 m and 1432.87 m, in the lowermost sedimentary rocks (Figure 20), by injecting brine (1.21 g/cc, 0.6 pH, 2.244 cp) and 15% HCl (1.233 cp and 1.068 g/cc at 70º F). Both fluids were injected in 5 mL intervals. Overall permeability is highest in the shallower sandstone. Permeability stays fairly constant with brine injection at both depths,

whereas acid injection causes an increase in permeability, particularly in the shallower test (Figure 20).

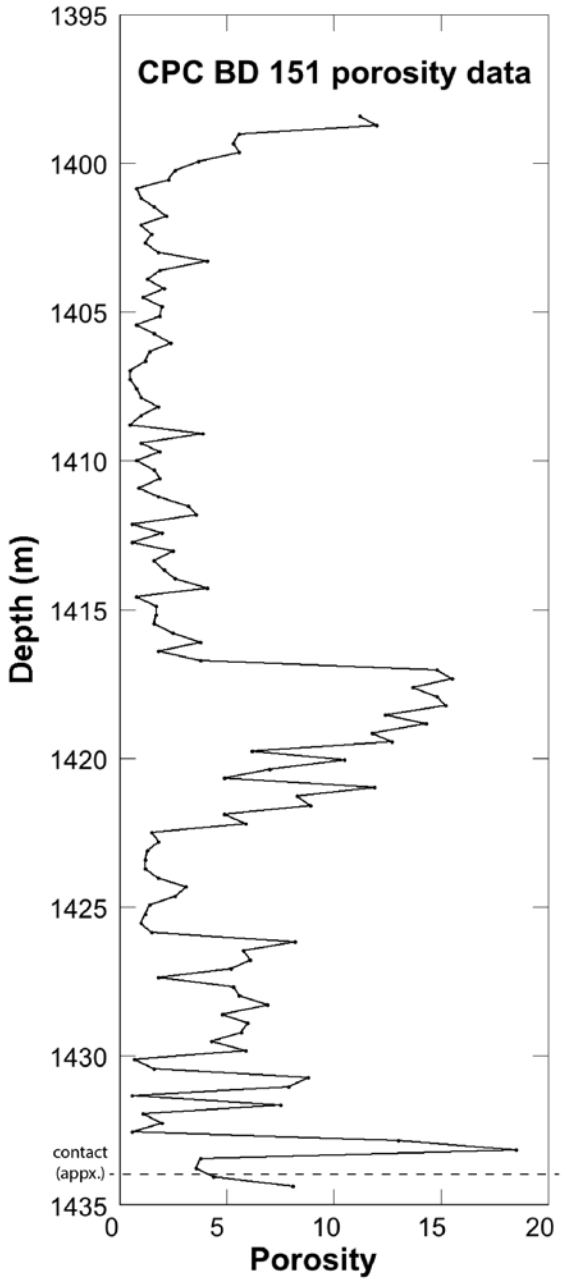

Figure 18: Legacy porosity data for the CPC BD-151 core, gathered by Maness Petroleum Laboratories. Porosity in the sandstone fluctuates between 2-5%, with higher (10-15%) zones at 1400 meters and 1418 meters. Porosity is highest at the contact (1434 meters).

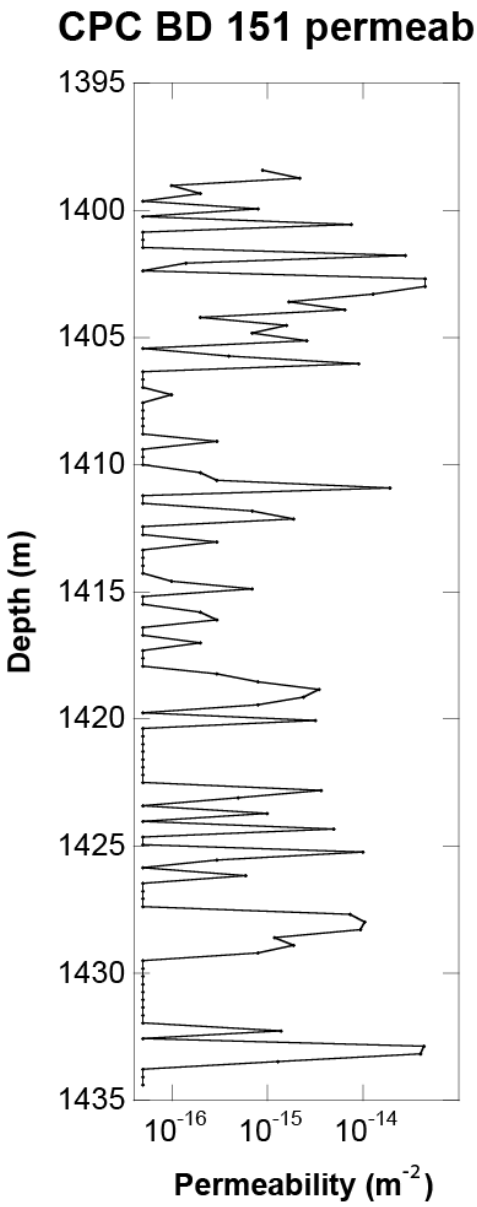

Figure 19: Legacy permeability data for the CPC BD-151 core, gathered by Maness Petroleum Laboratories. Values consistently fluctuate between $<10^{-17}$ to 10^{-13} m^{-2} throughout the 36 meters for which data were provided. Peaks are more frequent above 1420 meters. Permeability peaks to 10^{-13} m^{-2} at the contact (1434 m). Values aligning to 10^{-17} m^{-2} likely represent the lowest measurable permeability of the measuring device.

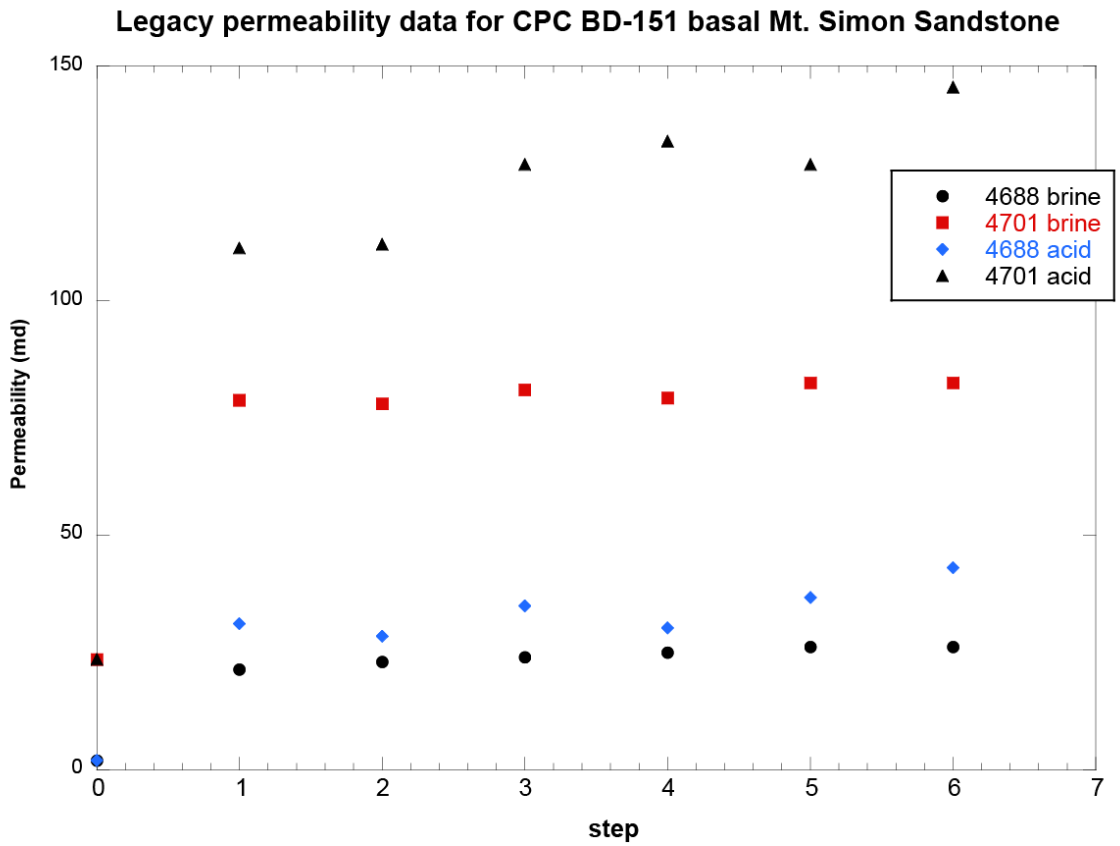

Figure 20: Legacy step permeability tests for brine and acid injection into basal sedimentary rocks at two depths in the CPC BD-151 core, gathered by Maness Petroleum Laboratories. Permeability stays fairly constant with brine injection, and increases slightly with acid injection. Permeability for brine and acid injection is highest in the shallower sandstone.

4.2 UPH-1 Borehole

A total of 16 samples over a depth of 20.5 meters were obtained from the UPH-1 core. Sample numbers reflect the depth (in feet) at which samples were taken.

4.2.1 Mesoscopic Description

The logged section of the UPH-1 core is comprised of 15 meters of Mt. Simon Sandstone and 7.9 meters of Precambrian granite (Figure 21, Appendix A). The Mt. Simon Sandstone here is tan and purple, cross-bedded, medium-grained, and well sorted, grading into an interbedded red

and green siltstone at around 600 meters depth (Figure 22). The interbedded siltstone is 5 meters thick, and grades over a short distance into an interbedded grus and siltstone layer (Figure 22). The interbedded grus layer is 2.8 meters thick, is friable and clay-rich, contains sub-angular granite clasts (>1-3 cm in diameter), and lies sharply in contact with Precambrian granite (Figure 22).

The Precambrian granite in this logged section is a pink, coarse-grained granite with no faults and few fractures (Figure 22). Clay alteration of feldspar appears to be weakly present at the contact (Figure 22), and is absent with depth.

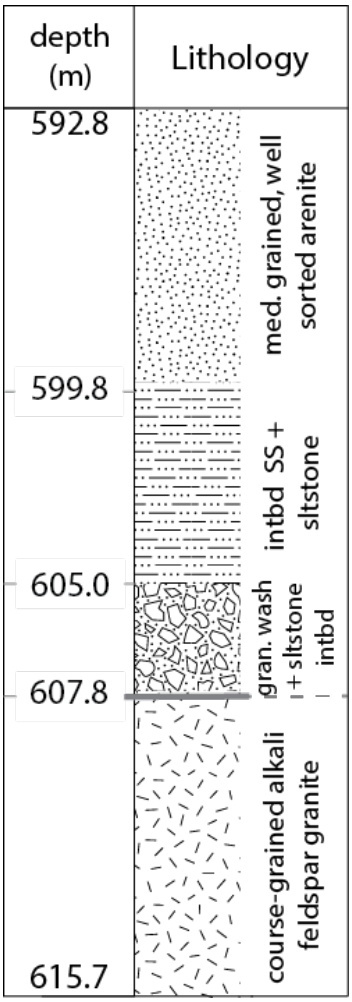

Figure 21: Generalized core log for the UPH-1 core, showing dominant lithologies from the logged section. Five major lithologies were identified and described at the UPH-1 core in Mt. Horeb, Wisconsin (sandstone, siltstone, granitic wash, weathered basement, fresh basement).

Figure 22: Core photos for the UPH-1 core from 593-616 m depth, in Mt. Horeb, Wisconsin. White arrows indicate up direction. White dashed line indicates location of contact (607.8 meters). Core is 3" in diameter.

4.2.2 Petrographic Analysis

A total of 7 thin sections from the UPH-1 core were analyzed (Appendix B). Two thin sections of the sandstone lithofacies of the Mt. Simon Sandstone reveal rounded to sub-rounded, well sorted, medium to coarse quartz grains cemented by quartz. Blue epoxy on these samples reveals a porosity of 8-12% (Figure 23a). One thin section of the siltstone lithofacies reveals sub-rounded to sub-angular, well sorted, very fine quartz cemented quartz grains, and a porosity of >3% (Figure 23b). The grus horizon consists of gravel-sized, sub-angular to sub-rounded, quartz and clay-altered feldspar grains in a poorly sorted very fine to coarse-grained matrix with clay cement (Figure 23c).

Thin sections of Precambrian granite reveal a coarse-grained alkali feldspar granite. Clay alteration of feldspar grains occurs at the contact, and appears to decrease with depth. Quartz and feldspar grains contain abundant microfractures, typically filled with clay, which are less

abundant with depth over a range of ~5 meters (Figure 23 d, e). Clay alteration of grains, interstitial clay, and clay-filled fractures are often accompanied by a relative increase in porosity.

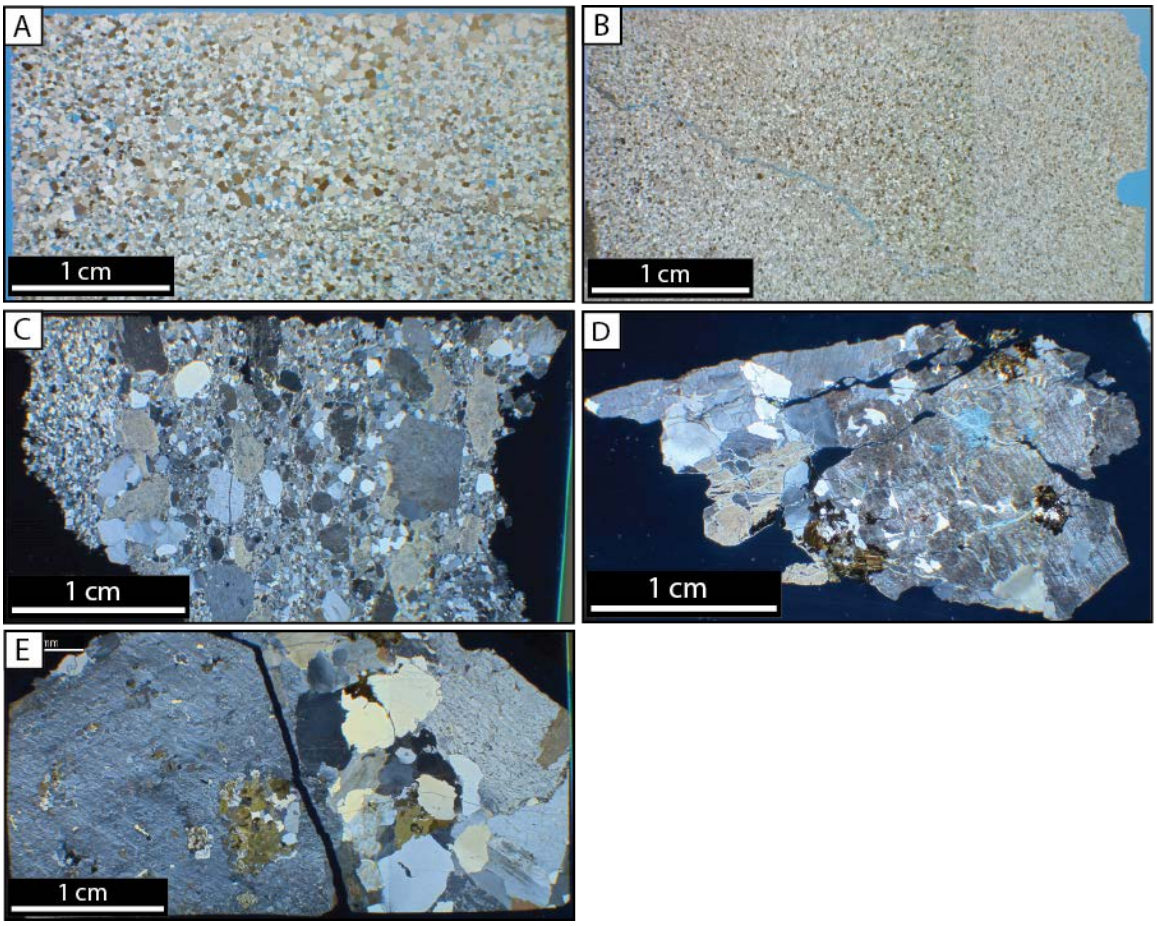

Figure 23: Photomicrographs of thin sections from the UPH-1 core, representative of the 5 main lithologies captured by the logged section. (A) Sample 1962.4, representative Mt. Simon Sandstone. (B) Sample 1973.8, silty Mt. Simon Sandstone. (C) Sample 1994A, grus horizon directly at the contact containing interstitial clay and clay-altered feldspar grains. (D) Sample 1994B, clay-altered alkali granite directly at the contact. Note increase in porosity (blue patches) in altered feldspar grains and along microfractures, relative to surrounding host. (E) Sample 2013.2, representative unweathered alkali granite host rock, 5.8 meters below the contact.

4.2.3 Mineralogical Analysis

X-ray diffraction (XRD) analyses on 14 of the 17 samples from the UPH-1 core (Table 3, Appendix C) shows that the Mt. Simon Sandstone primarily consists of quartz with minor

amounts of feldspar and illite, and trace amounts of glauconite and iron oxide. Nontronite (the Fe-rich end member of the smectite clay mineral group) is a major mineral component within 6 meters above the contact. The basement rocks directly at the contact are primarily quartz and feldspar with trace palygorskite and ankerite. The slightly altered basement consists mainly of quartz, minor feldspar and nontronite, and traces of biotite. Unaltered host granite consists mainly of quartz and feldspar (albite, microcline, anorthite), with minor amounts of biotite and/or phlogopite (Table 3).

Table 3: Interpretation of XRD results for samples from the UPH-1 core. Green indicates a major mineral phase (PANalytical X'Pert Highscore score of 0.5 or higher), yellow indicates a minor mineral phase (score of 0.1-0.5), and orange indicates a trace mineral phase (score of <0.1). Abbreviations of mineral name is present where applicable.

LITHOLOGY	SAMPLE ID	qtz	feldspar	clays	micas	carbonates	oxides
MT. SIMON	1943.5						
	1945.5			illite			
	1946						
	1962.4						
	1963.8			illite			Fe3O4
	1967				glauc.		
	1971						
	1971.5				musc.		rutile
	1973.8			nont.			SrFeMoOx
	1986.5			nont.	musc.		
BASEMENT	1994B			paly.		ank.	
	1997			nont.	bt		
	1998.5				bt		
	2013.2				phlogo.		

4.2.4 Geochemical Analysis

Major and trace element whole rock analyses were run on 3 samples from the UPH-1 core, capturing the geochemical makeup of the unaltered sandstone, grus, and unaltered basement lithologies (Appendix D). The grus is depleted in SiO_2 with respect to the unaltered sandstone,

and enriched in Al_2O_3 and K_2O with respect to the unaltered sandstone (Figure 24). The grus is slightly enriched in FeO with respect to the unaltered sandstone. The unaltered basement is primarily composed of SiO_2 (71.73 wt%), Al_2O_3 (14.07 wt%), and K_2O (7.00 wt%) (Figure 24). The unaltered basement is also slightly enriched in Na_2O, FeO, and CaO relative to the grus and unaltered sandstone (Figure 24).

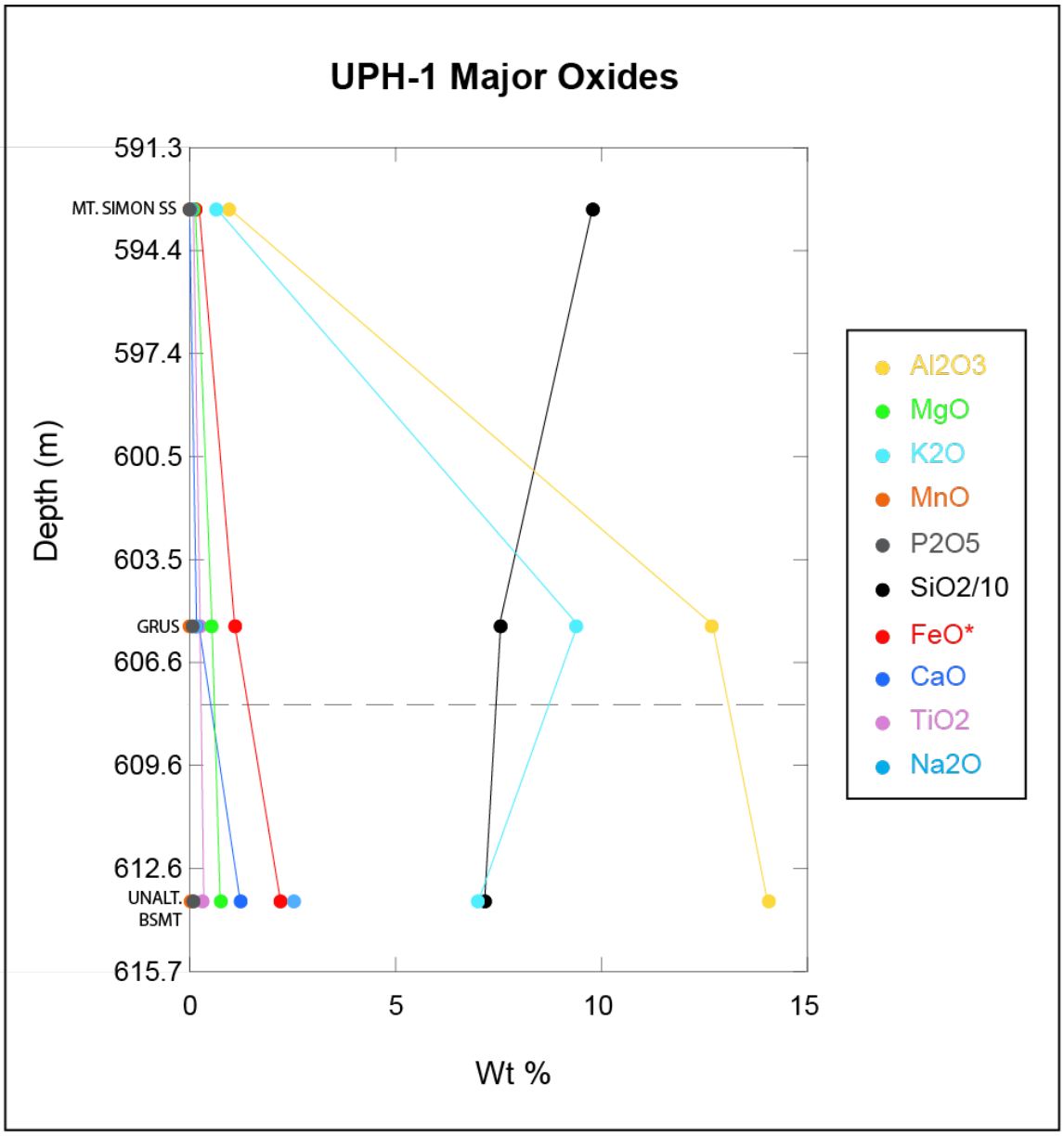

Figure 24: Whole rock geochemical data for all major oxides from samples from the UPH-1 core. The depth of the contact is indicated by the gray dashed line. See Appendix D for raw data.

Zirconium, barium, strontium, and rubidium are the primary trace elements constituents in the three analyzed samples (Figure 25, Appendix D). The unaltered sandstone contains 1216 ppm zirconium. All other trace elements fall below 15 ppm (Figure 25). The grus sample is enriched in barium, zirconium, rubidium, and strontium, and depleted in zirconium, with respect

to the unaltered sandstone. The unaltered basement sample is enriched in barium relative to the grus and the unaltered sandstone. Unaltered basement is slightly enriched in rubidium, strontium, and zirconium, relative to the grus (Figure 25).

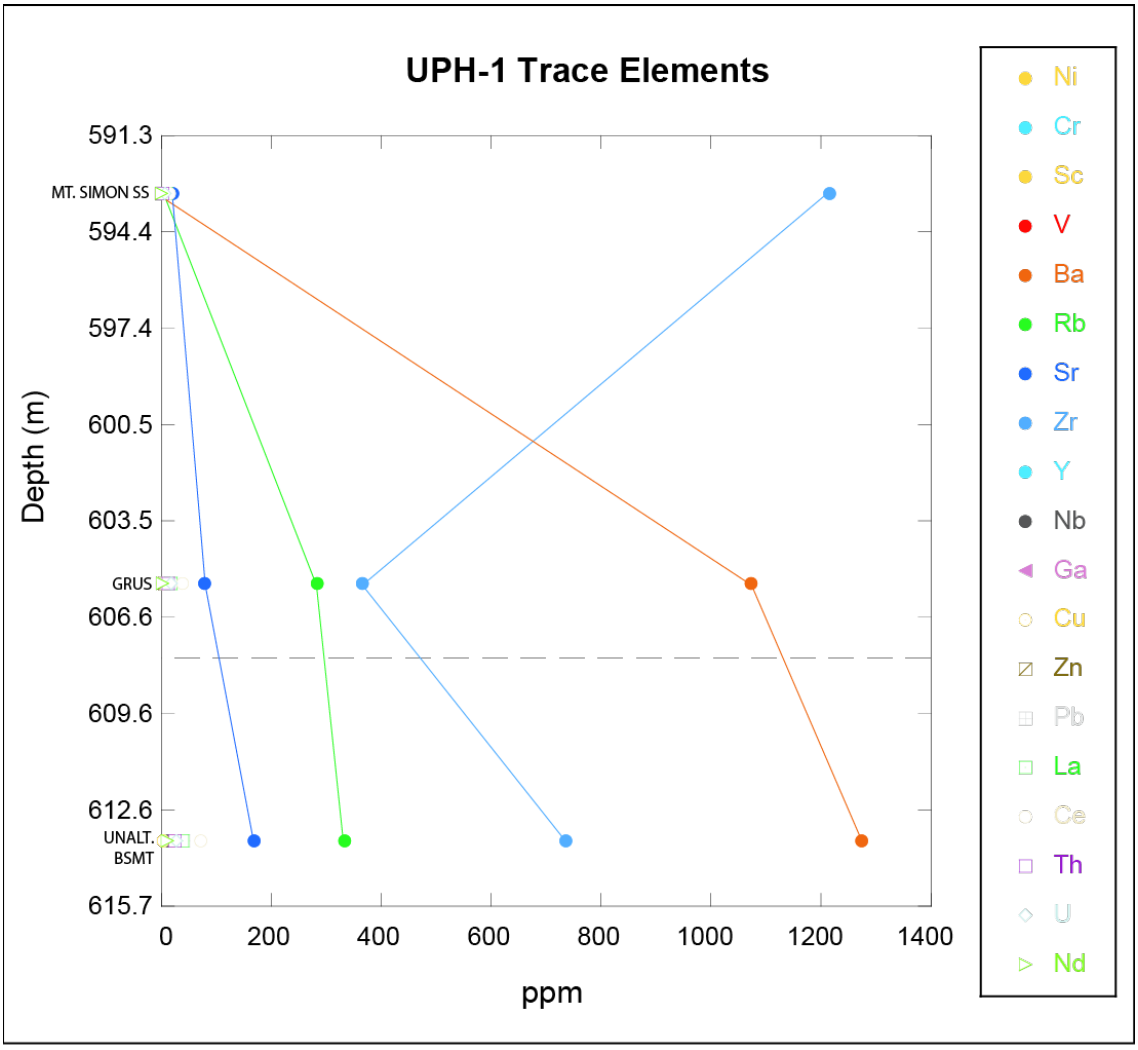

Figure 25: Whole rock geochemical data for all trace element concentrations in the samples from the UPH-1 core. The depth of the contact is indicated by the gray dashed line. See Appendix D for raw data.

4.3 Marquette, Michigan

4.3.1 Mesoscopic Description

The Marquette locality provided 2 sites in which the nonconformity zone is exposed in outcrop on two types of crystalline rock. At Hidden Beach, the nonconformity is only barely exposed for less than a meter, however, the overlying Neoproterozoic Jacobsville Sandstone is exposed for about 25 meters, and continuous exposures of the uppermost basement rocks are present for about 1 km. Other exposures were examined from sea kayak on Little Presque Isle (J.P. Evans, pers. comm., 2015) and also reported in Hamblin (1958). Patches of exposed contact at Hidden Beach and on Little Presque Isle reveal that the basal Jacobsville Sandstone is interbedded with a cemented conglomerate consisting of sub-angular to rounded jasperoid, gneiss, and greenstone clasts (Figure 26a). The overlying Jacobsville Sandstone contains vertical fractures with bleached horizons 15-90 cm wide (Figure 26b). The bleached horizons are only in the Jacobsville Sandstone, and tend to be associated with sub-vertical fractures and bedding planes. In some cases, fractures truncate at the basal conglomerate (Figure 26a). Local relief on the nonconformity at Little Presque Isle is around 5-10 meters, and epidote-iron oxide coated faults and fractures roughly align with the bleached fracture zones in the Jacobsville Sandstone (Figure 26c). The Compeau Creek Gneiss, with septa of the Mona Schist, underlies the Jacobsville at this site (Gair and Thaden, 1968b). Exposed surfaces appear fairly fresh due erosive processes occurring at the lake shore. Thin (>1-4 cm) linear veins consist of quartz, and in some cases, epidote. Small displacement (3-12cm) faults in the Compeau Creek Gneiss are epidote or quartz filled (Figure 26d). No faults were observed in the Jacobsville Sandstone.

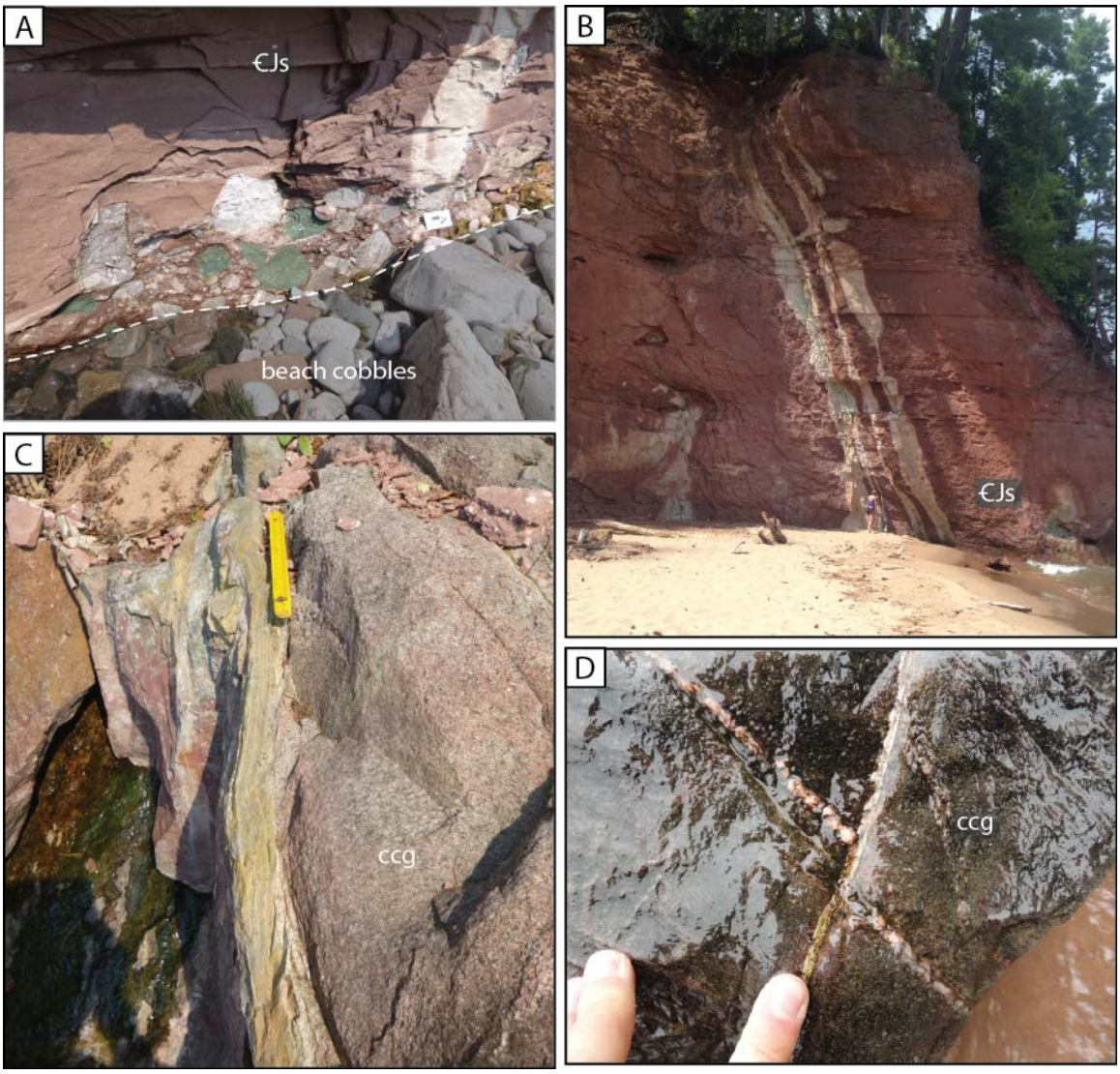

Figure 26: Outcrop photos of Hidden Beach and Little Presque Isle, Marquette, Michigan. (A) The Jacobsville Sandstone basal conglomerate. Note sub-vertical bleach fracture truncating at conglomerate layer. 15x18 cm field card for scale. (B) Bleached sub-vertical fractures in the Jacobsville Sandstone. Note person (1.68 m) for scale. (C) Epidote-iron oxide coated fault in the Compeau Creek Gneiss. These basement-hosted faults often align with the overlying bleached vertical fractures in the Jacobsville Sandstone. Yellow ruler (10 cm) for scale. (D) Epidote-coated small displacement fault offsetting a quartz vein in the Compeau Creek Gneiss. Offset is ~1 cm.

The Presque Isle site provides ~1 kilometer of exposed nonconformity, though the overlying Jacobsville Sandstone is commonly eroded away due to erosive lake shore processes. The contact is sinuous and has a topographic variation of ~2.5 meters over a span of 1100 meters

(Figure 27). The Jacobsville Sandstone here exhibits bleaching patterns that reflect zones of higher permeability (i.e. bedding planes, fractures) similar to that seen at Hidden Beach (Figure 28a). Iron oxide and/or clay alteration of the Jacobsville Sandstone is common (Figure 28b). The basal Jacobsville Sandstone contains tight, cohesive conglomerates and friable, incohesive basal conglomerate units, primarily consisting of jasperoid clasts, with some quartz, feldspar, and sandstone clasts (Figure 28a). The conglomerate exists as lenses and layers that vary laterally in thickness from 5 to 100 cm. Some conglomerate layers lie directly in contact with the serpentinized peridotite basement rock, whereas in other places, a layer of Jacobsville Sandstone lies between the conglomerate and serpentinized peridotite (Figure 28a,b, c). In some areas a regolith horizon up to 1 meter thick exists at the top of the basement (Figure 28d). The serpentinized peridotite basement rocks at this site range from black to red, with white web-like stockwork vein patterns (Figure 28e, f). Veins are often filled with jasperoid mineralization and are up to 10 cm thick (Figure 28f). The texture of the serpentinized peridotite ranges from crumbly and incompetent to moderately cohesive rock. Near-vertical fractures often exist in both the Jacobsville Sandstone and the serpentinized peridotite, although fracture density is often lower in the serpentinized peridotite, and fractures do not seem to bisect the contact. In some cases, fractures in the sedimentary rock truncate at the basal conglomerate layer and at the contact (Figure 29). The various geometric relationships between the Jacobsville Sandstone, conglomerate unit(s), regolith, basement rock, faults, and fractures, are documented through a series of lithologic columns in Figure 29. Normal, oblique, and strike-slip faults at Presque Isle are primarily basement-hosted. Areas that captured a full vertical section through the contact with faults are rare, however, we observed basement-hosted normal and oblique faults truncating at the contact, and a normal fault bisecting the contact (Figure 30). Three of the four faults observed at Presque Isle are associated with iron-oxide mineralization. The one faulted site that did not contain significant iron-oxide mineralization bisects the contact and basal conglomerate,

appearing as a silica-rich vein with a lozenge-like structure in the basement, on which slip surfaces were observed. This vein pinches out into the basal conglomerate, extending as an unmineralized, planar fault surface (Figure 30a). Slip surfaces on 4 faults observed at Presque Isle range in thickness from (<1-15mm).

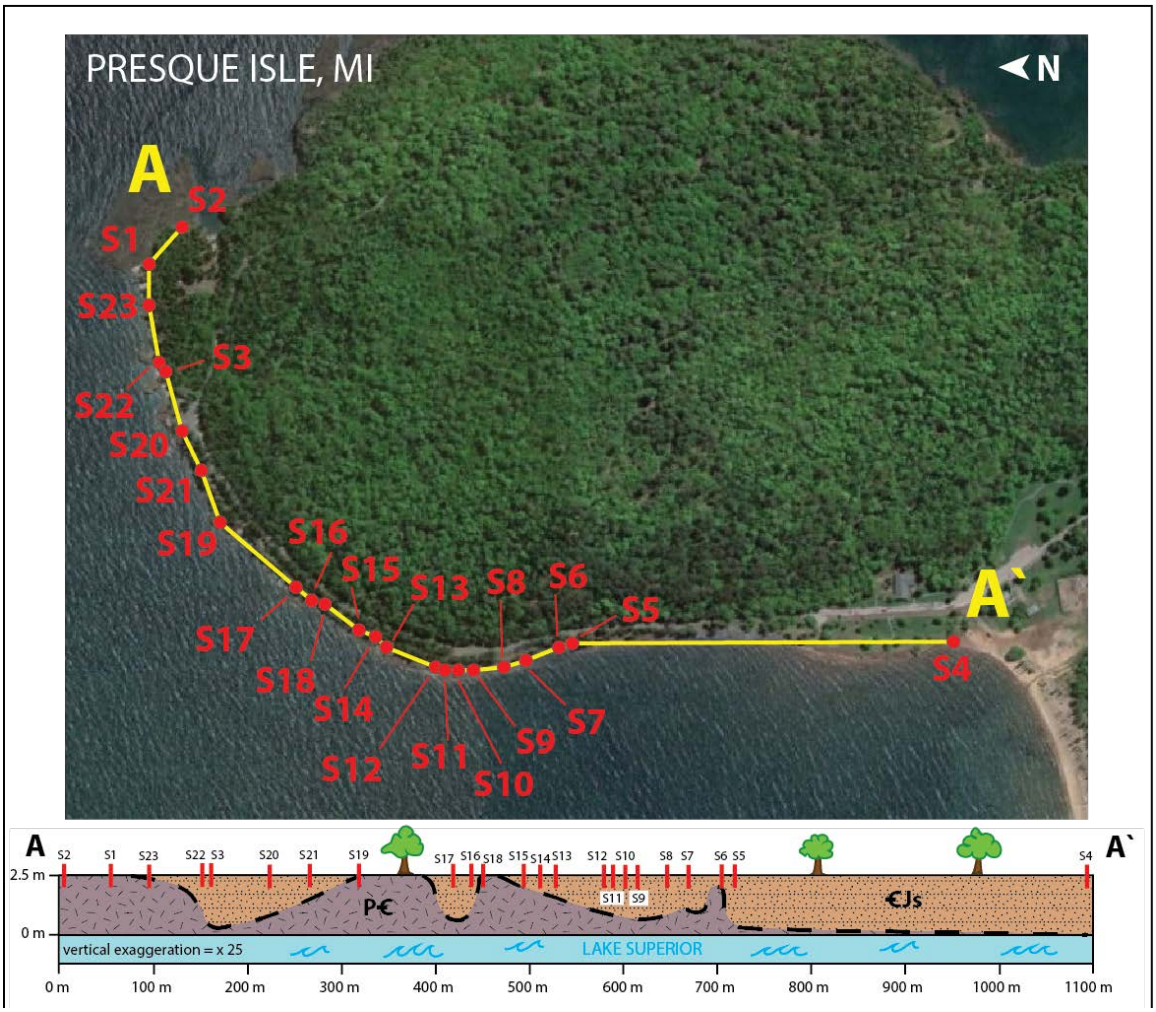

Figure 27: Topographic variation of the contact at Presque Isle was mapped using litho-stratigraphic profiles measured at each station (location of station indicated by red vertical line). The nonconformity along the ENE shore of Presque Isle varies vertically by 2.5 meters over a distance of 1100 meters.

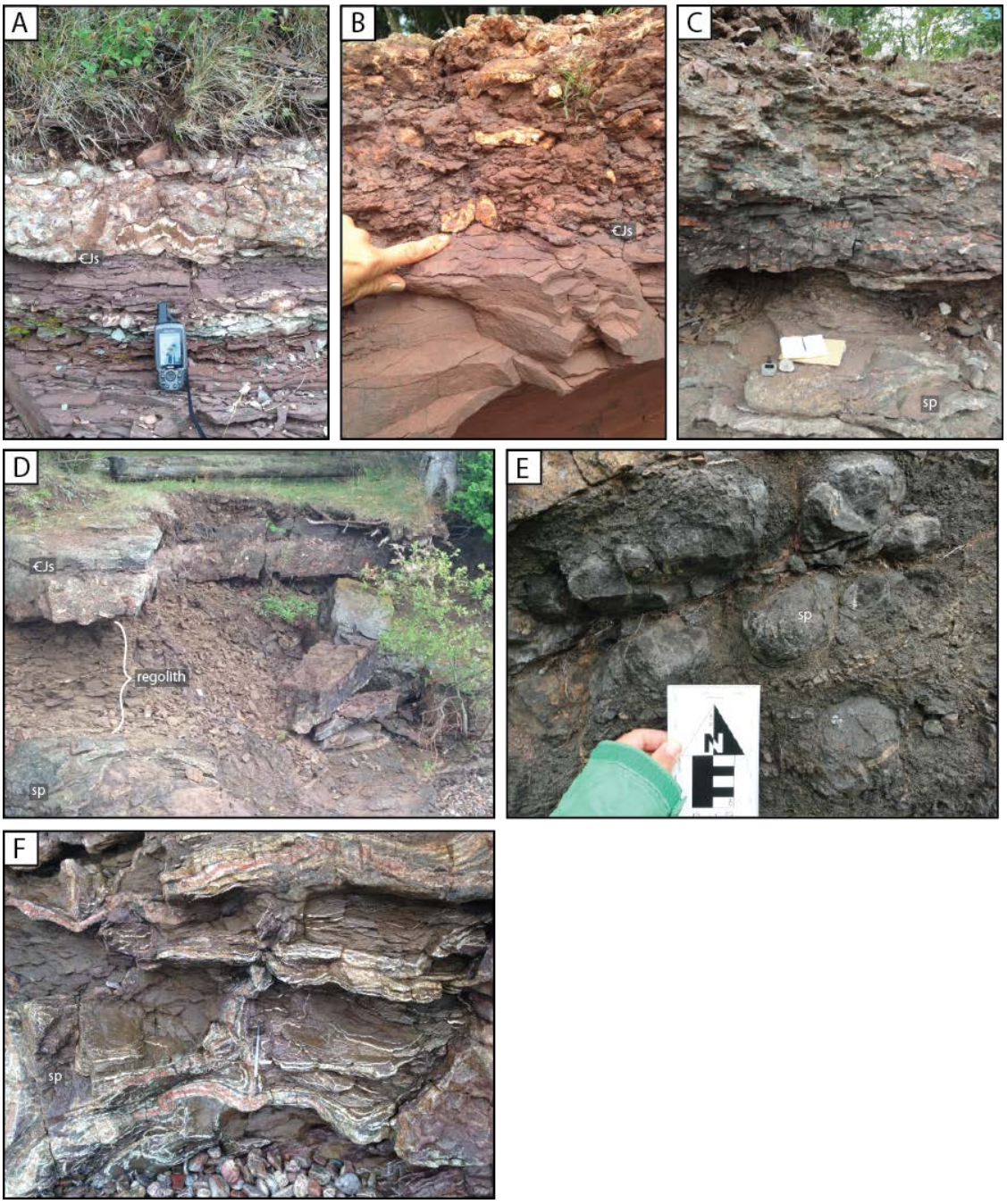

Figure 28: Outcrop photos of nonconformity exposures at Presque Isle, Marquette, Michigan. (A) Mineralized conglomerate in the Jacobsville Sandstone primarily consisting of jasperoid clasts. Note reduction along bedding planes. GPS (6x16 cm) for scale. (B) Significant iron oxide mineralization in the Jacobsville Sandstone and basal conglomerate unit. Hand for scale. (C) The basal conglomerate unit in the Jacobsville Sandstone lying directly in contact with serpentinized peridotite basement rocks. Compass (8x8 cm) for scale. (D) Regolith horizon (~80 cm thick) above the serpentinized peridotite at the contact. (E) Spheroidal weathering pattern in the serpentinized peridotite. Field card (15x8 cm) for scale. (F) Stockwork veining patterns and thick (<10cm) jasperoid veins in the serpentinized peridotite. Pen (15 cm) for scale.

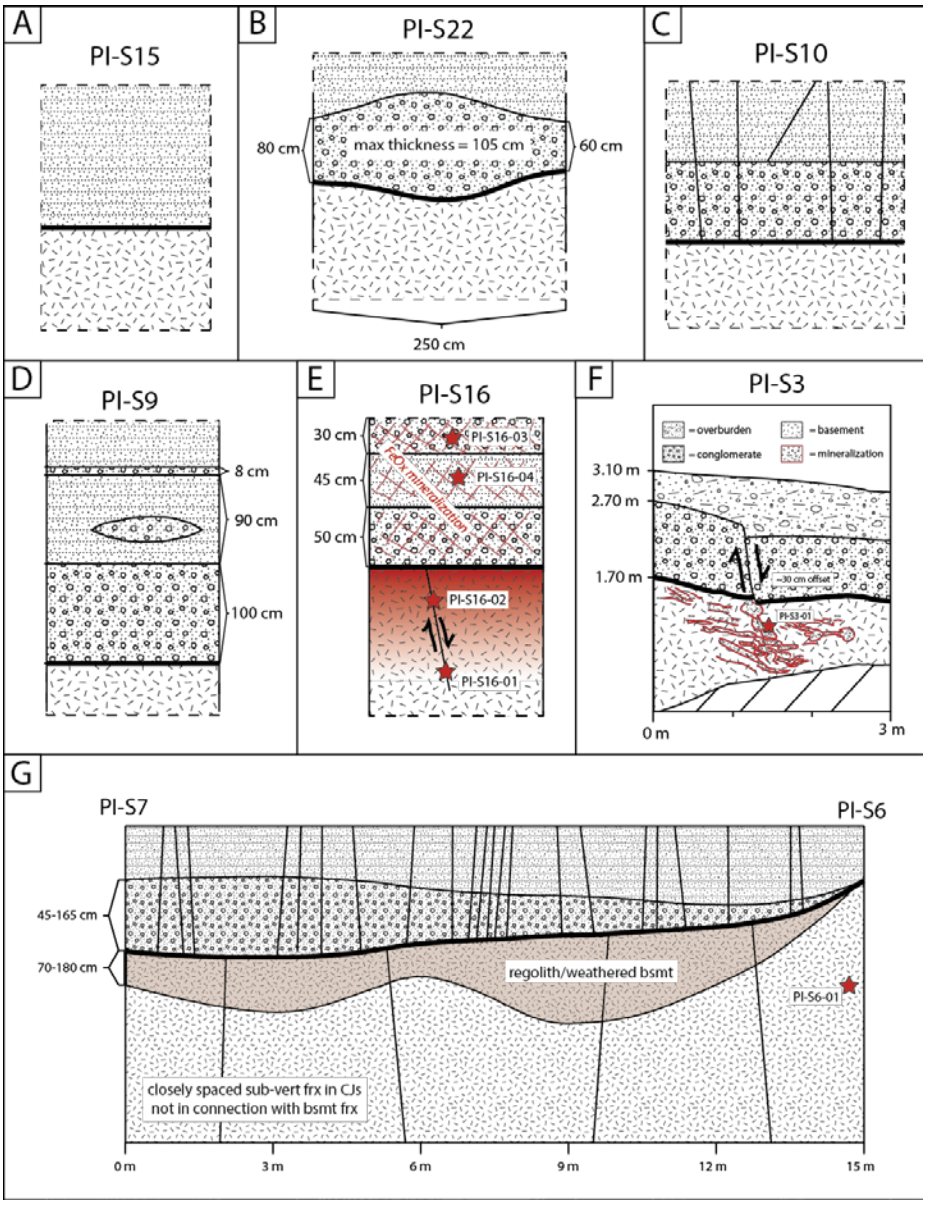

Figure 29: Litho-stratigraphic columns constructed from nonconformity exposures at Presque Isle, Marquette, Michigan. (A) Sharp contact between The Jacobsville Sandstone and serpentinized peridotite, faults and conglomerate absent. (B) Conglomerate horizon of varying thicknesses in contact with serpentinized peridotite, faults absent. (C) Conglomerate horizon in contact with serpentinized peridotite, fractures in the Jacobsville Sandstone truncating at basement, and at the conglomerate. (D) Variable distribution of conglomerate horizon in the Jacobsville Sandstone, including lenses and layers of variable thickness. (E) Fe-mineralization is concentrated in the Jacobsville Sandstone, and decreases with depth from the contact in the basement. Red stars indicate sample locations. Normal fault truncates at the contact. (F) Normal fault bisecting the contact. Fault appears as a silica-rich vein with a lozenge-like structure in the basement rocks. (G) Regolith at the top of the basement and basal conglomerate laterally pinching out. Fractures exist in the Jacobsville Sandstone and the basement, and are not in connection.

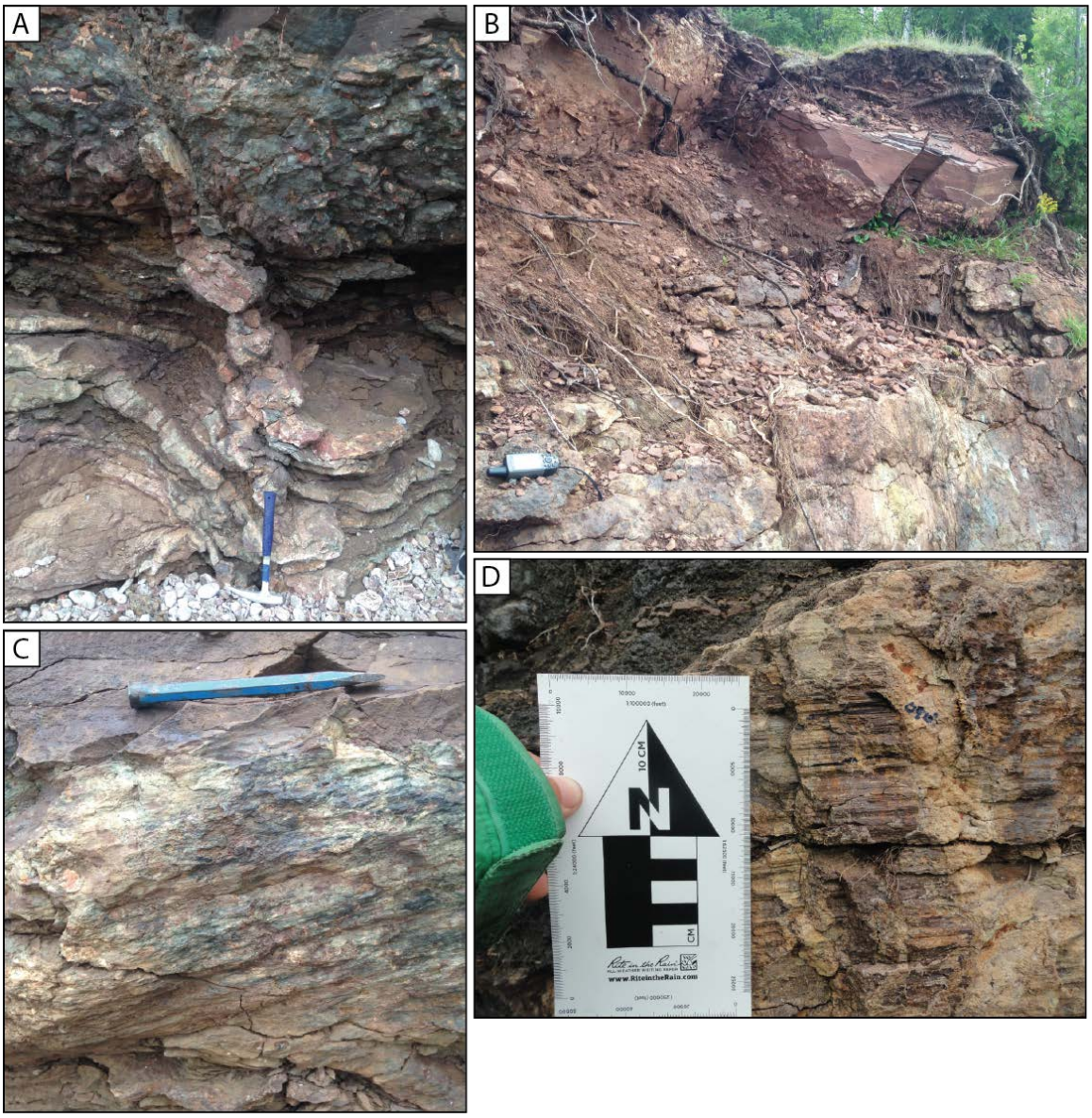

Figure 30: Field photographs of basement-hosted faults at Presque Isle, Marquette, Michigan. (A) Normal fault bisecting the contact and the basal conglomerate in the Jacobsville Sandstone. This fault presents itself as a silica-rich vein with a lozenge-like structure in the basement, which partially extend up into the offset mineralized conglomerate layer. Rock hammer (28 cm tall) for scale. (B) Dip-slip fault surface truncating at the contact. GPS (6x15 cm) for scale. (C) Oblique fault slip surface in serpentinized peridotite. Chisel (15 cm) for scale. (D) Mineralized strike-slip fault surface in darker, relatively less competent serpentinized peridotite. Tan mineralization is 1-1.5cm thick. Field card (15x8 cm) for scale.

4.3.2 Petrographic Analysis

Four thin sections from the Hidden Beach site and 17 thin sections from the Presque Isle site were analyzed (Appendix B). The Jacobsville Sandstone consists of fine-grained, angular, moderately sorted quartz and feldspar grains. A thin section capturing the transition from red sandstone protolith to a bleached horizon adjacent to a fracture at Hidden Beach reveals little change in texture and composition, and a reduction in hematite grain coatings and interstitial infilling from the red to the bleached sandstone (Figure 31a).

Incohesive conglomerates consist of rounded gravel- to small pebble-sized clasts of quartz and feldspar cemented by clay, hematite, and calcite (Figure 31b). Clasts are often rimmed by void-space, and some clasts appear altered (Figure 31b). Calcite cement is either sparry or amorphous (Figure 31c). Thin sections of the mineralized, competent conglomerate reveal little porosity, and dominantly consist of chalcedony in a fine-grained, poorly sorted, angular quartz grains in hematite cement. Clasts of the serpentinized peridotite basement host rock are rare but present (Figure 31d).

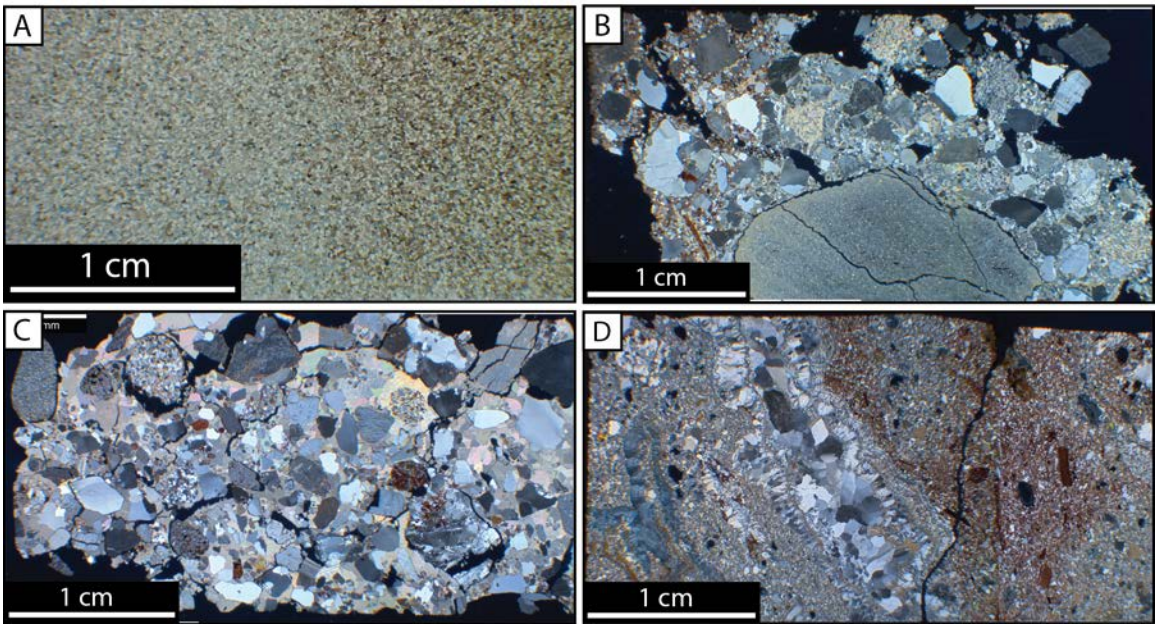

Figure 31: Photomicrographs of thin sections of the Jacobsville Sandstone and basal conglomerate, from Hidden Beach and Presque Isle, Marquette, Michigan. (A) Sample WET-5, transition between the bleached Jacobsville Sandstone (left) and the unbleached Jacobsville Sandstone host (right). (B) Sample WET-A, incohesive basal conglomerate. Note thin void space surrounding large clast, and slight alteration around rim of large clast. (C) Sample HB-S4-01, sparry calcite-cemented conglomerate. (D) Sample PI-S5-04, cohesive, fine-grained conglomerate consisting of quartz grains and Jacobsville Sandstone pebbles.

Thin sections of the serpentinized peridotite from Presque Isle host reveal a variable lithology of the basement rocks. Very altered, incohesive serpentinized peridotite samples consist of thin, stringy stockwork-textured dolomite veins in a matrix of relatively high (3-5%) porosity hematite-replaced serpentine, with small amounts of magnetite (Figure 32a). The more cohesive basement lithology consists mainly of patchy dolomite and recrystallized quartz with some hematite and magnetite. Veins are thin (>1-2 mm) and consist of fine-grained dolomite (Figure 32b). Thicker basement-hosted veins consist of both silica and calcite or dolomite. Silica veins are characterized by recrystallized amorphous quartz crystals or fibrous chalcedony crystals oriented perpendicular to vein boundaries. Calcite or dolomite veins crosscut the silica veins (Figure 32c). Calcite veins hosted in intact serpentine basement protolith can exhibit a fibrous texture in which parallel, straight-edged crystals have grown perpendicular to the vein orientation,

similar to the textures observed in calcite beef (Cobbold et al., 2013). These fibrous vein textures are also incorporated into crack-seal vein textures (Figure 32d).

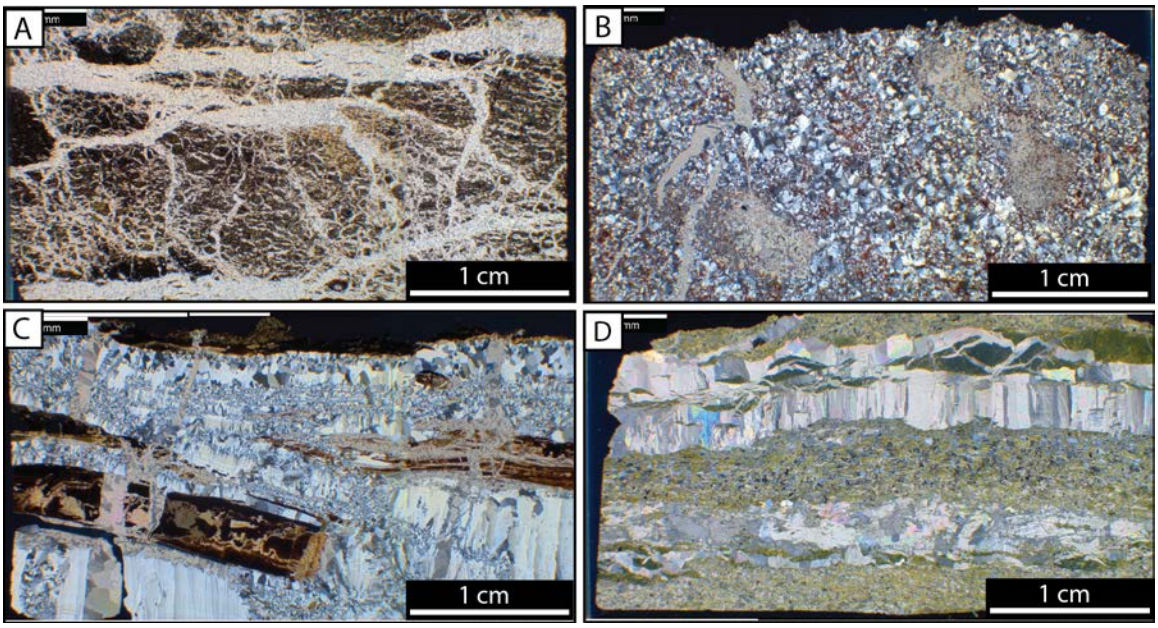

Figure 32: Photomicrographs of serpentinized peridotite host rock and veins from Presque Isle, Marquette, Michigan. (A) Sample PI-4, stockwork- to mesh-vein textures are observed in incohesive serpentinized peridotite. Veins are composed of dolomite, and host is highly altered and Fe-rich. (B) Sample PI-S5-01, cohesive, mineralized, serpentinized peridotite. Matrix is dominantly patchy fine-grained amorphous dolomite, iron oxide, and recrystallized quartz. Fine-grained dolomite veins cross-cut the matrix. (C) Sample PI-vein, chalcedony, dolomite, and calcite veins in serpentinized peridotite host. Calcite veins are oriented perpendicular to, and offset by, dolomite and chalcedony veins. (D) Sample CG-host, crack-seal and fibrous beef-like calcite veins in a relatively unaltered serpentinized peridotite host.

Six different types of basement-hosted slip surfaces from the Presque Isle serpentinized peridotite are seen in thin section (Figure 33). No slip surfaces from Hidden Beach were observed in thin section. Calcite slip surfaces are common, and are typically thick (2-20 m). Crystal texture ranges from coarse massive aggregates to fibrous crystals oriented perpendicular to slip. Shear along the slip surface is not apparent. Some calcite-rich slip surfaces contain fibrous serpentine, and show a relative increase in porosity (Figure 33a-c). Slip surfaces may also be composed of clay and radiating chalcedony oriented perpendicular to slip (Figure 33d,e).

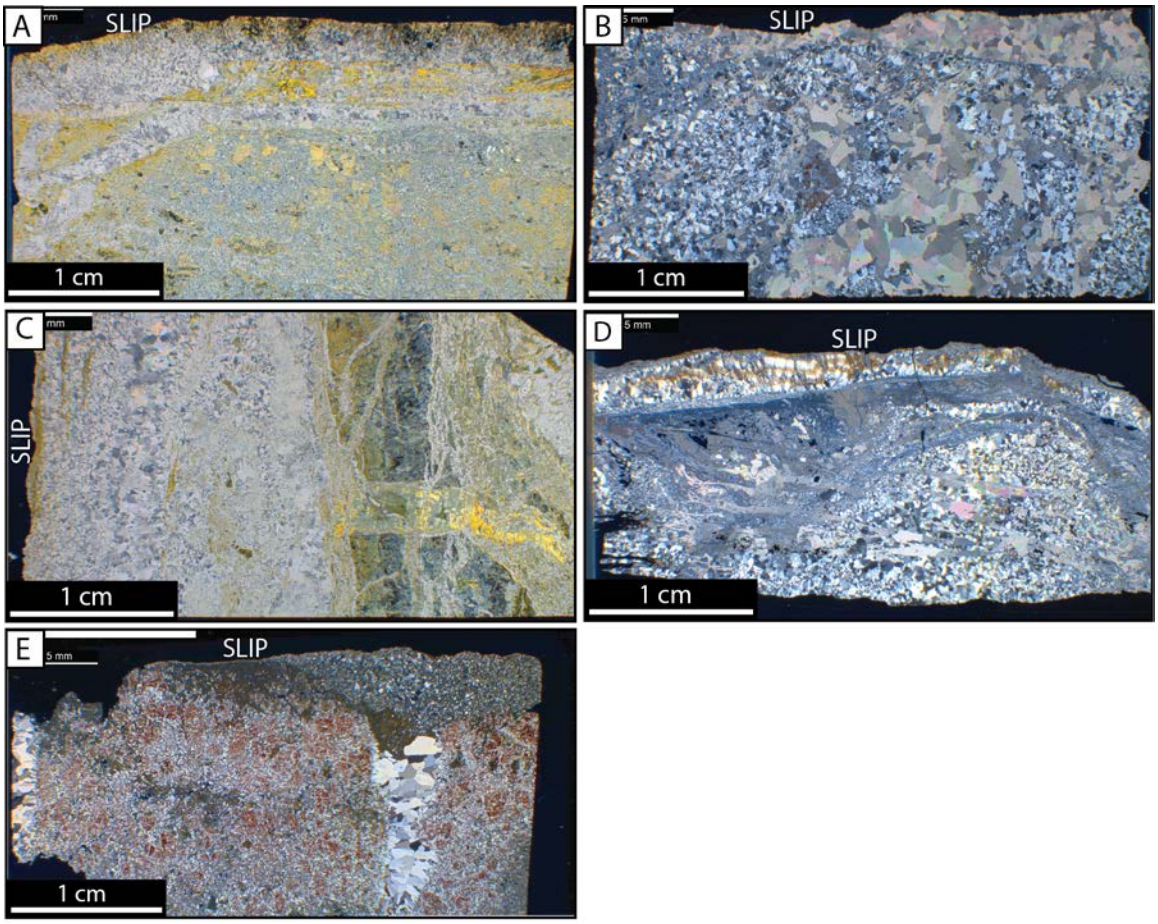

Figure 33: Photomicrographs of basement-hosted slip surfaces from Presque Isle, Marquette, Michigan. Location of slip surface is marked by word 'SLIP' in white for each microphotograph. (A) Sample PI-S2-02, calcite-rich slip surface dolomitized serpentinized peridotite. (B) Sample PI-S16-02, crystalline calcite slip surface in quartz-rich mineralized serpentinized peridotite. (C) Sample PI-S2-01a, thick calcite slip surface with anastomosing geometry in serpentinized peridotite. (D) Sample PI-S16-01, chalcedony slip surface in dolomitized serpentinized peridotite. The host rock directly beneath the slip surface is relatively porous. (E) Sample PI-S3-01, fine-grained quartz slip surface in relatively porous, Fe-rich serpentinized peridotite host. The slip surface cross-cuts a coarse-grained quartz vein.

4.3.3 Mineralogical Analysis

X-ray diffraction (XRD) analyses were done on all samples taken at the Presque Isle and Hidden Beach localities (Appendix C). The Jacobsville Sandstone is primarily composed of quartz and nontronite and trace amounts of hematite, rutile, vermiculite, zeolites, and clinochlore (Table 4). The conglomeritic basement layer consists mainly of quartz and nontronite, with trace

zeolites and iron oxide. Mineralogy of the serpentinized peridotite protolith is variable. Dolomite, serpentine minerals, quartz, iron oxide, and talc, are present in varying amounts. Dolomite and quartz are the most common major mineral phases. Lizardite, antigorite, chrysotile, iron oxide, and talc are generally minor phases. Veins within the basement rock consist of quartz, serpentine, dolomite, sepiolite, and talc. Slip surfaces are dominantly comprised of quartz with minor dolomite and trace oxides (Table 4).

Table 4: Interpretation of XRD results for samples Hidden Beach and Presque Isle, Marquette, MI. Green indicates a major mineral phase (PANalytical X'Pert Highscore score of 0.5 or higher), yellow indicates a minor mineral phase (score of 0.1-0.5), and orange indicates a trace mineral phase (score of <0.1). Abbreviations of mineral name is present where applicable.

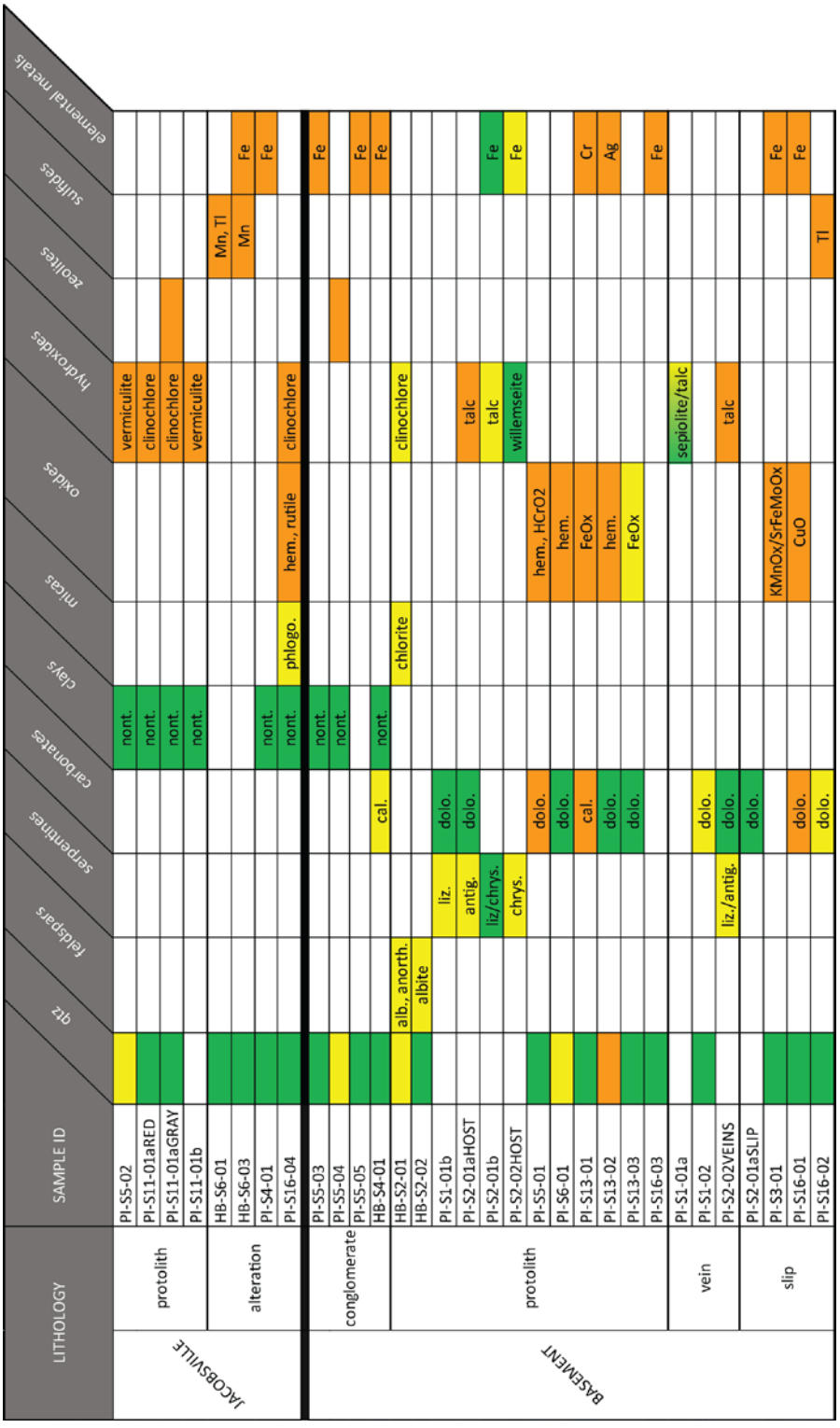

4.3.4 Geochemical Analysis

Major and trace element whole rock analyses were run on 11 samples from the Presque Isle locality (Appendix D). Sample include unaltered and altered Jacobsville Sandstone, the Jacobsville basal conglomerate, serpentinized basement host rock, basement hosted slip surfaces, and a basement hosted vein (Figure 34). The unaltered Jacobsville Sandstone is primarily composed of SiO_2 (77.9 wt%), Al_2O_3 (11.86 wt%) and K_2O (5.3 wt%). FeO (1.18 wt%) and MgO (2.58 wt%) make up a small portion of the unaltered Jacobsville Sandstone. All other major oxide constituents are >1 wt%. Alteration in the Jacobsville Sandstone appears as a minor depletion of K_2O, and a minor enrichment of FeO and MgO, relative to the unaltered Jacobsville Sandstone (Figure 34). The basal conglomerate is slightly enriched in SiO_2, and slightly depleted in Al_2O_3 and K_2O, relative to the unaltered Jacobsville Sandstone. The conglomerate also contains 1.42 wt% TiO_2; more than twice that of the unaltered and altered Jacobsville Sandstone (Figure 34). The geochemical makeup of the serpentinized peridotite basement rock is dominated by SiO_2, MgO, CaO, and FeO, however, the relative concentrations of these major oxides varies between samples. Sample PI-S2-01aHOST is dominantly composed of SiO_2 (35.6 wt%), MgO (31.5 wt%), CaO (14.78 wt%), and FeO (13.77 wt%) (Figure 34). Sample PI-S5-01 is enriched in SiO_2 and depleted in MgO, CaO, and FeO, relative to sample PI-S2-01aHOST. Sample PI-S13-02HOST is dominantly composed of SiO_2 (14.2 wt%), MgO (21.94 wt%), CaO (32.08 wt%), and FeO (24.53 wt%) (Figure 34). This sample also contains 4.78 wt% Al_2O_3. Basement hosted slip surfaces are dominantly composed of SiO_2, CaO, MgO, and FeO. PI-S2-01aSLIP is dominantly composed of CaO (51.42 wt%), MgO (31.02 wt%), and FeO (8.06 wt%), containing only 7.1 wt% SiO_2 (Figure 34). PI-S16-02 contains 62.8 wt% SiO_2, 20.72 wt% CaO, 13.39 wt% MgO, and 1.40 wt% FeO. SiO_2-enriched slip surfaces (PI-S16-01 and PI-S3-01) contain 90-93 wt% SiO_2, with low (<4 wt %) concentrations of FeO, CaO, and MgO (Figure 34). The basement hosted vein is composed of 53.76 wt% CaO, 36.16 wt% MgO, 4.56 wt% FeO, and 3.1 wt% SiO_2.

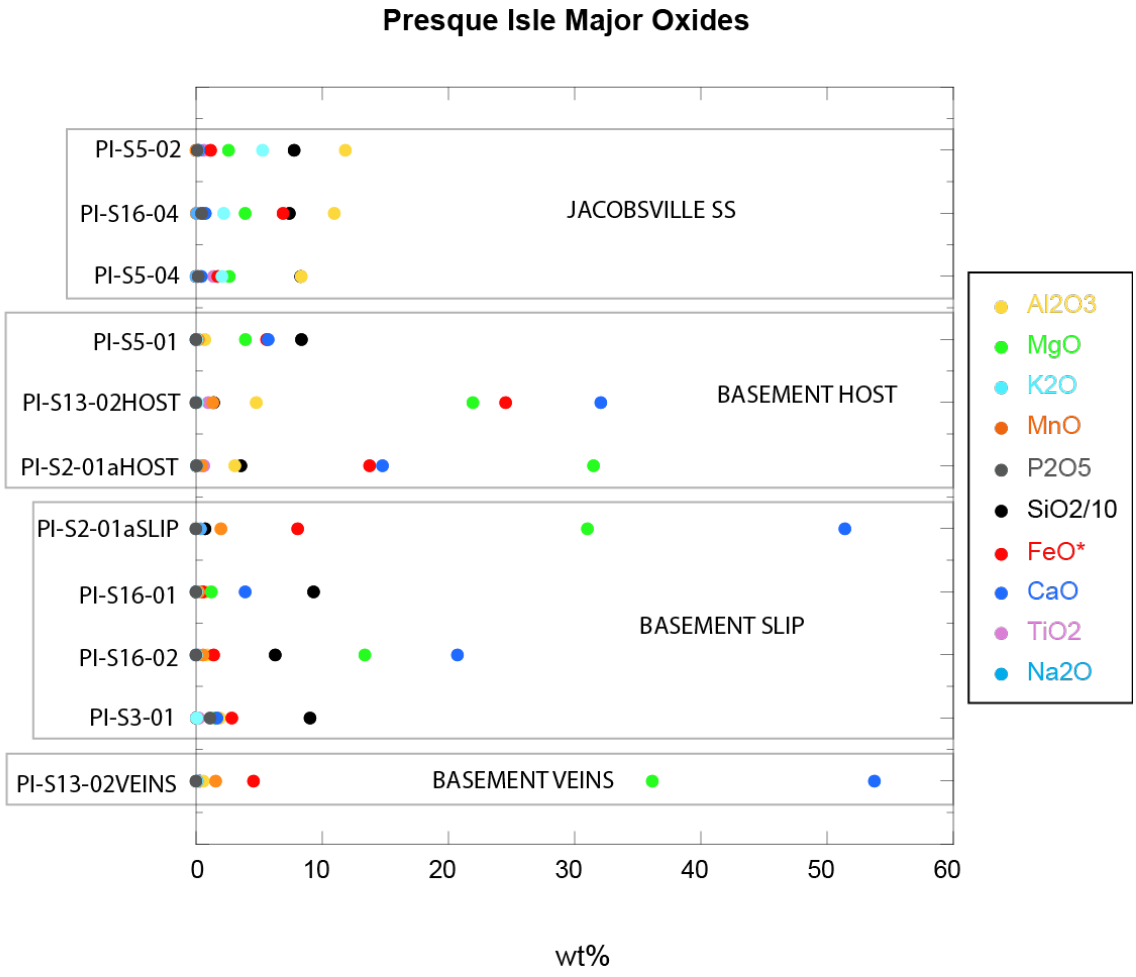

Figure 34: Whole rock geochemical data for all major oxides from samples from Presque Isle, Marquette, Michigan. Samples have been grouped by lithology or feature type. No relative depth is implied by the vertical layout presented here. See Figure 27 for sample locations. See Appendix D for raw data.

Nickel, chromium, vanadium, barium, zirconium, and copper are the main trace elements in the Jacobsville Sandstone samples (Figure 35). The altered Jacobsville Sandstone and the basal conglomerate are strongly enriched in nickel and zircon, and depleted in vanadium, barium, and copper, relative to the unaltered Jacobsville Sandstone (Figure 35). The unaltered Jacobsville Sandstone is enriched in chromium, whereas the conglomerate is depleted in chromium. Basement host samples are mainly enriched in nickel and chromium. Nickel concentrations range between 194-1154 ppm. Chromium concentrations range between 490-3370 ppm (Figure 35).

Slip surfaces are mainly enriched in nickel, chromium, and copper. Trace element concentrations in the dominantly CaO-MgO slip surface (PI-S2-01aSLIP) are low (>140 ppm) (Figure 35). In the other 3 slip surface samples, nickel concentrations range between 172-347 ppm, chromium concentrations range between 167-578 ppm, and copper concentrations range between 314-1197 ppm (Figure 35). The basement hosted vein contains 226 ppm chromium and 171 ppm nickel. All other trace element constituents in the basement hosted vein are >90 ppm (Figure 35).

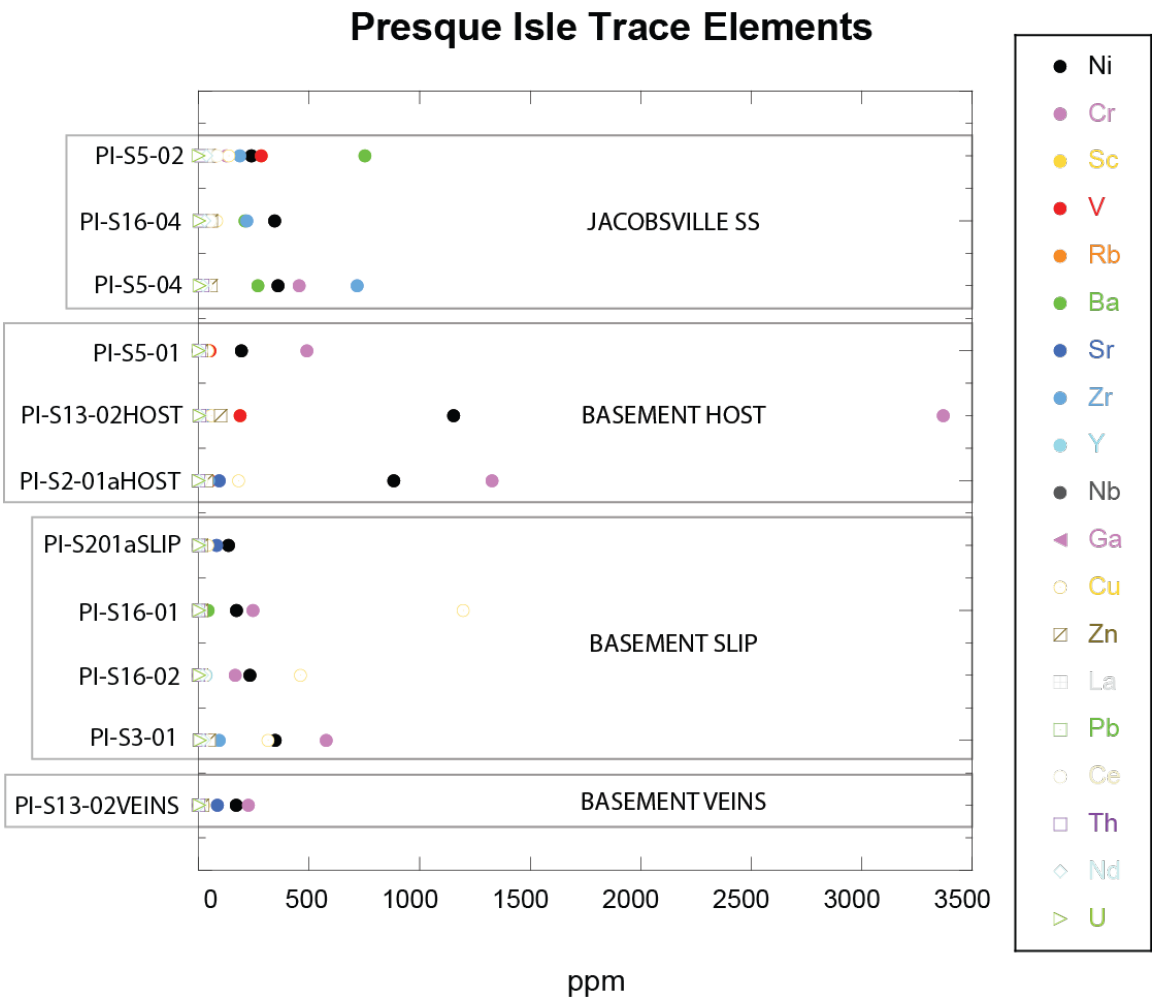

Figure 35: Whole rock geochemical data for all trace element constituents from samples from Presque Isle, Marquette, Michigan. Samples have been grouped by lithology or feature type. No relative depth is implied by the vertical layout presented here. See Appendix D for raw data.

One sample of calcite conglomerate cement from the Hidden Beach locality, and 9 calcite and dolomite veins, slip surfaces, and conglomerate cements from the Presque Isle locality, were analyzed for oxygen stable isotope ratios in order to investigate possible source fluids of mineralization using oxygen thermometry. The $\delta^{18}O_{SMOW}$ value for the Hidden Beach conglomerate cement is 20.89‰ (Table 5). Dolomite veins from Presque Isle range between 21.41 to 23.19‰. Dolomite slip surfaces from Presque Isle range between 22.18 to 23.17‰. Dolomite and calcite conglomerate cements from Presque Isle are 23.26‰ and 20.89‰, respectively. Calcite slip surfaces from Presque Isle range from 22.86 to 23.91‰ (Table 5).

Table 5: Oxygen stable isotope ratios for vein samples, slip surfaces, and conglomerate cements from samples from Presque Isle, Marquette, Michigan. Dolomite samples are indicated by a bold typeface. Blue-shaded cells indicate vein samples, orange-shaded cells indicate, slip-related samples, and purple-shaded cells indicate conglomerate-related samples. Calibrated data is precise to ±0.01‰.

Sample	Description	$\delta^{18}O$ ‰ (SMOW)	$\delta^{18}O$ ‰ (VPDB)
CG12-host	thick fibrous calcite **vein**	21.77	-8.86
PI-S2-02	calcite **vein** below slip surface	23.91	-6.79
PI-S13-01	calcite stringer **veins** below slip surf.	22.86	-7.81
PI-S16-01	calcite below slip surface	23.00	-7.68
HB-S4-01	calcite cemented conglomerate	20.89	-9.71
PI-vein	dolomite **veins** perpendicular to fabric	**21.41**	**-9.22**
PI-4	dolomite stringer **veins**	**23.19**	**-7.49**
PI-S5-01	dolomite **vein**	**22.31**	**-8.35**
PI-S2-01a	dolomite **slip** surface	**23.17**	**-7.51**
PI-S16-02	dolomite **slip** surface	**22.18**	**-8.47**
PI-3-15	fine-grained dolomite patches	**23.27**	**-7.41**

4.4 Cody, Wyoming

4.4.1 Mesoscopic Description

The Cambrian Flathead Sandstone and Precambrian granite contact west of Cody, Wyoming provides access to 40 meters of the nonconformity, and adjacent exposures of the basal

Flathead Sandstone, the uppermost section of basement rock, and a small fault that cuts the section, are also examined. An east-west trending map-scale fault that potentially cuts the worked area, and may tip out at the outcrop study site, was identified based on topographic features, areal imagery, and the observation of minor slip surfaces (Figure 36).

Figure 36: Map-scale fault in Cody, Wyoming. The orientation of the main outcrop (circled in yellow) at the Cody, Wyoming locality is roughly parallel to that of a probable fault (red). Slip on roughly E-W oriented surfaces at the main outcrop and secondary observation sites, and remote observations of probably fault gouge, indicate the presence of an E-W striking map-scale fault.

The 40 meters in map distance of contact exposed at the Cody locality is sinuous, and alteration along the contact varies laterally (Figure 37). Alteration of basement rocks is apparent at the eastern end of the exposure, decreasing to the west (Figure 37). The eastern 25 meters of the contact consists of a >5-50 cm thick weathered horizon at the top of the basement. The western 15 meters of the contact is underlain by a layer of horizontally laminated ‘granitic wash’, consisting of mostly clay and sub-rounded gravel-sized clasts of granite. The granitic wash is fairly unconsolidated in the bottom 85 cm, whereas the top 85 cm is cemented (Figure 38a,b). A

sinuous, ~30 cm thick, laminated iron oxide horizon lies below the horizontally laminated granitic wash horizon, possibly related to the mafic intrusive rocks in this portion of the exposure (Figure 38c). Near-vertical fractures bisect the contact, and sandstone- and basement-hosted fractures truncate at the contact. Small faults form in both the basement rocks and the sedimentary rocks. Sedimentary-hosted faults exhibit quartz, clay, and hematite mineralization on slip surfaces. Basement-hosted faults are typically quartz- or clay-rich, or chloritic. Faults are primarily roughly E-W oriented. One fault was found to bisect the contact (Figure 39).

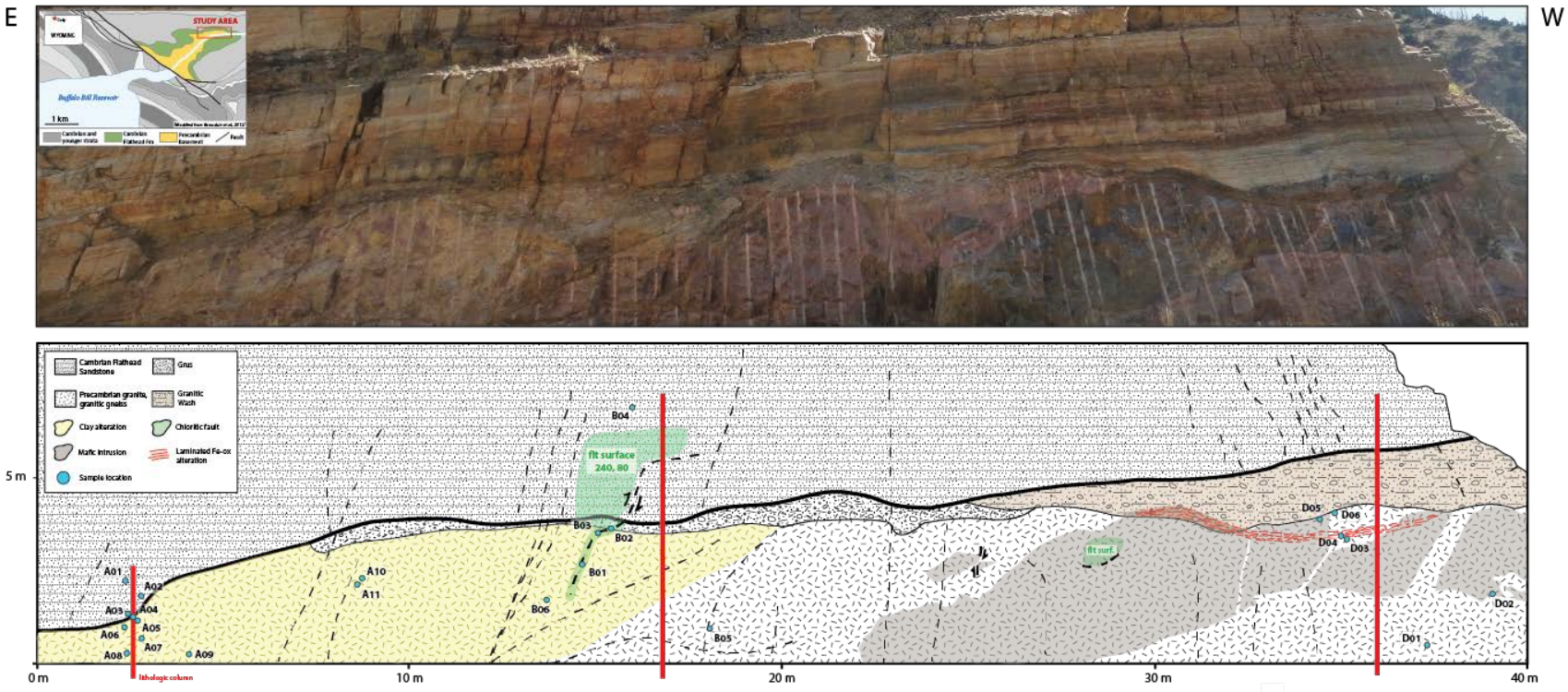

Figure 37: Field photograph and annotated tracing of the main outcrop in Cody, Wyoming. The contact between the Cambrian Flathead Sandstone and Precambrian granite and granitic gneiss is exposed in a road cut approximately 9 km west of Cody, Wyoming, in the shallow east-dipping limb of Rattlesnake Mountain. The Flathead Sandstone exhibits little alteration. Alteration is concentrated in the basement rocks along the contact, varying laterally in degree, type, and thickness. A clay alteration horizon (yellow) in the granitic basement rocks extends up to 2 meters or more below the contact in the eastern portion of the outcrop, and is sparse to absent in the western half of the outcrop. A cohesive, finely laminated 'granitic wash' horizon (tan) consisting of sub-rounded feldspar clasts in a clay-rich matrix lies directly below the contact in the western 15 meters of the outcrop. A sub-horizontal, Fe-rich, laminated alteration horizon (red streaks) cross cuts to granitic wash and uppermost portion of the basement. Fault surfaces are commonly chloritic, Fe-rich, or clay-rich.

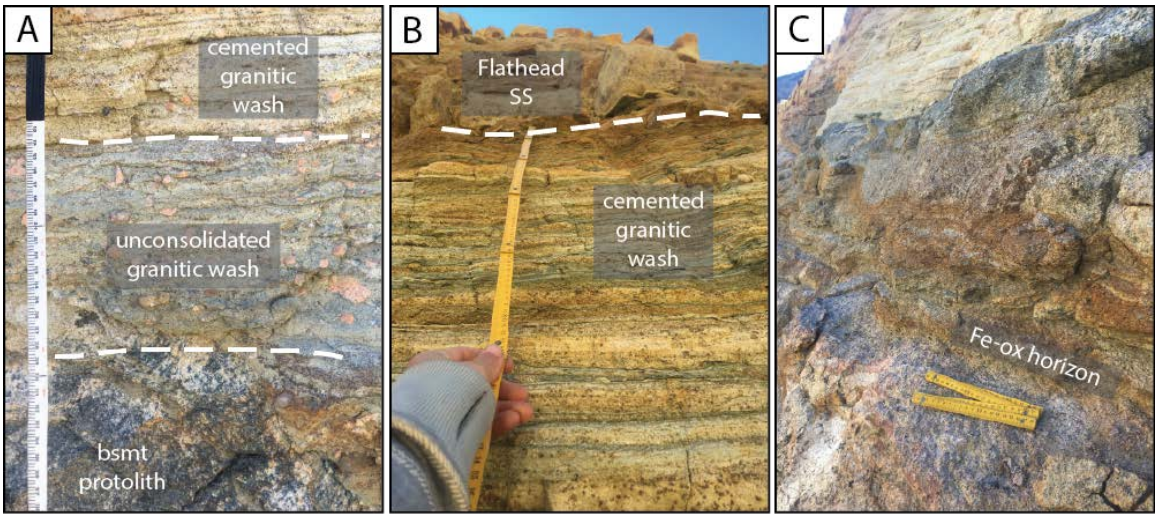

Figure 38: Field photographs from the granitic wash horizon in Cody, Wyoming. (A) Cemented and un-cemented granitic wash above mafic basement protolith. (B) Upper portion of cemented granitic wash, in contact with the Flathead Sandstone. (C) Laminated iron-oxide alteration horizon in mafic basement protolith below granitic wash horizon.

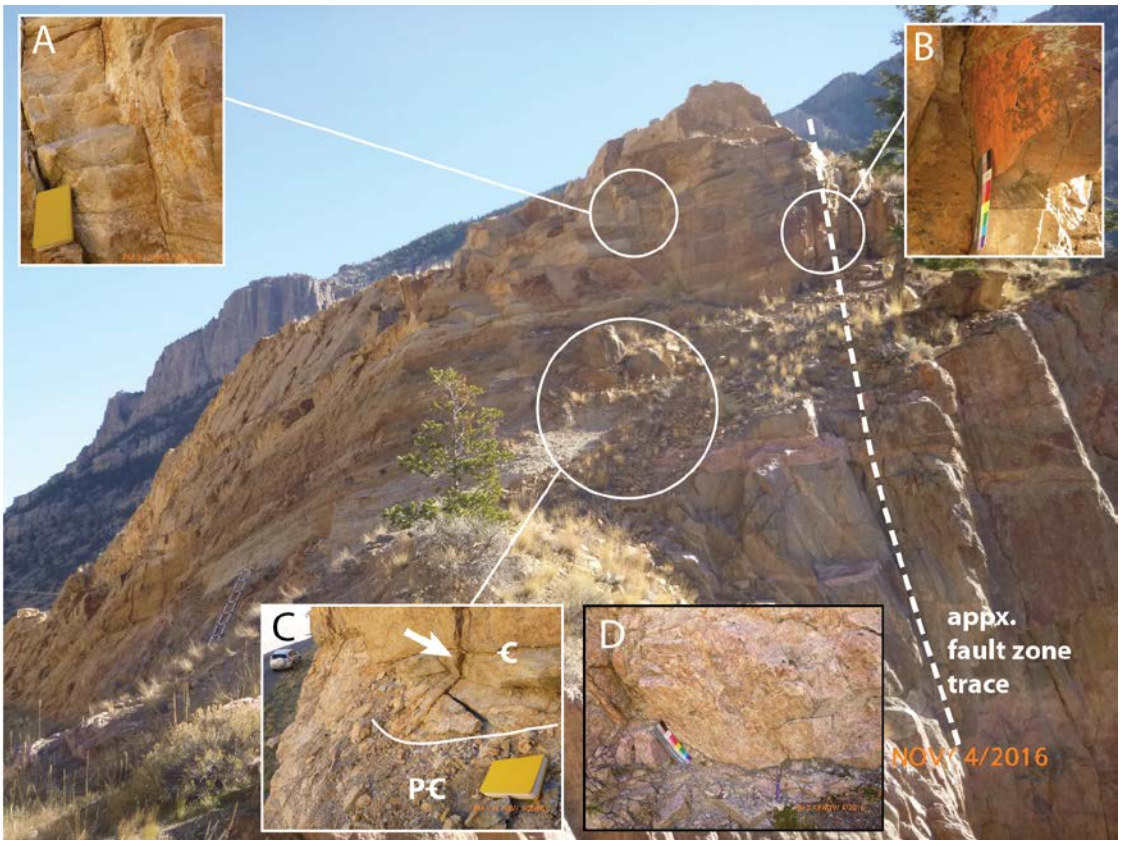

Figure 39: Outcrop photographs of basement- and sedimentary-hosted fault surfaces at the western end of the main outcrop in Cody, Wyoming. The approximate trace of the E-W oriented fault zone is indicated by the white dashed line. Faults pictured in A-D are oriented roughly along strike. Sandstone-hosted faults (A,B) contain quartz, clay, and hematite. (C) Fault (indicated by white arrow) likely bisecting contact. (D) Example of basement-hosted fault (photograph location not in this image).

4.4.2 Petrographic Analysis

A total of 13 thin section were analyzed (Appendix B). Thin sections from the Flathead Sandstone reveal an annealed quartz arenite with fine to coarse, poorly sorted, rounded to sub-rounded grains. Pore-spaces are typically filled with iron-oxide (Figure 40a). The sandstone in the deformation bands appear as silt-sized to very fine, poorly sorted, angular grains. Undeformed sandstone has an estimated porosity of around 13%, significantly decreasing within the deformation bands to <5% (Figure 40b). Thin sections capturing the unconsolidated granitic wash layer at the contact reveal brecciated angular quartz and feldspar grains within a very fine

brecciated quartz, feldspar, clay, and iron oxide matrix (Figure 40c). One thin section capturing the cemented granitic wash layer reveals moderated sorted, medium-grained, rounded quartz cemented by calcite and clay(?). Spots of iron oxide appear to form around large pore spaces (Figure 40d).

Thin sections of pink granite protolith reveal a coarse-grained alkali granite with few muscovite lathes (Figure 40e). A ~3-6mm thick mineralized fracture surface in the alkali granite consists of clay-sized to very fine grains of angular quartz and feldspar (Figure 40f). Thin sections of slip surfaces in the alkali granite reveal a protolith with clay-altered feldspar. Slip surfaces are unmineralized, and are characterized as relatively finer-grained brecciated host rock (Figure 40g). Crack-seal calcite veins from the mafic intrusive basement rock show evidence for multiple phases of fluid flow and fluctuations in fluid pressures (Ramsay, 1980). Textures within the crack-seal veins include brecciated calcite grains, sheared fibrous calcite grains (similar to calcite-beef texture), and dogtooth calcite grains (Figure 40h).

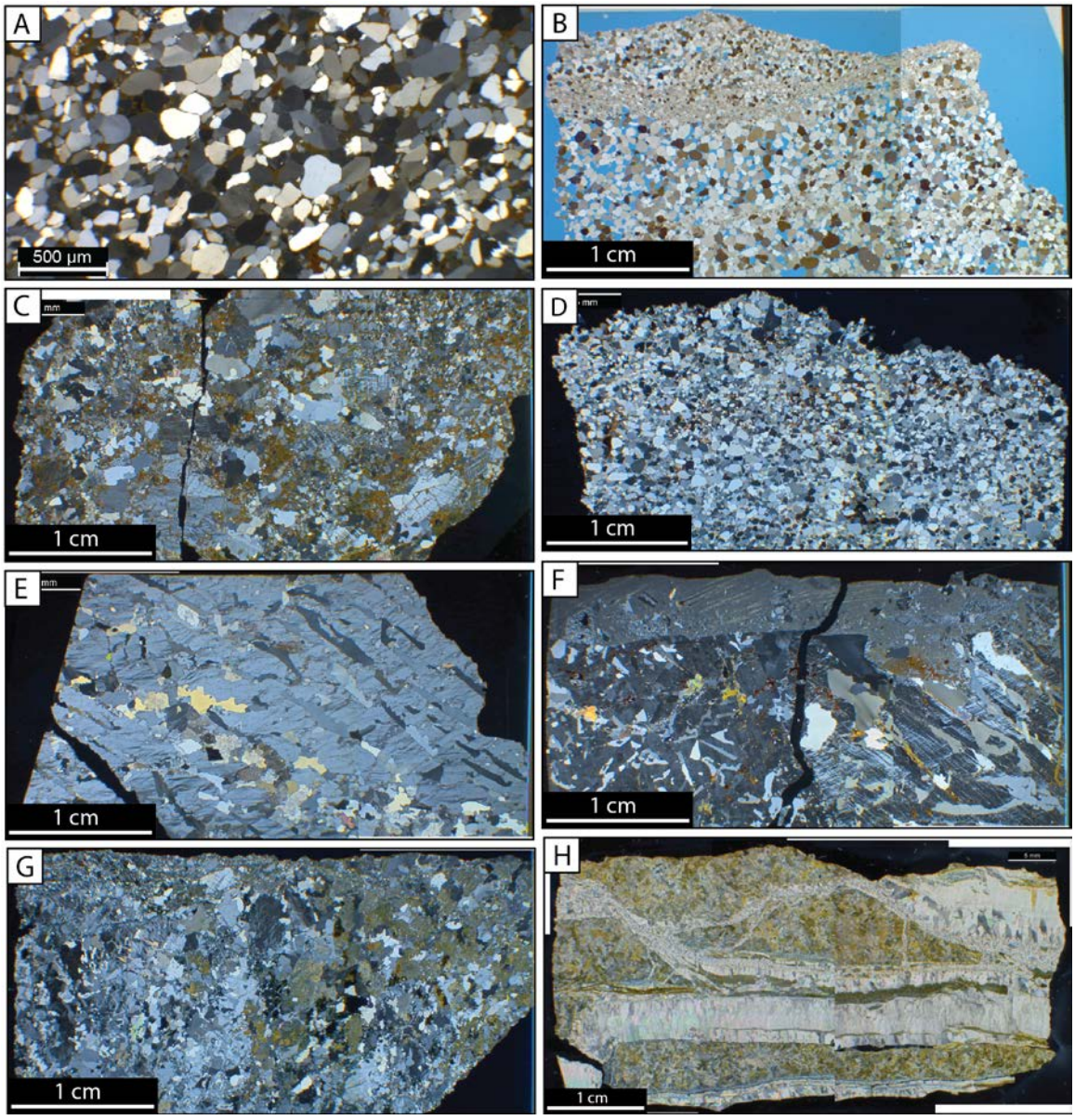

Figure 40: Photomicrographs of samples from Cody, Wyoming. (A) Sample CWY-A01, Flathead Sandstone with hematite and/or iron-rich clay filling pore spaces. (B) Sample CWY-E06, variation in porosity in the Flathead Sandstone due to reduction of grain size in deformation bands. (C) Sample CWY-A03, grus layer from eastern portion of the main outcrop, consisting of angular, brecciated quartz and feldspar grains in a clay-rich matrix. (D) Sample CWY-E01, cemented granitic wash from the western portion of the main outcrop, primarily consisting of calcite-cemented quartz grains, and hematite-filled pore spaces. (E) Sample CWY-A10, unaltered alkali granite. (F) Mineralized fracture surface (top, 4-6 mm thick) in unaltered alkali granite, consisting of brecciated host rock in a matrix of clay and clay-sized quartz grains. (G) Slip surface in alkali granite (top). Slip surfaces are characterized by brecciation of host rock and a decrease in grain size along the surface. (H) Sheared fibrous calcite veins in mafic intrusive basement rock. Veins are 1-8 mm thick and often exhibit a crack-seal texture.

4.4.3 Mineralogical Analysis

X-ray diffraction (XRD) analyses were done on a total of 34 samples (Table 6, Appendix C). Samples analyzed include unaltered host rocks, altered host rocks, mineralization, and slip surfaces, in the Flathead Sandstone and the Precambrian granite. Unaltered Flathead Sandstone is primarily composed of quartz, and in some cases, contains trace amounts of kaolinite and iron oxide. Altered Flathead Sandstone is dominantly composed of quartz, with traces of feldspar, kaolinite, phlogopite, ankerite, and iron oxide (Table 6). Mineralization in the form of deformation bands, as well as slip surfaces in the sandstone, are both dominantly composed of quartz, and sometimes trace amounts iron oxide. Unaltered pink granite is dominantly composed of quartz and feldspar, with trace kaolinite. The unaltered mafic intrusion is dominantly composed of quartz, with minor biotite, phlogopite, and gismondine (zeolite). The pink granite typically alters to clays (illite, kaolinite, nontronite, and dickite), and phlogopite becomes a more common minor constituent. Very altered granite samples are depleted in quartz and feldspar, and consist primarily of clay minerals. Calcite is found in trace amounts in 3 out of 10 altered basement host samples (Table 6). Altered mafic intrusive rock primarily consists of quartz, with trace clays (dickite, palygorskite, halloysite) and iron oxide. Mineralization in the pink granite consists mainly of quartz, with minor clays (dickite, kaolinite) and feldspar. Mineralization in the mafic intrusive rock is dominantly calcite with minor quartz. Fault surfaces are quartz dominated, with minor or trace feldspar and mica, and trace palygorskite and dickite (Table 6).

Table 6: Interpretation of XRD results for samples from Cody, Wyoming. Green indicates a major mineral phase (PANalytical X'Pert Highscore score of 0.5 or higher), yellow indicates a minor mineral phase (score of 0.1-0.5), and orange indicates a trace mineral phase (score of <0.1). Abbreviations of mineral name is present where applicable. Gray shading on sample ID cells indicates mafic basement.

LITHOLOGY		SAMPLE ID	qtz	feldspar	clay	mica	carbonate	zeolites	-O/-OH	sulfides
Flathead SS	host	A01			kaol				Fe	
		A02							Fe	
		E05b								
	altered	A03			kaol		ank			
		A04		san.	kaol	phlog.	ank		Fe	
	mineralized	E06								
	fault surface	B04								
		E04							Fe	
		E05a								
		E07								
Basement	host	A08			kaol					
		A09host								
		A10								
		D02				bt, phlog		gismondine		
	altered	A05			illite, dickite					
		A06			illite / kaol, dickite				Fe	
		A07			nont	phlog				
		A11			nont / dickite	musc				
		B06								
		D03			nont	phlog	calcite			
		D04			kaol, dickite	phlog				
		D05			dickite, palyg, halloy				Fe	
		E01			nont		calcite			
		E02					calcite			
	mineralized	A09surf			kaol, dickite					
		F01			illite / kaol				rutile	
		Q1					calcite		birnessite	
	fault surface	A12							Fe	
		B01								tin sulfide
		B02			palygorskite					
		B03							rutile	
		D07				phlog				
		D08			dickite	bt			CaCuPbSbTeCl-ox	
		F03				musc				

4.4.4 Geochemical Analysis

Major and trace element whole rock analyses were run on 7 samples from the Cody, WY locality (Appendix D). Samples include unaltered Flathead Sandstone, a sandstone-hosted slip surface, cemented and un-cemented granitic wash, altered basement at the contact, and basement hosted slip surfaces (Figure 41). The geochemical makeup of the Flathead Sandstone and the sandstone hosted slip surface are dominantly composed of SiO_2 (>90 wt%) (Figure 41). Al_2O_3 is enriched in the sandstone hosted slip surface (5.79 wt%) relative to the Flathead Sandstone host (2.48 wt%). All other major oxide constituents for the Flathead Sandstone and sandstone hosted

slip are >1 w% (Figure 41). The granitic wash samples are dominantly composed of SiO_2 (77.0-89.9 wt%) and Al_2O_3 (3.09-10.53 wt%). The unconsolidated granitic wash (CWY-D03) is more enriched in Al_2O_3, than the cemented granitic wash (CWY-E01) (Figure 41). Both granitic wash samples contain between 1.14-3.66 wt% FeO, 1.04-2.95 wt% K_2O, and 3.90-4.26 wt% CaO (Figure 41). The altered basement sample from the contact is enriched in SiO_2 (79.0 wt%) and Al_2O_3 (16.6 wt%). K_2O composes 2.58 wt% of the altered basement. All other major oxide constituents are >1 wt% (Figure 41). Basement hosted slip surfaces are mainly composed of SiO_2 (75.0-77.7 wt%), Al_2O_3 (13-41-14.84 wt%), and K_2O (4.94-8.16 wt%) (Figure 41). One slip surface contains 3.78 wt% Na_2O. The remaining major oxide constituents for basement hosted slip surfaces are <1 wt% (Figure 41).

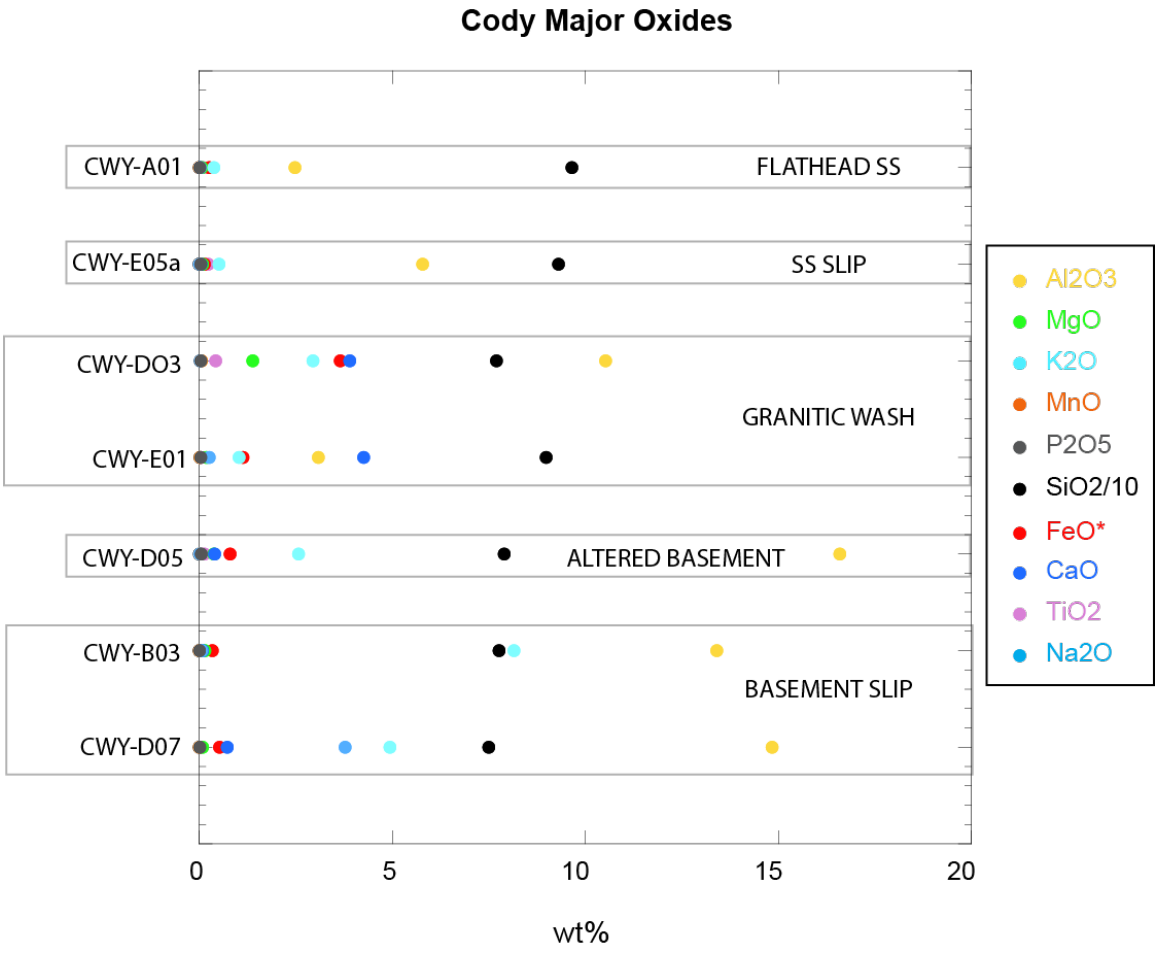

Figure 41: Whole rock geochemical data for all major oxides from samples from Cody, Wyoming. Samples have been grouped by lithology or feature type. No relative depth is implied by the vertical layout presented here. See Appendix D for raw data.

The dominant trace element constituents at the Cody locality are barium, zirconium, strontium, and rubidium (Figure 42, Appendix D). The Flathead Sandstone is mainly comprised of zirconium (1051 ppm). The sandstone hosted slip surface is depleted in zirconium relative to the sandstone host, but contains slightly more barium, strontium, and rubidium, as well as 138 ppm cesium (Figure 42). The unconsolidated granitic wash sample (CWY-D03) contains 1242 ppm barium, whereas the cemented granitic wash sample (CWY-E01) contains 79 ppm (Figure 42). The altered basement sample at the contact is mainly enriched in strontium (163 ppm) and barium (364 ppm). One basement hosted slip surface (CWY-B03) is highly enriched in barium

(2790 ppm) and slightly enriched in strontium and rubidium (119 and 116 ppm, respectively). The other basement hosted slip surface (CWY-D07) is relatively depleted in all trace elements (>170 ppm for each trace element) (Figure 42).

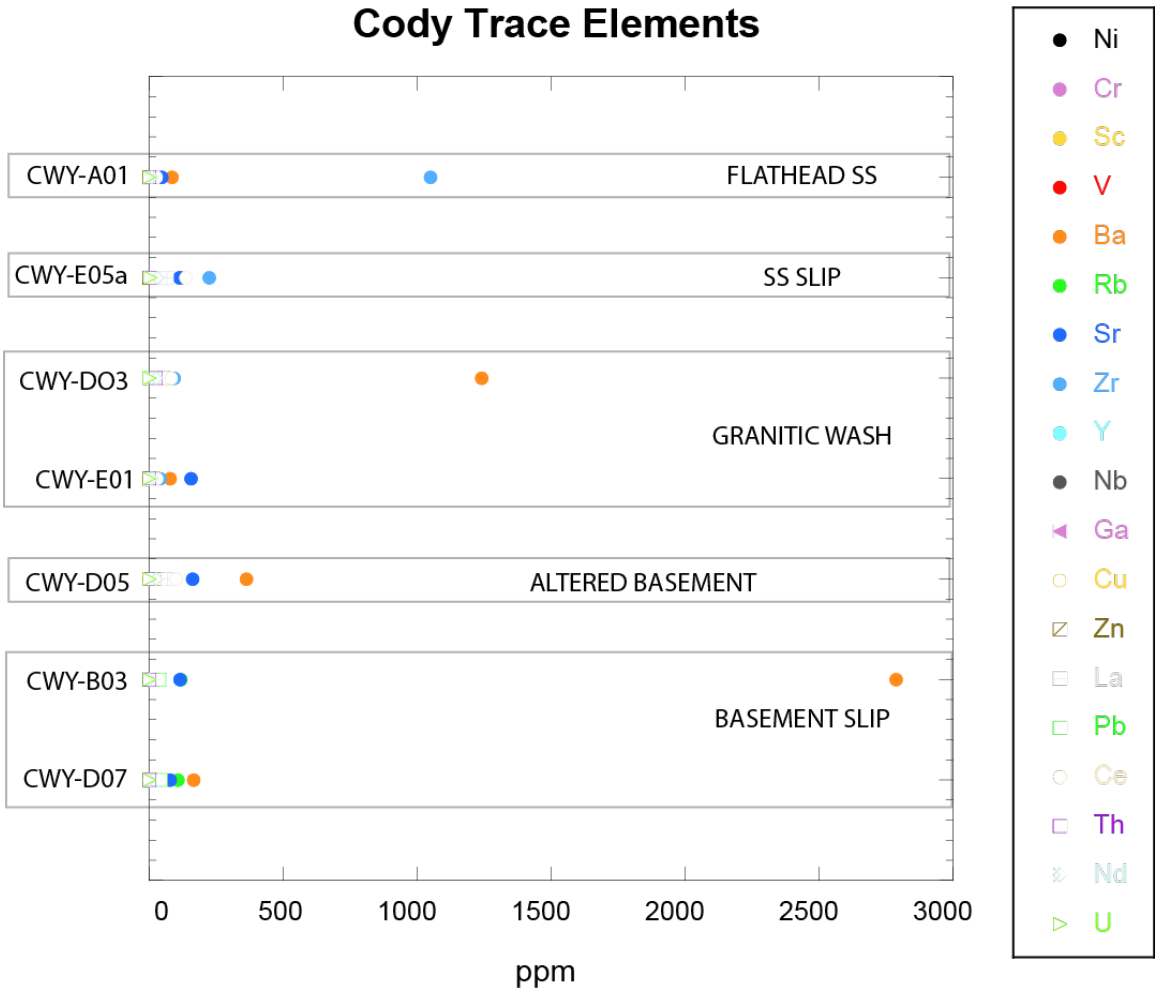

Figure 42: Whole rock geochemical data for all trace element constituents from samples from Cody, Wyoming. Samples have been grouped by lithology or feature type. No relative depth is implied by the vertical layout presented here. See Appendix D for raw data.

4.5 Ross Lake Area, Wind River Range, Wyoming

4.5.1 Mesoscopic Description

We examine the distribution and nature of the exposed basement rocks in the Ross Lake, Wyoming area in order to examine the nature of the Precambrian sub-crop meters to 100 meters below the great nonconformity. The site has a high degree of topographic relief, exhibiting multiple distinct fracture sets (Figure 43a). The Precambrian rocks here consist of granitic gneiss with mafic intrusions. Talus-filled gouge zones measuring 5-10 meters wide and walled by vertical cliff faces are fairly common (Figure 43b). No evidence of slip was observed in these zones. These zones were not easily accessed, therefore, mostly remote observations were made. Alteration at the surface is nonexistent, likely due to the glacial history of the area. Thin (1-3 mm) veins are predominantly consisting of epidote are common (Figure 43c). Mineralized slip surfaces are rare, and are commonly composed of either quartz or chlorite (Figure 43d,e). A vertically dipping fault zone strikes E-W and is 3-10 meters wide (Figure 43f). Offset is unknown. Fracture intensity decreases with increasing distance from the fault zone.

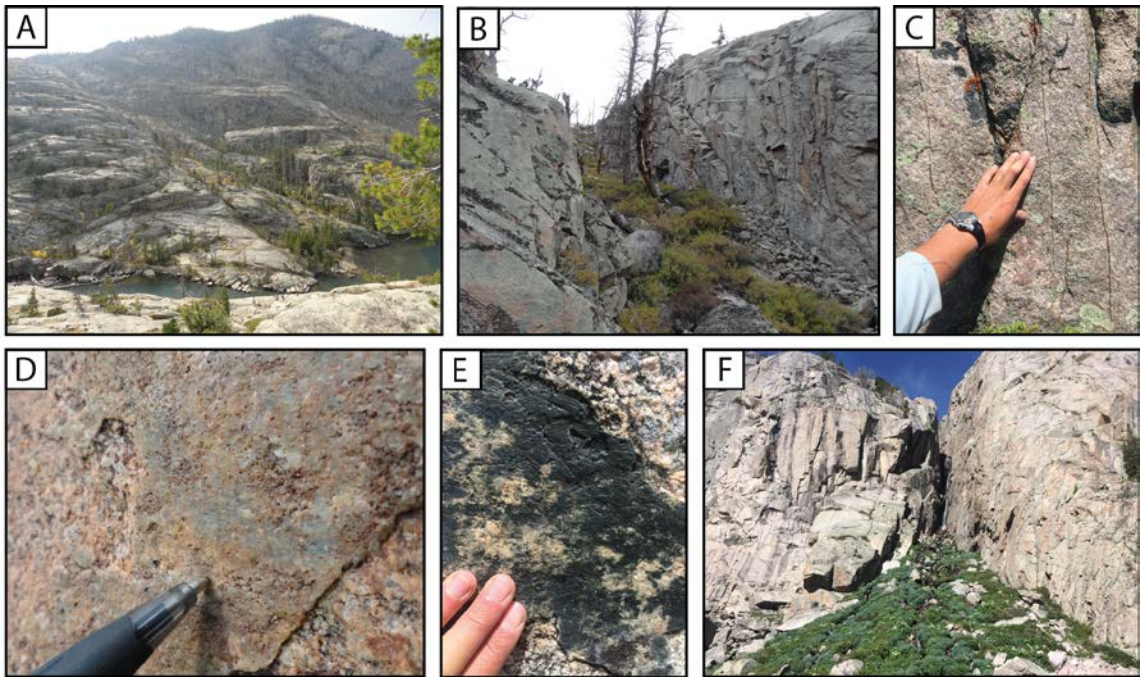

Figure 43: Field photographs from the Ross Lake Area, Wind River Range, Wyoming. (A) Map-scale topographic relief of the top of the basement. (B) Talus-filled 'gouge zone' (~5-10 meters wide). (C) Vertical, thin (1-3 mm), epidote veins in granitic gneiss. (D) Quartz mineralization on an oblique slip surface in granitic gneiss. (E) Chloritic oblique slip surface in granitic gneiss. (F) E-W trending fault zone on west side of Ross Lake. Base of vegetated talus zone is ~40 meters.

4.5.2 Fracture Analysis

Aerial fracture analysis of the ~14 km^2 area of basement exposures reveals mainly E-W and NW-SE trending major fracture zones, in which the highest fracture density is about 24 fracture zones/km (Figure 44). A total of 5 fracture transects were done in 3 different areas in order to determine meso-scale fracture intensity values and decipher fracture sets (Figure 45). At Area 1, a NNW-SSE trending transect indicates a fracture intensity of 0.89 fr/m, and an E-W trending transect indicates a fracture intensity of 0.51 fr/m. At Area 3, a N-S trending transect indicates a fracture intensity of 2.74 fr/m, and an E-W trending transect indicates a fracture intensity of 0.21 fr/m. At Area 4, one NE-SW trending transect was done across a 2 to 5 meter-wide, E-W oriented fault zone (likely related to the larger fault zone described previously),

however, fracture data was not reliable enough to calculate fracture intensity due to difficult field conditions (Figure 45).

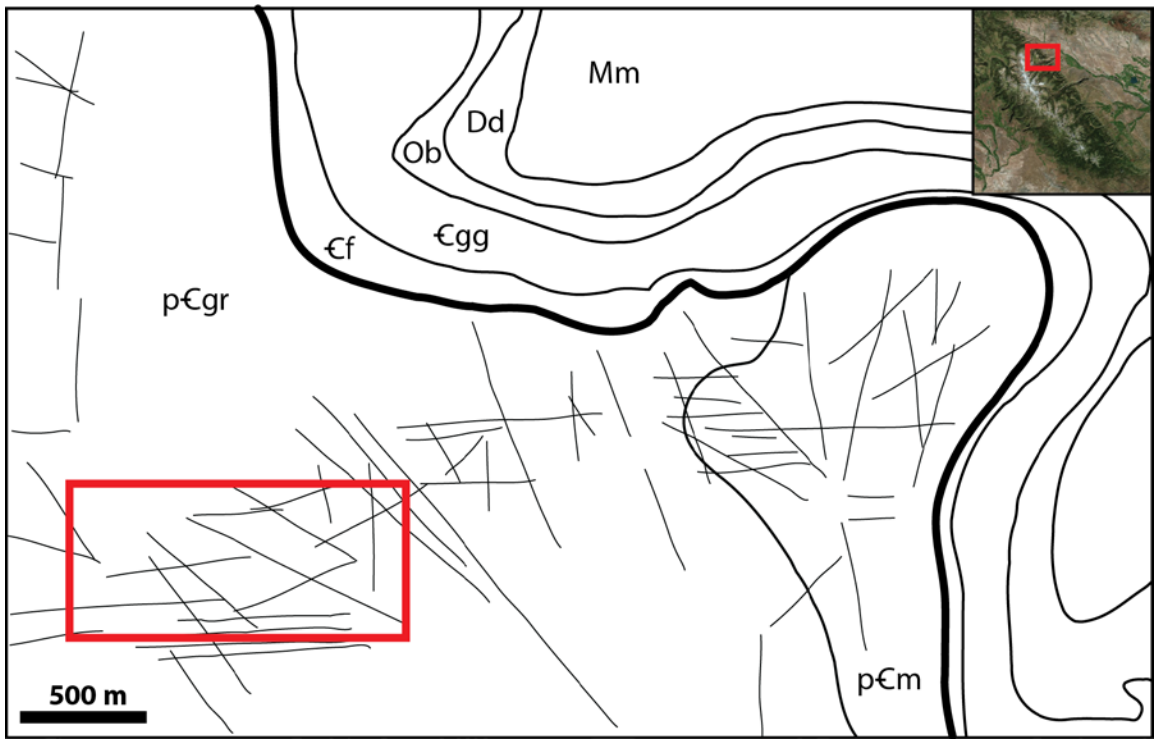

Figure 44: Tracing of major fracture zones in the ~14 km^2 of exposed basement near Ross Lake, Wind River Range, Wyoming, based on Google Earth imagery. The worked area here is outlined by the red box. Modified from Granger et al., (1971).

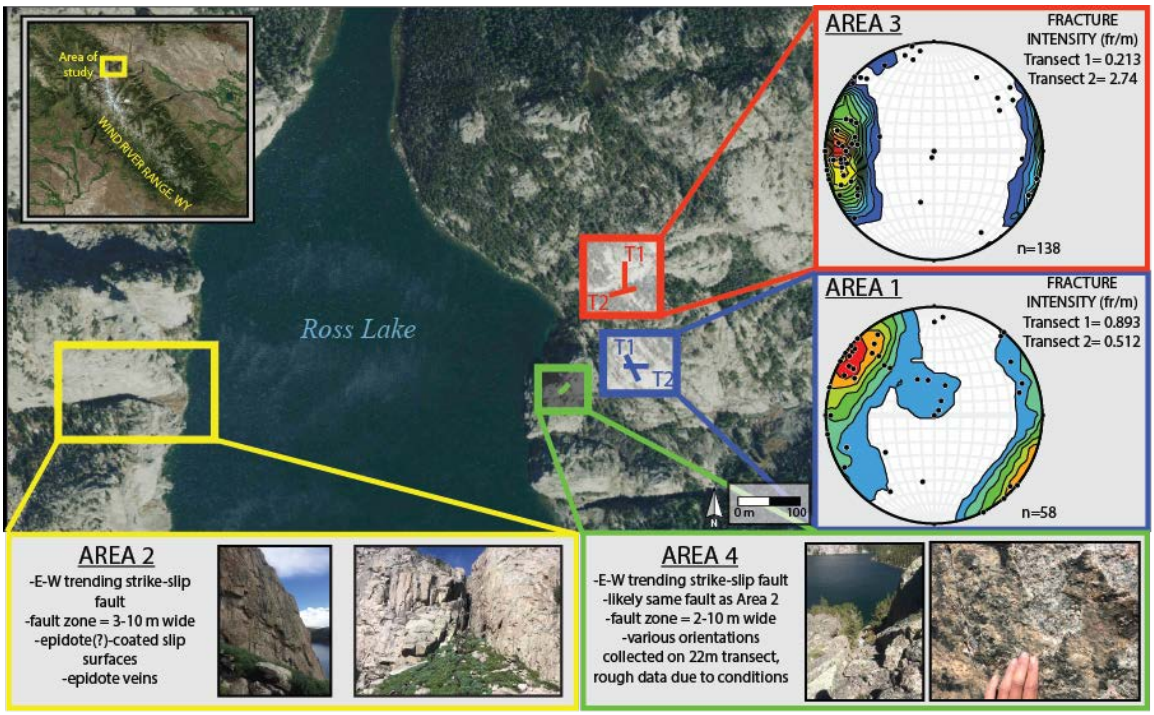

Figure 45: Fracture analysis results from the Ross Lake Area, Wind River Range, Wyoming. Archean gneiss exposures reveal a dominantly WNW-ESE fracture set. One major E-W trending fault zone was investigated on either side of Ross Lake. Minor slip surfaces in these areas (Areas 2 and 4) indicate strike-slip motion.

5. Analysis

Through characterization of the nonconformity sites, and a review of analyses of other sites from the literature, we identify three categories of hydrologically significant nonconformity types in this study. These are: 1) basal conglomerate, 2) weathered and/or altered horizon (i.e., regolith, grus, granitic wash), and 3) mineralized contacts. Regolith refers to horizon of bedrock which has been weathered by surface processes, with little or no evidence of transport (Pain, 1991). Grus is a type of regolith in which the source rock is a felsic crystalline rock, resulting in a clay-rich material (Migon and Thomas, 2002). Granitic wash is a weathered material which is compositionally equivalent to the source rock, however, evidence of transport is present (Pettijohn et al., 2012). We stress that the three major contact type categories do not completely encapsulate the full range of geological scenarios that may be found at the nonconformity zone, but are a sampling of what one could expect to find at the nonconformity zone (Figure 5) based on what we document from our five case studies. Here we examine the geologic properties of each contact type from a hydrological prospective to hypothesize how the specific properties of each contact type pertain to fluid transport along the nonconformity. We predict the geologic features discussed below to be either conduits (permeability high relative to surrounding rock) or barriers (permeability low relative to surrounding rock), based on the geologic properties they display.

5.1 Basal Conglomerate Contacts

The presence of a basal conglomerate at the contact is observed in the Jacobsville Sandstone at Hidden Beach and Presque Isle, Michigan. Texturally, the basal conglomerate falls into two hydrologically distinct categories: 1) tight, well-cemented layer, which would likely act as a low permeability barrier to flow, and 2) friable, poorly cemented horizon, which may act as a conduit to flow (Figure 46). Thin sections of the two differing conglomerates reveal porosity in

both samples. Porosity in the tight conglomerate is vuggy and disconnected (Figure 46a), whereas the friable conglomerate has effective porosity in the form of fractures and void spaces along clast boundaries (Figure 46b). Geochemically, the tight conglomerate is more clay-rich relative to the friable conglomerate, further indicating that it may act as a low-permeability barrier to fluid flow (Table 4). The tight conglomerate type appears to be more common than the friable variety at the Marquette, Michigan sites, however, this may not hold true elsewhere. The basal conglomerate at the Marquette, Michigan sites is spatially and geometrically variable. The basal conglomerate exhibits variations in lateral thickness, ranging from <10-100 cm. Conglomerate layers form lenses, are interbedded with the host sedimentary unit, and often pinch out. The basal conglomerate lies in contact with basement rock in some places, or is, in some places, absent all together (Figure 47).

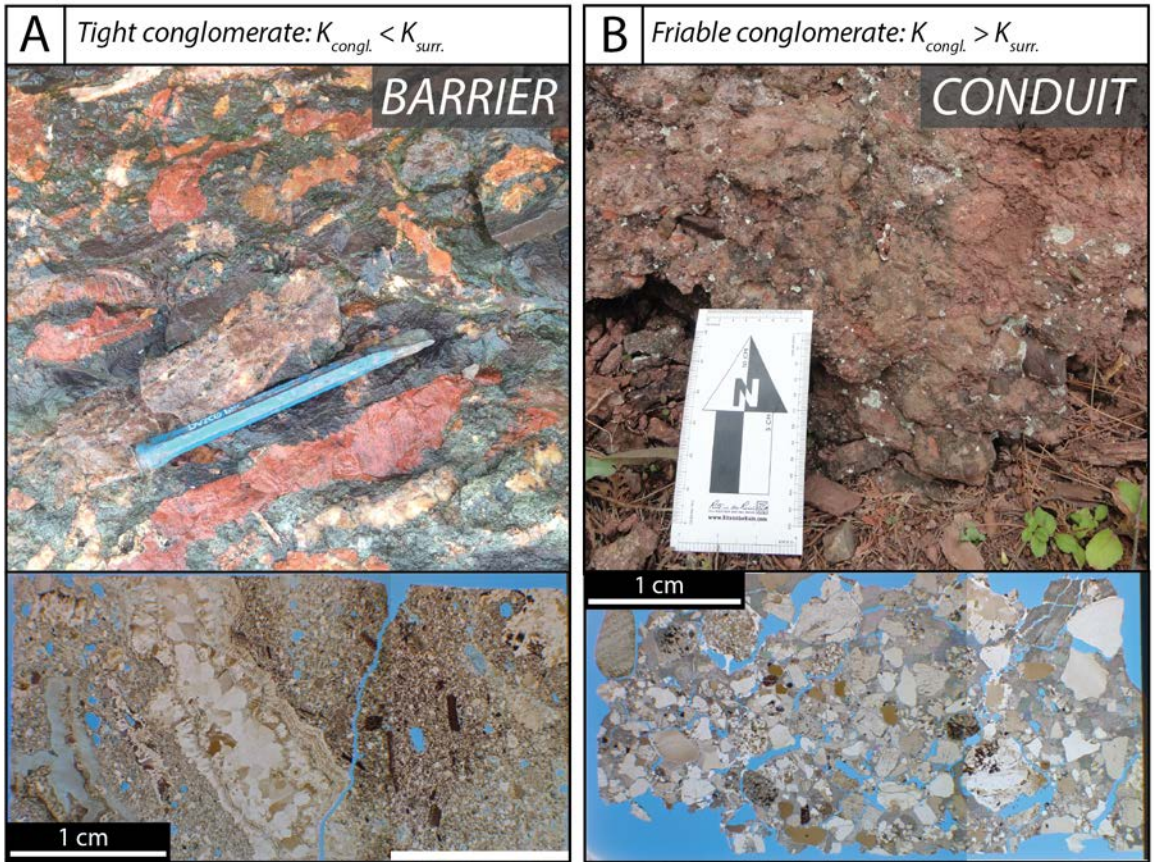

Figure 46: Barrier- versus conduit-type basal conglomerate layers. (A) Tight, well-cemented conglomerate layer at Presque Isle, Marquette, Michigan. Ineffective porosity is present in this type of conglomerate, and therefore likely has a low permeability (K) relative to the surrounding rocks. Chisel (15 cm) for scale. (B), poorly-cemented conglomerate at Hidden Beach, Marquette, Michigan. The interconnected porosity in this conglomerate type indicates that it may have a high K, relative to the surrounding rocks. Field card (8x15 cm) for scale.

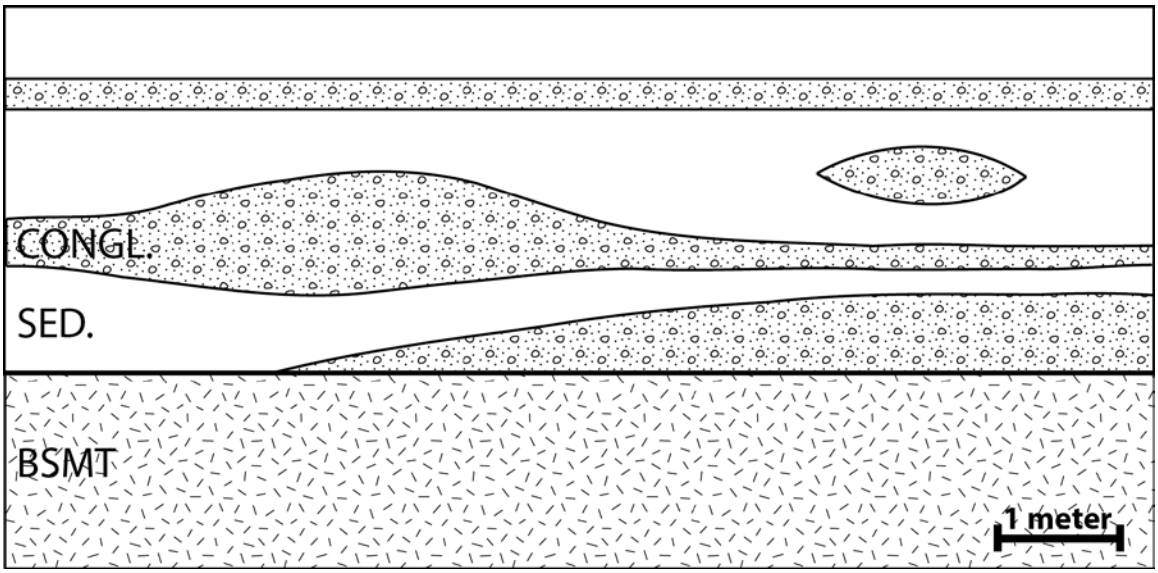

Figure 47: Schematic diagram depicting the range of basal conglomerate geometries observed at Presque Isle, Marquette, Michigan. Geometries include lateral changes in thickness (pinch-outs, bulges, lenses) and direct and indirect contact with underlying basement rocks. In addition to the scenarios depicted here, the basal conglomerate may be completely absent in places.

Additionally, the presence of basal conglomerates at the contact has been observed in the field at sites separate from this project (Figure 48). East of Willard, Utah, we observe a very well cemented basal conglomerate with rounded pebble- to cobble-sized clasts in the Cambrian Tintic Quartzite, directly in contact with Precambrian Farmington Canyon Complex. At Devil's Lake State Park and Parfrey's Glen State Natural Area, near Merrimack, Wisconsin, basal conglomerates in the Cambrian Parfrey's Glen Formation overlie the Precambrian Baraboo Quartzite (Figure 48). The basal conglomerate in Devil's Lake State Park consists of pebble- to boulder-sized rounded quartzite clasts. Many of the boulders are approximately 1-2 meters in diameter. The basal conglomerate at Parfrey's Glen State Natural Area consisted mainly of sub-angular to rounded pebble- to boulder-sized quartzite clasts in an incohesive sandstone host. The conglomerate layers here are mainly thin (approximately <50 cm) and are interbedded with incohesive sandstone. The conglomerates here are interpreted to have been eroded off of basement highs (described as 'islands') due to Cambrian tropical storms, and were subsequently

dispersed offshore in basement lows (Dott and Attig, 2004). Other notable basal conglomerates have been described in southwestern Ontario (Easton and Carter, 1995) and the Grand Canyon, Arizona.

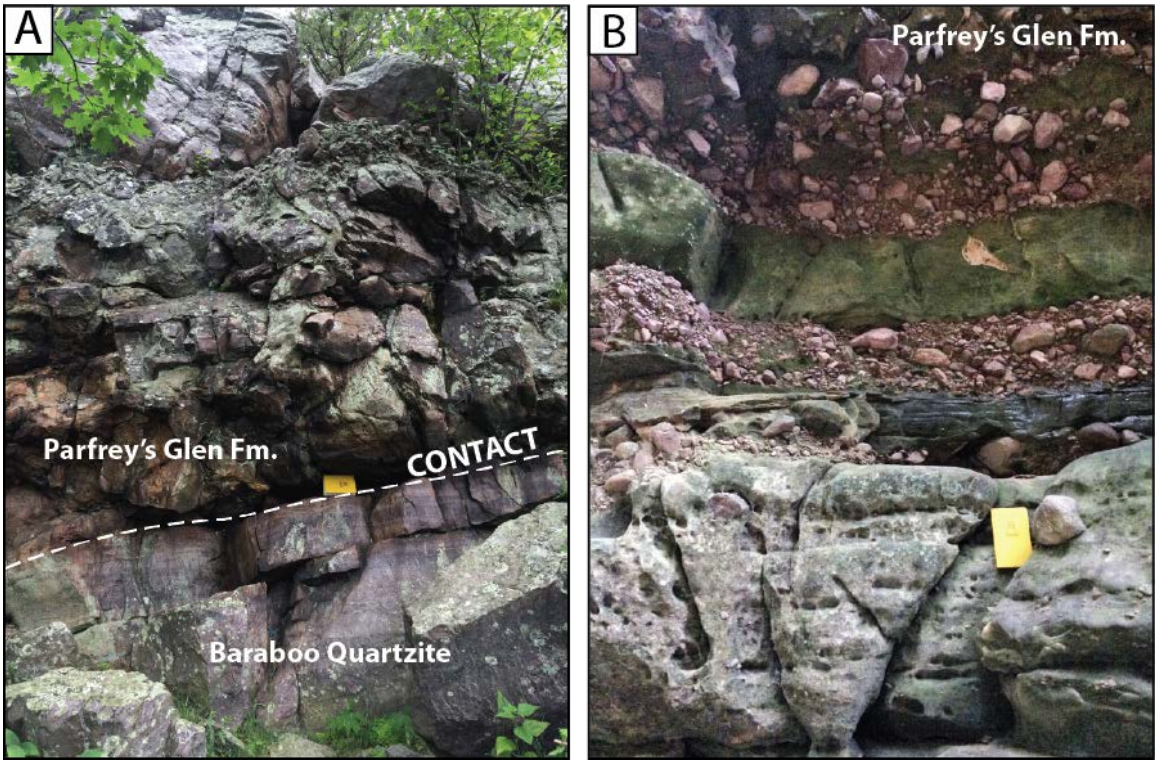

Figure 48: Examples of basal conglomerates at (A) Devil's Lake State Park, and (B) Parfrey's Glen State Natural Area. Both are located near Merrimack, Wisconsin, where the Cambrian Parfrey's Glen Formation lies nonconformably above the Precambrian Baraboo Quartzite. The contact is only expose at Devil's Lake State Park. Field notebook (12x19 cm) for scale.

5.2 Weathered and/or Altered Horizon Contacts

We observe three different types of weathered horizons at the contact at three different localities. Weathered horizons likely contain some degree of alteration, such as alteration of feldspars to clay minerals. The process by which these alteration minerals are formed differentiates this contact type from the 'mineralized' contact type, in which chemical alteration of the host rock is due to fluid-rock interaction as externally sourced fluids move along the

contact, rather than from in situ surface weathering processes. The geochemistry of alteration minerals in weathered profiles resembles that of the host rock, whereas a mineralized horizon may be enriched in elements not found in the host rock. Additionally, textures revealed in thin section, such as sericitization of feldspar grains, can also be used to distinguish between weathering-related chemical alteration and mineralization. At Presque Isle, some sites exhibit a regolith horizon at the top of the serpentinized peridotite, in contact with the overlying Jacobsville Sandstone (Figure 49). This regolith horizon is between 50 and 200 cm thick, and is characterized as a very friable, unconsolidated, fine-grained material, which generally retains the color and texture of the underlying host rock (Figure 49a). Dolomite- and silica-rich veins seen in the host rock are often preserved in the overlying regolith. In places the regolith horizon has completely weathered away, leaving a gap between the basement rock and overlying strata (Figure 49b). The hydrological implications of a regolith horizon at the contact is highly dependent on the host rock from which it formed, but in the case of the Presque Isle regolith, we predict that it may act as a conduit to flow based on the highly incohesive texture and tendency to weather easily.

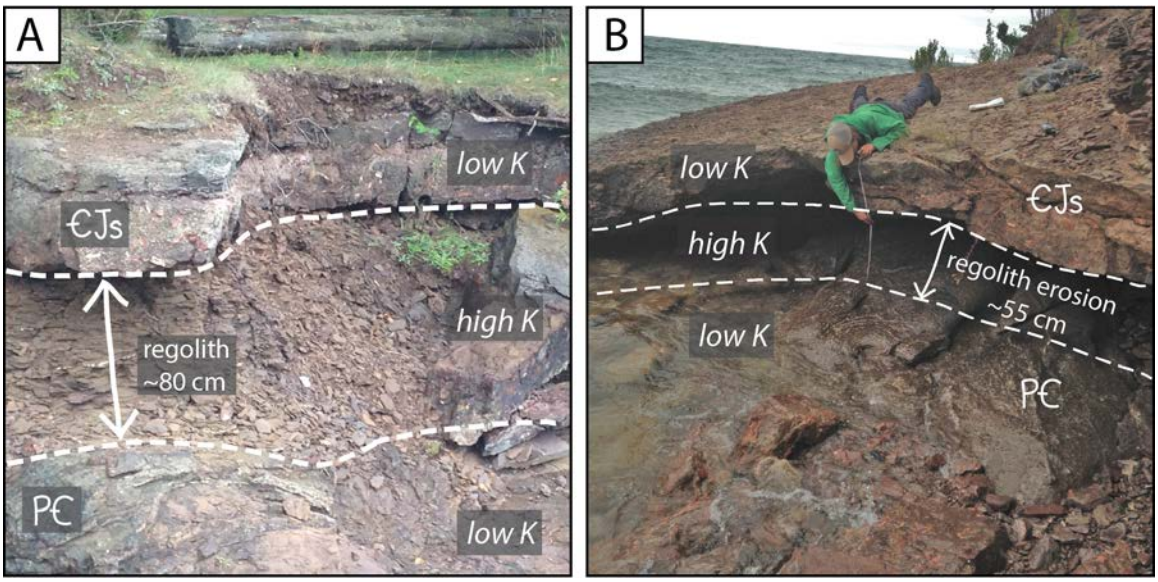

Figure 49: Regolith horizons at the contact at Presque Isle, Marquette, Michigan. Relative permeability (K) of layers are indicated. (A) Regolith is significantly less competent than surrounding rock. (B) The friable nature of the Presque Isle regolith makes it particularly susceptible to weathering. Here the regolith has been eroded away by wave action on the lake shore, leaving a gap between the underlying basement host rock and the overlying Jacobsville Sandstone mineralized basal conglomerate.

A grus horizon lies directly at the contact in parts of the Cody, Wyoming outcrop (Figure 50). This weathered horizon is defined as grus rather than regolith or granitic wash based on the felsic parent rock, lack of evidence of transport, and relative clay content. The <5-30 cm thick grus horizon is characterized by sub-angular gravel- to pebble-sized granite clasts in a very friable, clay-rich matrix. Iron-oxide mineralization along a fracture boundary that bisects the grus horizon and adjacent lithologies is evidence of the movement of oxidizing fluids along a fracture plane (Figure 50).

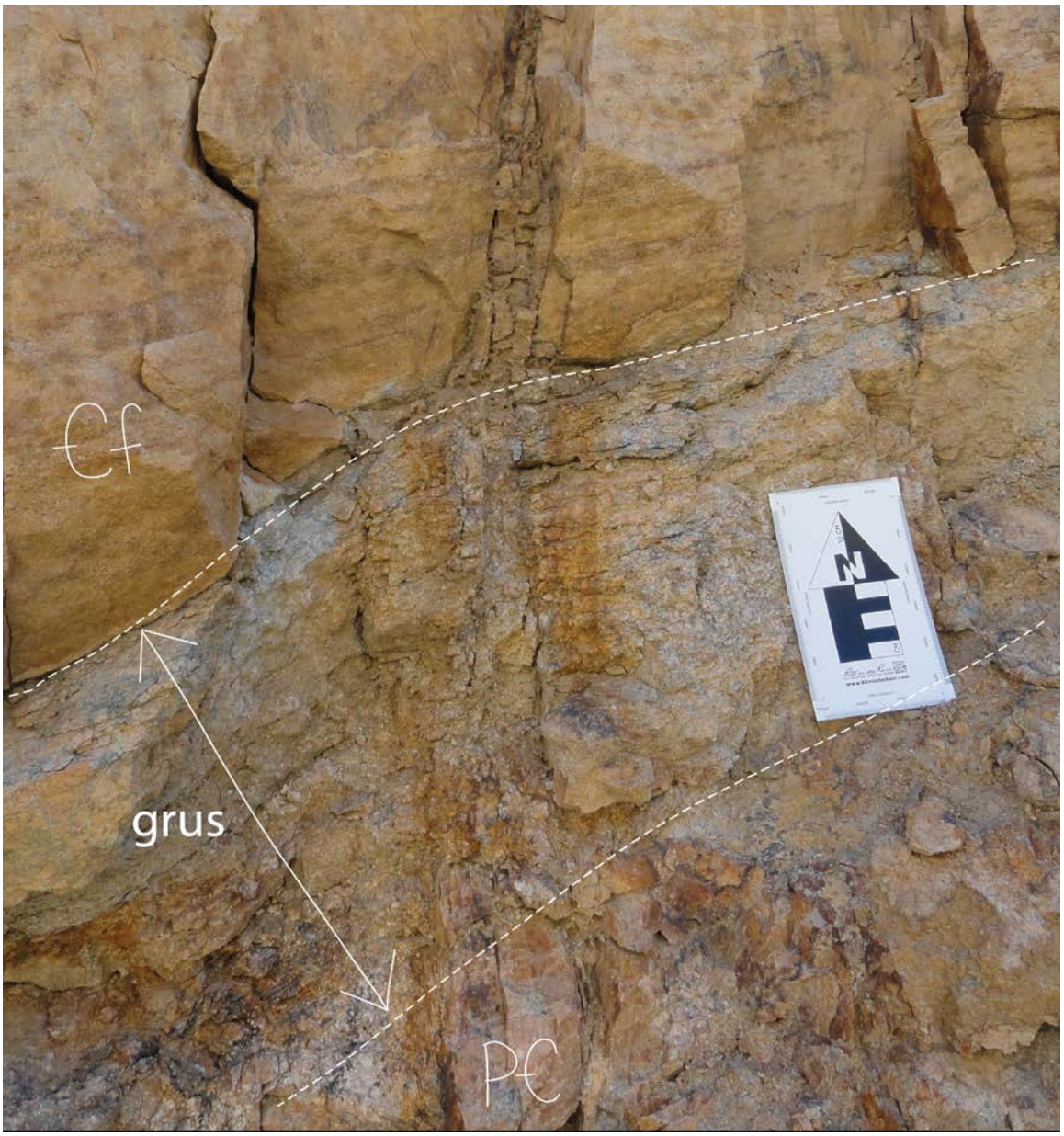

Figure 50: Grus at the contact at Cody, Wyoming. Iron-oxide staining along the fracture boundary in the grus layer may be indicative of oxidizing fluid movement through fractured zones. Field card (15x8 cm) for scale.

Granitic wash is observed at the Cody, Wyoming outcrop and in the UPH-1 core (Figure 51). In the UPH-1 core, the interbedded nature of the grus-like material is indicative of transport of a once in-situ weathered material, thus we define it as a granitic wash. The 2.8-meter-thick

interbedded granitic wash layer is characterized as a relatively incohesive, clay-rich material, containing sub-angular pebble-sized granite clasts (Figure 51a). The granitic wash horizons in Cody, Wyoming are laminated and contain sub-rounded to rounded granite clasts, indicating transport. This granitic wash is very similar to the clay matrix-rich granitic wash seen in the UPH-1 core, with the main physical difference being that the granitic wash in Cody is laminated and contains clasts that are more rounded (Figure 51b). The high clay content of the Cody granitic wash indicates that it may acts as a low-permeability barrier to fluid flow. In addition, the laminations in this material may control fluid migration in a more anisotropic manner, relative to an unlaminated material (Figure 51b).

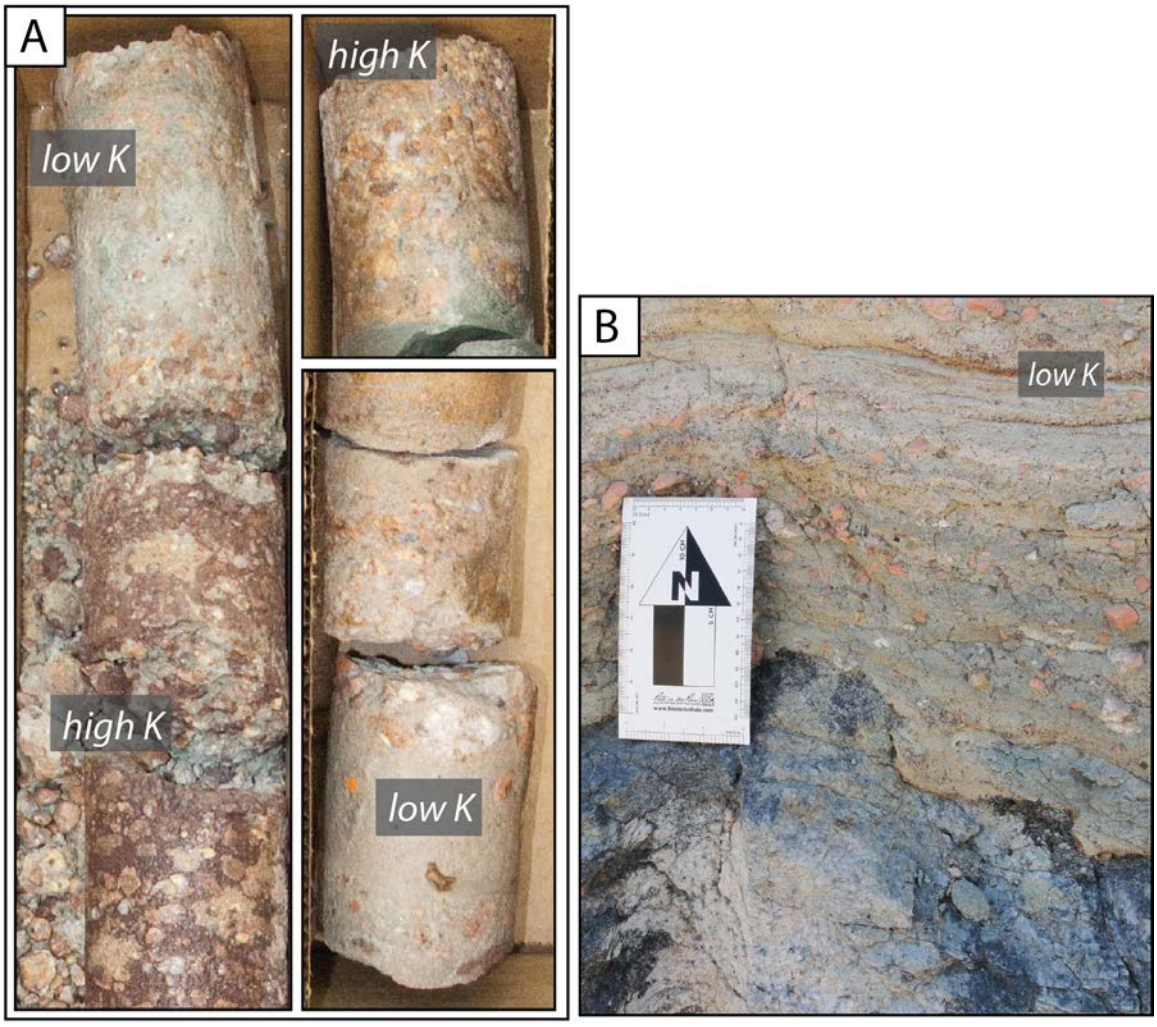

Figure 51: (A) Granitic wash in the UPH-1 core. Relatively less clay-rich, clast-supported granitic wash is accompanied by iron oxide alteration, whereas the more clay-rich, matrix supported material is not. This may be indicative of microvariations in permeability due to differences in the clast to matrix ratio of the material. (B) Laminated, clay-rich granitic wash in Cody, WY. This material likely has a low permeability due to high clay content, relative to surrounding rock. Laminations would likely cause this material to behave anisotropically.

A weathered horizon was not observed in the CPC cores. Easton and Carter (1995) document a weathered contact zone in core from southwestern Ontario, which also samples the Grenville Front Tectonic Zone. The cores they documented contain a 2- to 5-meter-thick zone of weathering and alteration at the contact in the uppermost basement rocks, at the contact between Cambrian sandstone and Precambrian granitic gneiss. They describe this as a ‘paleo-regolith’

which is primarily characterized by saussuritization of plagioclase, development of authigenic K-feldspar, and corrosion and chloritization of mafic minerals (Easton and Carter, 1995).

The three types of weathered/altered horizons presented here are all unconsolidated. Even when subjected to lithostatic loads of >20 MPa, these materials may retain their unconsolidated characteristics. One possible way to explain this may be that basement highs are acting as structural supports similar to pillars or columns, where unconsolidated weathered/altered materials in basement lows have pinched out, and stresses are supported at these basement contacts, effectively lessening the load on the materials between these highs.

5.3 Mineralized Contacts

Evidence for post-deposition or post-weathering mineralization at the contact is observed at Hidden Beach and Presque Isle in Marquette, Michigan, in the CPC BD-139 and CPC BD-151 cores, and at Cody, Wyoming. Dolomitized basement rock and iron-oxide mineralization of sedimentary and basement rocks are the primary types of mineralization seen at these sites. Significant iron-oxide mineralization (in which FeO is enriched by >5 wt% relative to host), and relatively high (<1000 ppm) concentrations of Ni and Cr, are observed at 3 locations at Presque Isle in the ultramafic basement host and the overlying sedimentary strata (Figure 28b, Figure 34, Figure 35). Evidence for dolomitization is observed in the uppermost basement rocks in the CPC BD-139 core (Figure 14b,d,e), (and likely the CPC BD-151 core, though this is solely supported by macroscopic observation) and in the Presque Isle serpentinized peridotite (Figure 32). Dolomitized basement rocks are defined by a >10 wt% enrichment of both CaO and MgO, relative to host rocks. Additionally, calcite, ankerite, and anhydrite exist in veins and slip surfaces in the basement rocks at Presque Isle and in the CPC BD-139 core (Table 1, Table 4). Calcite-cemented conglomerates and/or weathered horizons are also present at both sites in Marquette, Michigan, and at Cody, Wyoming (Figure 31, Figure 40d).

5.3.1 Iron-Oxide Mineralization

Concentrated iron-oxide mineralization of the nonconformity zone is related to the presence of ultramafic basement rocks at Presque Isle. Significant iron-oxide mineralization is absent at Hidden Beach, where felsic basement rocks underlie the same basal sedimentary unit. Significant iron-oxide mineralization is also absent from all other sites examined in this project, particularly where the sedimentary units are underlain by felsic basement rocks. Ultramafic rocks are geochemically defined as low silica, high Fe-Mg-Mn igneous rocks (Sen, 2013), therefore it is likely that the serpentinized peridotite host rock at Presque Isle is the source of the iron-oxide mineralization.

Spatially, iron oxide mineralization of the nonconformity zone correlates with the presence of faults, occurring at 3 out of the 4 faulted sites (PI-S2, PI-S13, and PI-S16) examined at Presque Isle, whereas all other sites do not contain significant iron oxide (Figure 30, Figure 34). The host rocks and, in one case, the overlying Jacobsville Sandstone, at these 3 faulted are enriched in iron-oxide, indicating that an oxidizing fluid may have once flowed through the zones. The one faulted site that did not contain significant iron-oxide mineralization bisects the contact where the basal conglomerate is directly in contact with basement rock, and appears as a silica-rich lozenge-like vein in the basement, on which slip surfaces were observed (Figure 30a). The lack of iron-oxide mineralization at this fault may be due to the relative permeability of the lozenge-like vein. It is possible that this structure acted as a barrier-type fault due to its tightly mineralized structure, inhibiting significant fluid flow, and thus iron-oxide mineralization, throughout the zone.

5.3.2 Carbonate Mineralization

The presence of carbonate-mineralized contacts at sites with varying lithologies, specifically in gneisses, indicates that carbonate-mineralization of the nonconformity zone is independent of basement rock composition, and reflects alteration from an external source. At

Hidden Beach, parts of the Jacobsville Sandstone basal conglomerate are cemented by calcite, and underlain by gneiss. Basement-hosted carbonate mineralization is widespread at Presque Isle, as calcite slip-surfaces, dolomite and calcite veins, and as patches of dolomitized host rock. At Cody, Wyoming, the laminated granitic wash is calcite-cemented, and crack-seal calcite veins are present in mafic basement-hosted fault gouge. In the CPC BD-139 core, dolomitized gneiss hosts calcite and anhydrite veins.

The ubiquitous nature of carbonate mineralization at the contact prompts the investigation of the source of the fluid and potential heat that drove this alteration. We use stable isotope oxygen thermometry to constrain fluid temperatures using our oxygen stable isotope data, which relies on the temperature dependency of stable isotopic fractionation to determine the temperature of the fluids from which minerals precipitated (Friedman et al., 1977). If we assume that the mineral in question precipitated under isotopic equilibrium condition, the $\delta^{18}O$ value of the mineral depends on the temperature and the $\delta^{18}O$ value of the water from which it precipitated (Urey, 1947). The key relationships for this method are:

$$1000ln\alpha_{dolomite-water} = \frac{2.73\times10^6}{T^2} + 0.26 \qquad (3)$$

where,

$$1000ln\alpha_{dolomite-water} = \delta^{18}O_{dol} - \delta^{18}O_{water} \qquad (4)$$

and

$$1000ln\alpha_{calite-water} = \frac{2.78\times10^6}{T^2} - 2.89 \qquad (5)$$

where

$$1000ln\alpha_{calite-water} = \delta^{18}O_{cal} - \delta^{18}O_{water} \qquad (6)$$

Where α is the fractionation factor, $\delta^{18}O_{water}$ is the oxygen isotope ratio value for the source fluid, $\delta^{18}O_{cal}$ and $\delta^{18}O_{dol}$ are the oxygen isotope ratio values of the precipitated mineral, and T is the temperature of the source fluid in Kelvin (Vasconcelos et al., 2005; Sharp, 2007; Friedman et al., 1977). Our measured $\delta^{18}O_{cal}$ values satisfy one of the three variables for this relationship, leaving us with two unknowns: the $\delta^{18}O_{water}$ value of the source fluid from which the mineral precipitated, and the temperature of that source fluid. By setting our measured $\delta^{18}O_{cal}$ values as the independent variable, and the temperature as the dependent variable, we can solve for the isotopic signature of the source fluid and compare our calculated values to those presented in the literature. If our calculated values are consistent with the values seen in the literature, we consider that temperature range to be a possible solution. We chose to test 3 different temperature ranges, which we inferred from mineralogical and textural observations and the geologic history of the area. These are: 1) hydrothermal fluid source, 2) basinal brine fluid source, and 3) present-day meteoric water source.

Due to the complicated geologic history of the Presque Isle serpentinized peridotite, where the nonconformity represents up to 2 billion years of missing history, and due to the scarcity of available literature on the area regarding timing, temperatures, and depths associated with paragenesis of the Presque Isle serpentinized peridotite, constraining an accurate temperature range for the mineralization of the original peridotite cannot be done with confidence. The dolomitization seen at Presque Isle is thought to be a product of metasomatic events specific to peridotite, rather than a product of fluids flowing along the nonconformity. Lewan (1972) documents the metasomatic history of the Presque Isle serpentinized peridotite, which includes: 1) serpentinization of the peridotite body, 2) dolomitization of the serpentinized peridotite, 3) regolith formation. The dolomite must have formed prior to the deposition of the Jacobsville Sandstone based on the presence of dolomite veins within the regolith, which formed due to surface weathering conditions. Since this alteration occurred before the nonconformity existed,

determining the origin of the source fluid is not relevant to our research questions, therefore we only apply oxygen thermometry to the samples from the CPC BD-139 core.

We used the present-day geothermal gradient (25 ºC/km) and the depth range of 1405-1410 meters (depth of CPC BD-139 samples) to estimate the temperature of a meteoric source fluid to be 35 ºC. The expected $\delta^{18}O_{water}$ value based on local meteoric water lines is around -12 ‰ (SMOW) (Faure, 2009). Using these values, our calculated $\delta^{18}O_{water}$ values range from -7.19 to -2.48 ‰ (SMOW). This range is high of the values reported in the literature; therefore, we do not consider groundwater to be a likely source fluid (Figure 52).

MEASURED $\delta^{18}O_{(calcite)}$		CALCULATED $\delta^{18}O_{(water)}$ (SMOW)				
Sample ID#	$\delta^{18}O_{(cal)}$ (SMOW)	Hydrothermal		Basinal brine		Meteoric
		70 °C	170 °C	49 °C	63 °C	35 °C
CPC-4611A	23.07	2.33	11.80	-0.85	1.34	-3.34
CPC-4623	19.23	-1.51	7.95	-4.7	-2.51	-7.19
CPC-4630.5	23.93	3.20	12.66	0.01	2.2	-2.48
Target $\delta^{18}O_{(fluid)}$ (SMOW) (from literature)		5-20‰ (Sharp, 2007)		-0.5-3‰ (lo-T), 1-5‰ (hi-T) (Clayton et al., 1966)		-12‰ (Faure, 2009)

Figure 52:Oxygen isotope thermometry data. $\delta^{18}O_{water}$ values were calculated for different source fluid temperature ranges using our measured $\delta^{18}O_{calcite}$ values, using Equations 5 and 6.The calculated $\delta^{18}O_{water}$ values were then compared to the values presented in the literature for each source fluid scenario. If the calculated values match the target values, the source fluid scenario is considered plausible. Green text indicates a plausible source fluid scenario, and red text indicates an unlikely source fluid scenario. Based on our results, the calcite veins in the CPC BD-139 core likely precipitated from a low temperature hydrothermal fluid, or a warm basinal brine.

Using the present-day sample depths, we calculate the temperature of a basinal brine source fluid to be 49-63 ºC (Cercone, 1984), using the geothermal gradient during late Paleozoic basin subsidence in the Michigan Basin (35-45 ºC/km), which is also consistent with Girard and Barnes (1995). We acknowledge that these depths have likely changed during the late Paleozoic (Everham and Huntoon, 1999), however, subsidence rates in intracratonic basins are typically

greatest in the center, and the CPC BD-139 core is on the margin where subsidence rates were likely slower. Taking subsidence into account results in a higher temperature range, yielding a range even closer to that of the hydrothermal fluid scenario presented below. For the lower temperature estimate, the $\delta^{18}O_{water}$ value should be between -0.5 to 3‰ (SMOW), and for the higher temperature estimate, the $\delta^{18}O_{water}$ value should be between 1 to 5‰ (SMOW) (Clayton et al., 1966) (Figure 53). Our calculated $\delta^{18}O_{water}$ values for a basinal brine source range from -4.70 to 0.01‰ (SMOW) for the lower temperature brine, and -2.51 to 2.20‰ (SMOW) for the higher temperature brine. The calculated $\delta^{18}O_{water}$ values for the higher temperature brine scenario match the values reported in the literature fairly well, therefore we infer that a basinal brine that flowed along the nonconformity may be a plausible source fluid for the calcite veins in the CPC BD-139 core (Clayton et al., 1966). This also may be supported by the chemical composition of Michigan Basin brines, which are reported to be highly concentrated Ca-Na-Cl brines (Wilson and Long, 1993). The relatively high concentration of Ca in typical Michigan Basin brines may provide the constituents necessary for carbonate mineralization along the contact.

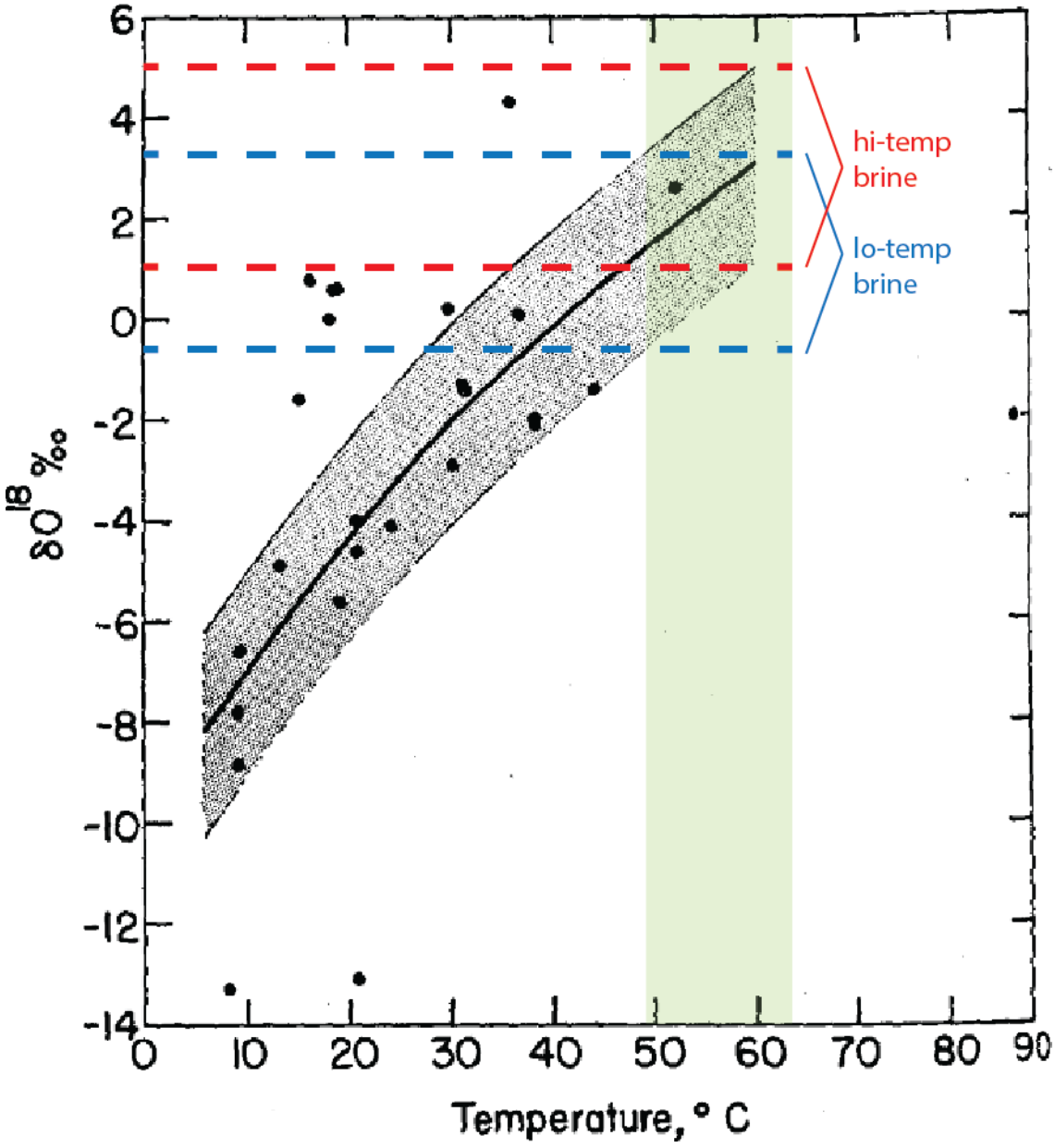

Figure 53: Variation of brine O^{18}/O^{16} ratio with well temperature for the Michigan Basin. The equilibrium curve is drawn for calcite of δ =+25.3‰. The green box represents the temperature range we determined for the basinal brine scenario. The values presented here indicate that our calculated source fluid $\delta^{18}O$ values should be between -1 and 5 ‰ (SMOW) for a warm basinal brine source fluid, and -0.5 to ~3 for a cool basinal brine source fluid. Modified from Clayton, et al., (1966).

Hydrothermal alteration in these rocks is supported by the presence of hydrothermally associated minerals in the CPC BD-139 core, such as zeolites, vermiculite, and clinochlore,

therefore, we test a hydrothermal fluid source for our highest temperature scenario (Kerr, 1955) (Table 1). A plausible temperature range for a hydrothermal fluid source for these rocks is difficult to constrain without fluid inclusion data, therefore we look to the literature for fluid inclusion data for rocks from the surrounding area. Fluid inclusions from post-dolomitization calcite from middle-Ordovician strata in southwestern Ontario, roughly 100 km south of the CPC BD-139 bore hole, indicate homogenization temperatures of between 70-170 ºC (Coniglio et al., 1994) (Figure 54). The measured $\delta^{18}O_{cal}$ values of the calcites from which this temperature range was inferred from fall between about -10 to -6‰ (VPDB), which is very close to our measured $\delta^{18}O_{cal}$ range of -11.33 to -6.77‰ (VPDB) (Coniglio et al., 1994) (Table 2). We apply this temperature range, yielding calculated $\delta^{18}O_{water}$ values between -1.51 to 3.20‰ (SMOW) for the lower temperature (70 ºC) hydrothermal source, and 7.95 to 12.66‰ (SMOW) for the higher temperature (170 ºC) hydrothermal source (Figure 52). Specific measured oxygen isotopic values for deep-seated hydrothermal fluids in the Michigan Basin are scarce. However, the calculated $\delta^{18}O_{water}$ values for the 170 ºC fluid sources resemble those of primary igneous and metamorphic waters (Figure 55). If we assume that these fluids were circulating within the metamorphic basement rock, we expect the $\delta^{18}O_{water}$ values to reflect the isotopic signature of that host rock, resulting in enriched $\delta^{18}O_{water}$ values (~5-20‰ (SMOW)) (Figure 55). The assumption that these hydrothermal fluids are basement-derived is consistent with the work of Coniglio et al. (1994), Ma et al. (2009), Barnes et al. (2008), and Luczaj et al. (2006), who suggest that reactivation of fault and fracture networks in the Precambrian basement in the Michigan Basin is responsible for the circulation of basement-derived hydrothermal fluids, resulting in the precipitation of hydrothermal dolomite reservoirs. The hypothesis that this carbonate mineralization is hydrothermally related is further supported by the observation of other hydrothermally associated minerals in the CPC BD-139 core, such as zeolites, vermiculite, and clinochlore (Kerr, 1955) (Table 1).

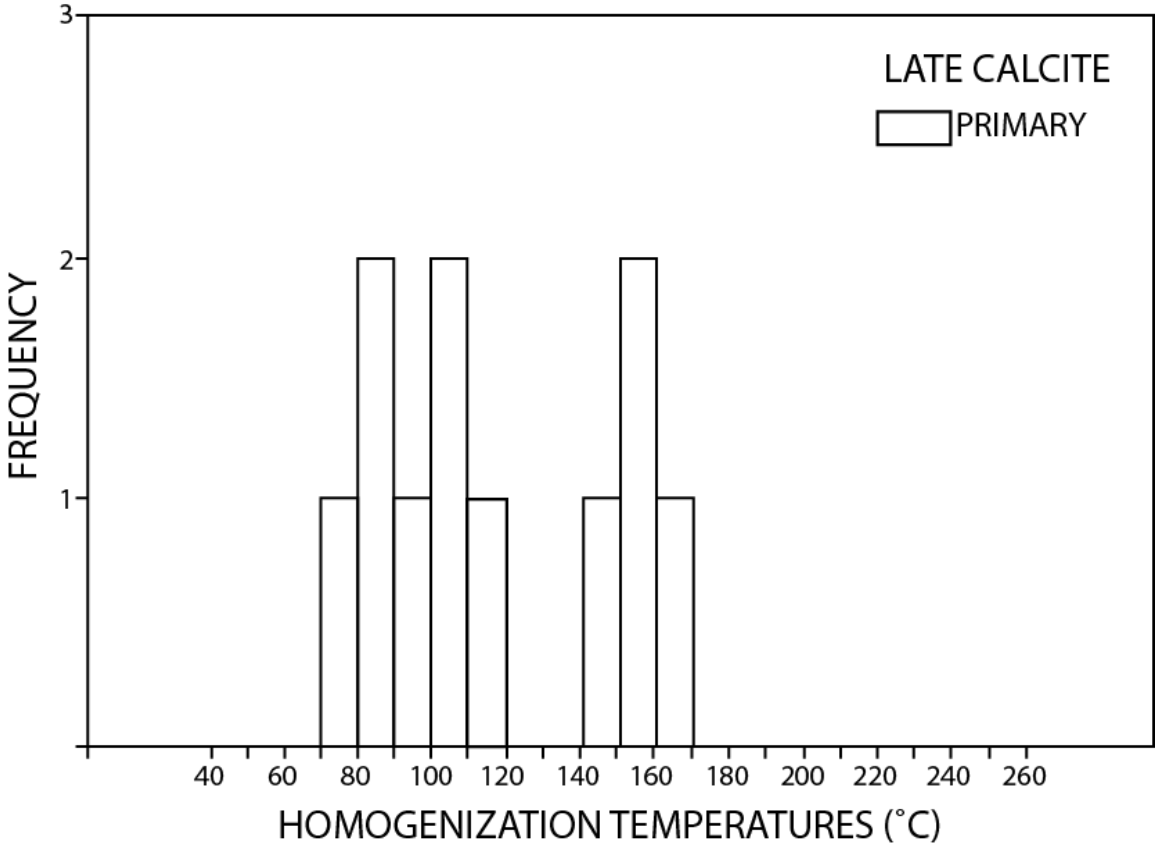

Figure 54: Histogram showing the distribution of homogenization temperatures from fluid inclusions in late (post-dolomitization) calcite in southwestern Ontario. From Coniglio et al. (1994).

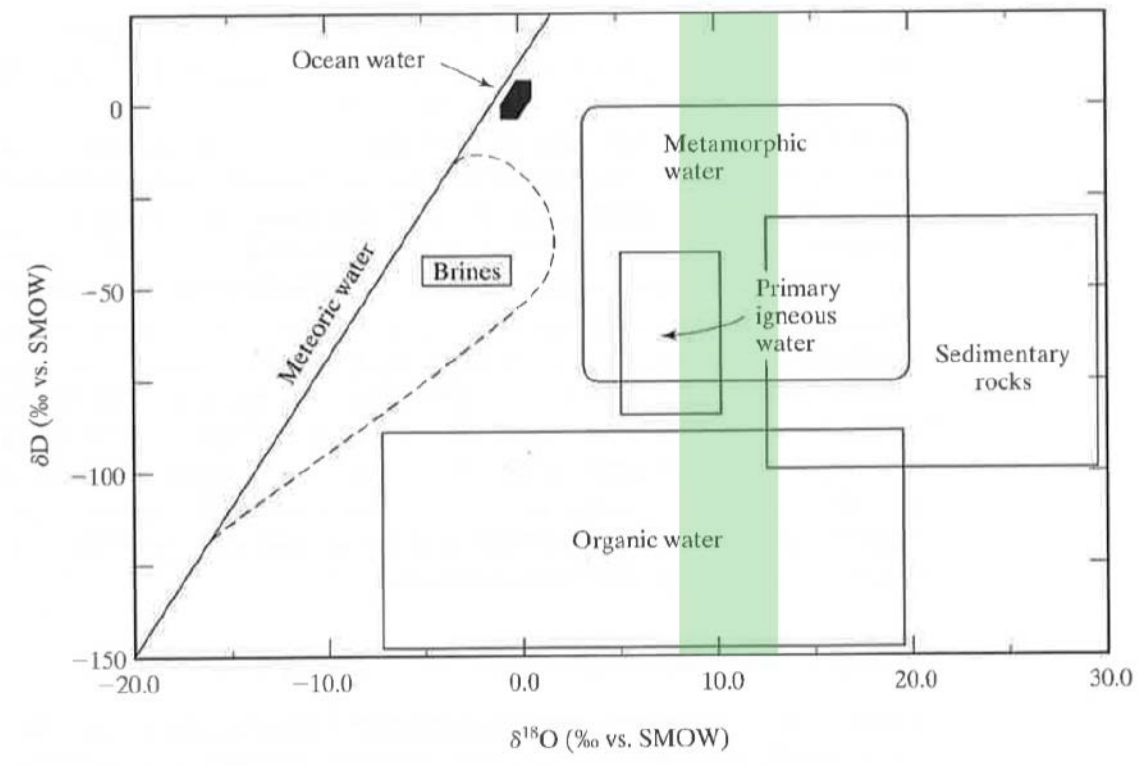

Figure 55: “Generic” isotopic fields for waters of different origins. The vertical green band indicates our calculated range of $\delta^{18}O_{water}$ (SMOW) values, based on the 170 ºC hydrothermal source fluid scenario. From Sharp, (2007).

6. Discussion

We identify three dominant nonconformity types through the characterization of the five main study sites examined here. These are: 1) Basal conglomerates, 2) weathered horizons, and 3) mineralized nonconformities, observed at the contact zone in outcrop, in core, and in the literature, and therefore represent likely common contact types which may be encountered in a deep injection environment (Figure 56). Each of these contact types vary geometrically and are likely to be fractured or faulted (Kerner, 2015; Hesseltine et al., 2016; E.S. Petrie, pers. comm., 2017). Additionally, combinations of these contact types may be present, such as the iron oxide mineralized conglomerate at Presque Isle, or the calcite-cemented weathered horizon in Cody, Wyoming (Figure 56). The permeability of the contact zone relative to the surrounding rock has significant influence on the propagation of fluid pressure (Zhang et al., 2013). The presence of a low-permeability barrier at the nonconformity decreases fluid pressure propagation, therefore decreasing risk for injection-induced seismicity (Figure 57) (Zhang et al., 2013; Ortiz, 2017).

Detailed site assessment and research into basin history and/or regional geology in the areas where brine injection occurs will likely improve seismic mitigation efforts. Our study indicates that special attention must be paid to the geology of the contact zone due to the hydrologically distinct properties it may exhibit. Detecting or predicting which type of contact is present, and how that contact behaves hydrologically, is critical to risk assessment.

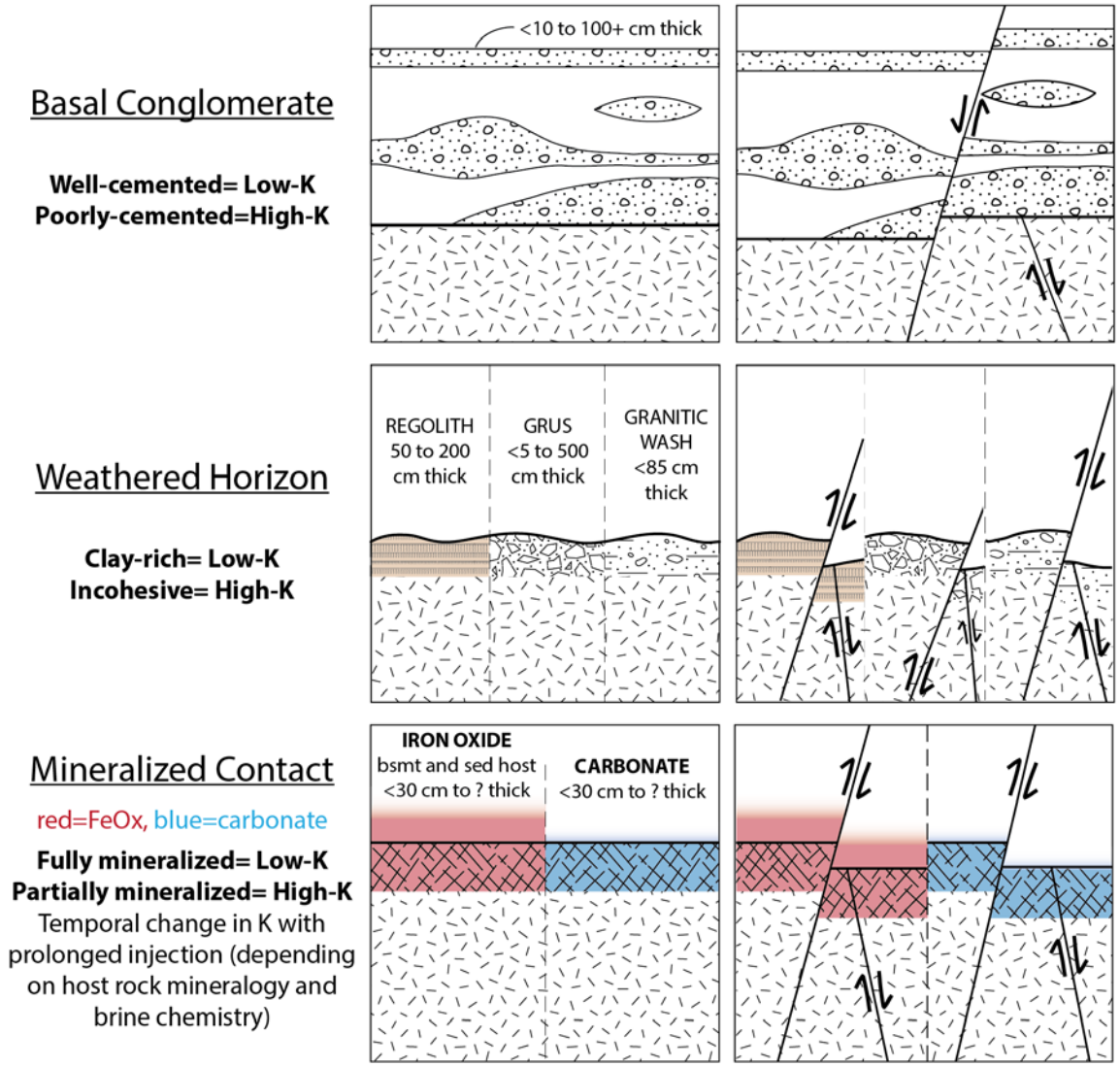

Figure 56: Overview of the 3 main contact types and associated permeability. Low permeability horizons are likely associated with low seismic risk with injection, according to Zhang et al., (2013) and Ortiz, (2017). Faulting may be basement-hosted, or offset the contact. Drawings are not to scale.

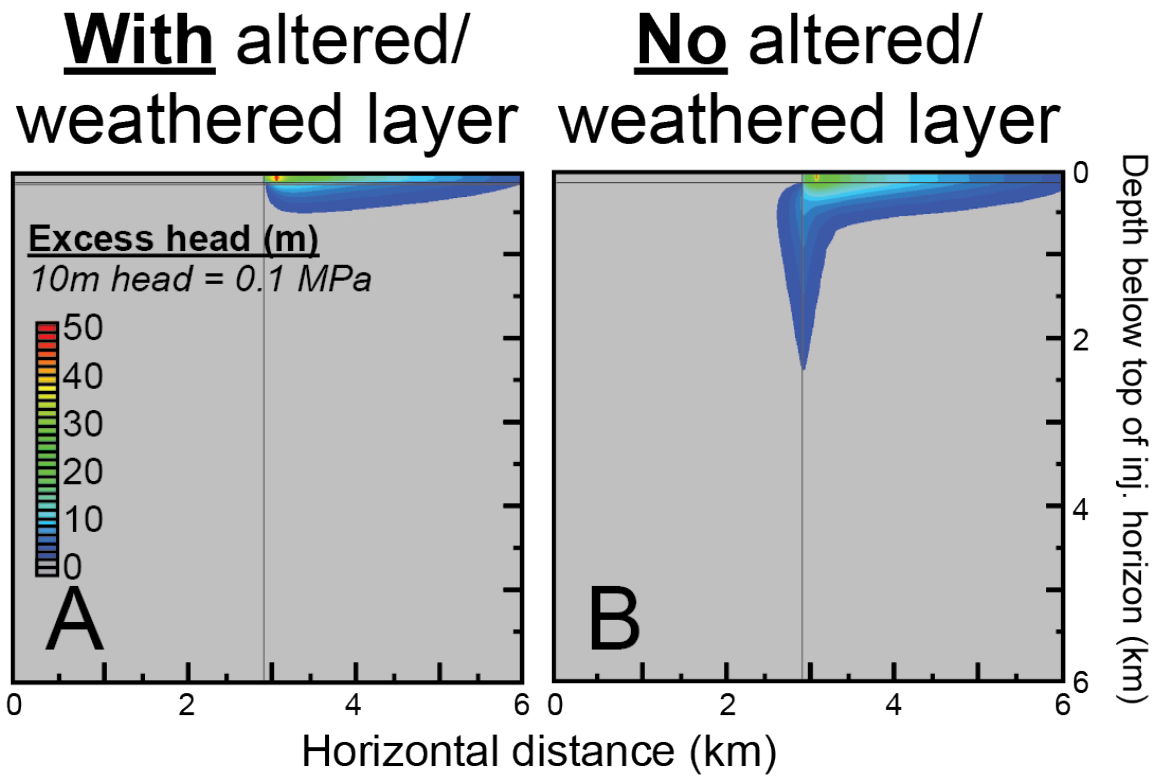

Figure 57: Hydrological modeling of injection with and without a low-permeability seal at the contact. Excess heads after 4 years of constant-rate injection for Paleozoic conduit-barrier fault scenario with (A) 20-m-thick low-permeability altered/weathered basement horizon (represented by two horizontal gray lines), and (B) no altered/weathered basement horizon. Vertical gray lines indicate location of the fault zone. Note the compartmentalization of the reservoir by the fault core in both cases and relatively little downward pressure diffusion when a low-permeability layer is present. Results are zoomed in to the top 6 × 6 km of the model domain. Transition from gray to dark blue contour (and all subsequent contour lines) denotes a 2-m increase in hydraulic head (0.02 MPa). From Ortiz, (2017).

6.1 Contact Types and Associated Seismic Risk

Contact scenarios associated with a low-risk injection environment (in which a low-permeability barrier exists at the contact) include well-cemented basal conglomerates, clay-rich grus or granitic wash, and fully-mineralized horizons. High-risk injection environments (high-permeability nonconformity zones) include partially mineralized horizons and friable zones, such as poorly-cemented basal conglomerates, regolith, and clast-rich grus or granitic wash. Fault-sealing may occur due to faulting of the contact, depending on the degree of offset, whereas

basement faults truncating at the contact may serve as flow conduits. Fracturing of these different contact types can greatly affect permeability, and therefore, associated seismic risk. Observations of highly deformed basement rocks in the Wind River Range indicate that fracture intensity can be as high as 2.74 fr/m (Figure 45). The nature and density of fracture networks in the basement, as well as the mechanical properties of the materials at the contact, directly impact the hydrological connectivity of the contact zone. Mechanically strong horizons, such as a well-cemented conglomerate, may respond to stresses in a brittle manner, resulting in more abundant open-mode fractures, whereas mechanically weaker materials, such as a clay-rich grus, may behave more ductilly, resulting in fewer hydrologically effective fracture networks (Ferrill et al., 2016).

6.2 Site Assessment

These observations provide a framework to help define the nature of the nonconformity in a range of injection sites. Detection of these types of contacts may be possible with wire-line logging and sampling of the borehole if the borehole penetrates basement rock. Information from neighboring boreholes, analyses of local basement surface topography, regional geology, and basin history of the area, can supplement wire-line logs, and serve as predictive tools to determine the type of contact present if the borehole does not reach basement rock. High-resolution gamma, porosity, and sonic wire-line logs may provide adequate data for identifying the type of contact zone present. Data from spectral gamma ray logs can be used to detect clay-rich horizons, such as a grus, granitic wash, or clay-rich conglomerate. Porosity and sonic logs may be used to determine the competency of the rocks at the contact, helping to distinguish between friable horizons, such as regolith, some types or grus, or poorly-cemented conglomerates.

If a borehole does not reach basement rock, information can be extrapolated from the geologic history of the area. Areas that have experienced Paleozoic tectonism could expect to encounter mineralization at the contact due to hydrothermal fluids sourced from reactivated

basement faults, such as the mineralization that has occurred in the CPC cores (Ma et al., 2009). Thicker weathered horizons may be expected in areas where the time gap between basement rocks and sedimentary rocks is longer, or in sheltered areas, such as on the flanks of basement highs. Additionally, alteration and weathering may present itself differently for different host rocks. Areas underlain by felsic basement rocks might anticipate a higher clay content in weathered horizons than areas underlain by mafic basement rocks due the higher feldspar content. Furthermore, the distribution of these contact types may be controlled by basement topography. Basement depressions may correlate to sedimentation zones, resulting in conglomerates or granitic wash horizons, whereas basement highs may correlate to weathered zones, such as regolith and grus (Dott, 1974; Bowen et al., 2011) (Figure 58). Weathered horizons have the potential to be 200+ meters thick in stable continents, such as Australia, however, this is not the case in the United States, where the formation of thick weathering horizons was likely stripped or affected by the continental-scale marine transgression during the Cambrian and early Ordovician known as the ‘wave-base razor’ (Peters and Gaines, 2012). This results in the relatively thin (<1 to 5 meter) weathered horizons observed here and at other sites in North America (Duffin, 1989; Easton and Carter, 1995; Peters and Gaines, 2012).

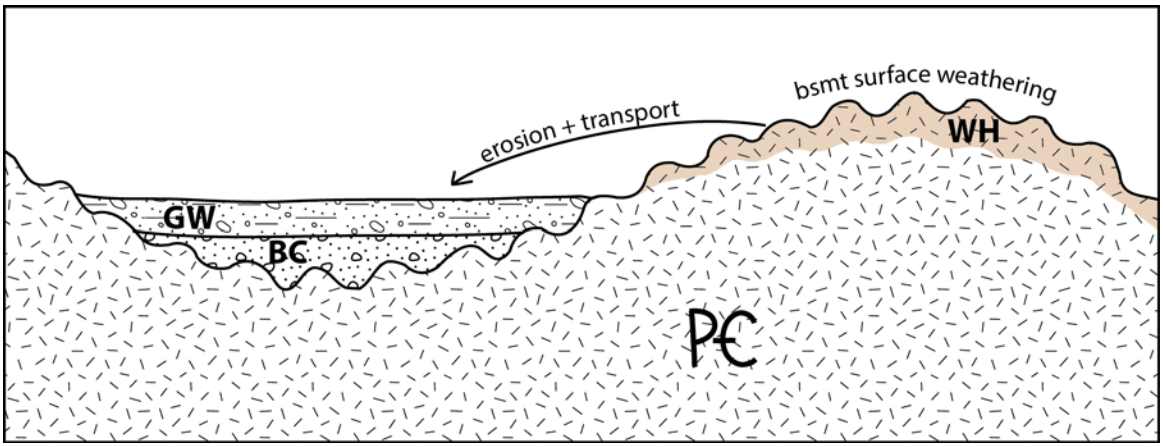

Figure 58: Schematic diagram of basement topography influencing distribution of contact types. Weathered horizons (WH, tan), such as regolith or grus, likely form on basement highs were the effects of surface weathering are more intense. Materials eroded off of basement highs are likely transported and deposited in basement lows, forming basal conglomerates (BC) or granitic wash (GW) horizons (Dott, 1974). Vertical distance is not to scale. Lateral variation of basement surface topography may occur at the meter- to kilometer-scale.

6.3 Anticipated Changes in Permeability with Brine Injection

The injection of concentrated brines into or near the contact zone likely results in a variety of fluid-rock interactions over time. Low temperature hydrothermal/warm basinal brine mineralization in the CPC BD-139 core may be an analog for how injected fluids might flow at the nonconformity, and suggests that we might anticipate mineralization in active injection wells over time, depending on the chemical composition of injected brines and the mineralogy of the host rock. For example, results from a geochemical modelling experiment of deep well brine injection in the Paradox Valley, Colorado indicated that a large mass of anhydrite would precipitate as a result of water-rock interactions at certain temperature-pressure conditions, resulting in a 'plugging' of the permeable zone in the well (Kharaka et al., 1997). Additionally, oil field scaling is a well-known process in which mineralization occurs due to disturbances in pressure and/or temperature, or by mixing of waters of different compositions- which could likely occur with the injection of concentrated, potentially warm brines with pressure (Sorbie and Mackay, 2000). On the other hand, injection of acidic brines may have the potential to increase

permeability when injected into certain host rocks, such as carbonates, or rocks containing carbonate mineralization (Figure 20). This occurs in the CPC BD-151 core, which likely contains the same dolomitized basement rocks seen in the CPC BD-139 core ~6.5 km away (Figure 20).

6.4 Future Work

The results presented in this study serve as a starting point for site-specific, geology-based assessment of Class II injection wells. The predictions for permeability and future fluid-rock interactions discussed here are supported by our data and the literature, however, further research should be done to test these predictions. Future studies may include permeability experiments on the different contact types, mapping of contact types as a function of basement topography, and experiments or modeling of fluid-rock interaction for each contact type.

7. Conclusions

We examined outcrop and core analogs of the sedimentary-Precambrian nonconformity in the central United States in order to investigate the range of rock properties that may exist within the contact zone, with the intent on determining the nature of fluid flow through the contact zone. Outcrops were studied in Marquette, Michigan, Cody, Wyoming, and the northeastern Wind River Range, Wyoming. Core study included the CPC BD-139 and CPC BD-151 cores from St. Clair County, Michigan, and the UPH-1 core, from Stephenson County, Illinois. We characterized the structure, lithology, mineralogy, and geochemistry of the rocks at each of these sites, where applicable.

We identified 3 major contact zone scenarios through characterization of these 5 main sites. These are: 1) Basal conglomerate, 2) Weathered horizons (regolith, grus, granitic wash), and 3) Mineralized contact (carbonate and iron-oxide mineralization). Contacts with tight, well-cemented basal conglomerates may act as low-permeability barriers to flow or as a high-permeability conduit in the case of a friable, poorly-cemented conglomerate. Regolith and clay-poor/clast-supported grus or granitic wash at the contact likely acts as a high-permeability conduit. Clay-rich/matrix supported grus or granitic wash likely acts as a low-permeability barrier. Fully mineralized contacts may act as barriers to flow, whereas partially mineralized contacts may act as conduits to flow. The permeability of the contact may change over time with sustained brine injection due to fluid-rock interactions.

Identification of these zones may be possible with wire-line logging (spectral gamma, porosity, and sonic logs) or study of core if the borehole penetrates basement. For wells that do not penetrate basement, information from neighboring boreholes, regional geology, basin history, or basement topography may be useful in predicting the type of contact present.

References

Barnes, D.A., Parris, T.M., and Grammer, M., 2008, Hydrothermal Dolomitization of Fluid Reservoirs in the Michigan basin, USA, http://www.searchanddiscovery.com/pdfz/documents/2008/08075barnes/images/barnes.pdf.html (accessed March 2017).

Beaudoin, N., Leprêtre, R., Bellahsen, N., Lacombe, O., Amrouch, K., Callot, J.-P., Emmanuel, L., and Daniel, J.-M., 2012, Structural and microstructural evolution of the Rattlesnake Mountain Anticline (Wyoming, USA): New insights into the Sevier and Laramide orogenic stress build-up in the Bighorn Basin: Tectonophysics, v. 576–577, p. 20–45, doi: 10.1016/j.tecto.2012.03.036.

Bell, L.H., and Middleton, L.T., 1978, An Introduction to the Cambrian Flathead Sandstone, Wind River Basin, Wyoming; Resources of the Wind River Basin: Wyoming Geological Association, 30th Annual Field Conference, Guidebook, p. 79–88.

Bowen, B.B., R.I. Ochoa, N.D. Wilkens, J. Brophy, T.R. Lovell, N. Fischietto, C.R. Medina, and J.A. Rupp. 2011, Depositional and Diagenetic Variability within the Cambrian Mount Simon Sandstone: Implications for Carbon Dioxide Sequestration: Environmental Geosciences v. 18, p. 69-89, doi:10.1306/eg.07271010012.

Brace, W. F. "Permeability of Crystalline Rocks: New in Situ Measurements." Journal of Geophysical Research: Solid Earth 89, (June 10, 1984): 4327–30. doi:10.1029/JB089iB06p04327.

Calais, E., Han, J.Y., DeMets, C., and Nocquet, J.M., 2006, Deformation of the North American Plate interior from a decade of continuous GPS measurements: Journal of Geophysical Research, v. 111, 23 p., doi: http://dx.doi.org.dist.lib.usu.edu/10.1029/2005JB004253.

Cercone, K.R., 1984, Thermal History of Michigan Basin: America Association of Petroleum Geologists Bulletin, v. 68, p. 130–136.

Clayton, L., and Attig, J.W., 1990, Geology of Sauk County, Wisconsin: Wisconsin Geological and Natural History Survey Information Circular 67, http://www.koubadrilling.com/well-drilling/docs/sauk-county-geological-report.pdf (accessed July 2017).

Clayton, R.N., Friedman, I., Graf, D.L., Mayeda, T.K., Meents, W.F., and Shimp, N.F., 1966, The origin of saline formation waters; Part 1, Isotopic composition: Journal of Geophysical Research, v. 71, p. 3869–3882.

Coates, M.S., Haimson, B.C., Hinze, W.., and Van Schmus, W.R., 1983, Introduction to the Illinois deep hole project: Journal of Geophysical Research, v. 88, p. 7267–7275.

Cobbold, P.R., Zanella, A., Rodrigues, N., and Løseth, H., 2013, Bedding-parallel fibrous veins (beef and cone-in-cone): Worldwide occurrence and possible significance in terms of fluid overpressure, hydrocarbon generation and mineralization: Marine and Petroleum Geology, v. 43, p. 1–20, doi: 10.1016/j.marpetgeo.2013.01.010.

Coniglio, M., R. Sherlock, A. E. Williams-Jones, K. Middleton, and S. K. Frape. “Burial and Hydrothermal Diagenesis of Ordovician Carbonates from the Michigan Basin, Ontario, Canada.” In Dolomites, edited by Bruce Purser, urice Tucker, and Donald Zenger, 231–54. Blackwell Publishing Ltd., 1994. doi:10.1002/9781444304077.ch14.

Cooley, Maurice E. “Artesian Pressures and Water Quality in Paleozoic Aquifers in the Ten Sleep Area of the Bighorn Basin, North-Central Wyoming.” U.S. Geological Survey Water-Supply Paper. Department of the Interior, 1986. https://pubs.usgs.gov/wsp/2289/report.pdf.

Crone, A.J., De Martini, P.M., Machette, M.N., Okumura, K., and Prescott, J.R., 2003, Paleoseismicity of two historically quiescent faults in Australia; implications for fault behavior in stable continental regions: Bulletin of the Seismological Society of America, v. 93, p. 1913–1934.

Denison, R.E., Lidiak, E.G., Bickford, M.E., and Kisvarsanyi, E.B., 1984, Geology and geochronology of Precambrian rocks in the Central Interior region of the United States: U.S. G.P.O., Professional Paper USGS Numbered Series 1241–C, http://pubs.er.usgs.gov/publication/pp1241C (accessed June 2017).

Dixon, T.H., Mao, A., and Stein, S., 1996, How rigid is the stable interior of the North American Plate? Geophysical Research Letters, v. 23, p. 3035–3038, doi: http://dx.doi.org.dist.lib.usu.edu/10.1029/96GL02820.

Domrois, S., Marshak, S., Abert, C.C., and Larson, T.H., 2015, ArcGIS Maps Depicting Topography of the Basement-Cover Contact (the Great Unconformity), and the Traces of Faults and Folds, in the Cratonic Platform of the United States: American Association of Petroleum Geologists Search and Discovery Article #30410.

Dott, R. H., 1974, Cambrian Tropical Storm Waves in Wisconsin: Geology v. 2, p. 243–46.

Dott, R.H., and Attig, J.W., 2004, Roadside Geology of Wisconsin: Mountain Press Pub., 368 p.

Duffin, M.E., 1989, Nature and origin of authigenic K-feldspar in Precambrian basement rocks of the North American midcontinent: Geology, v. 17, p. 765–768, doi: 10.1130/0091-7613(1989)017<0765:NAOOAK>2.3.CO;2.

Duffin, M.E., Lee, M., Klein, G. deVries, and Hay, R.L., 1989, Potassic diagenesis of Cambrian sandstones and Precambrian granitic basement in UPH-3 deep hole, Upper Mississippi Valley, U.S.A.: Journal of Sedimentary Research, v. 59, p. 848–861, doi: 10.1306/212F908E-2B24-11D7-8648000102C1865D.

Dutton, Clarence Edward. 1882, Tertiary History of the Grand Canon District. University of Arizona Press.

Easton, R.M., and Carter, T.R., 1995, Geology of the Precambrian Basement Beneath the Paleozoic of Southwestern Ontario, in Ojakangas, R.W., Dickas, A.B., and Green, J.C. eds., Basement Tectonics 10, Springer Netherlands, Proceedings of the International Conferences on Basement Tectonics, v. 4, p. 221–264, doi: 10.1007/978-94-017-0831-9_26.

Ellsworth, W.L., 2013, Injection-Induced Earthquakes: Science, 341, p. 142, doi: 10.1126/science.1225942.

Environmental Protection Agency, and Underground Injection Control, 2015, Class II Oil and Gas Related Injection Wells: United States Environmental Protection Agency, https://www.epa.gov/uic/class-ii-oil-and-gas-related-injection-wells (accessed June 2017).

Evans, J.P., Berry, M., Allred, I., Nielson, K., and Parslow, D., 2013, How many Class II wells present a risk for induced seismicity?, https://gsa.confex.com/gsa/2013AM/webprogram/Paper226615.html (accessed June 2017).

Everham, W.D., and Huntoon, J.E., 1999, Thermal history of a deep well in the Michigan Basin; implications for a complex burial history (A. Foerster, Ed.): Kluwer Academic/Plenum Publishers; New York; NY, http://search.proquest.com.dist.lib.usu.edu/georef/docview/52420903/D1E9596410E24127PQ/1 (accessed March 2017).

Faure, G., 2009, Isotopes: Principles and Applications: John Wiley & Sons, 897 p.

Ferrill, D.A., A.P. Morris, S.S. Wigginton, K.J. Smart, R.N. McGinnis, and D. Lehrmann. "Deciphering Thrust Fault Nucleation and Propagation and the Importance of Footwall Synclines." Journal of Structural Geology v. 85, no. (April 1, 2016): p. 1–11. doi:10.1016/j.jsg.2016.01.009.

Frailey, S.M., J. Damico, and H.E. Leetaru, 2011"Reservoir Characterization of the Mt. Simon Sandstone, Illinois Basin, USA." Energy Procedia, 10th International Conference on Greenhouse Gas Control Technologies, v. 4, (January 1, 2011): 5487–94. doi:10.1016/j.egypro.2011.02.534.

Friedman, I., O'Neil, J.R., and Fleischer, M., 1977, U. S. Geological Survey Professional Paper: U. S. Geological Survey Professional Paper, p. 12.

Gair, J.E., and Thaden, R.E., 1968a, Geology of the Marquette and Sands Quadrangles, Marquette County, Michigan: Geological Survey Professional Paper 397, https://pubs.usgs.gov/pp/0397/report.pdf (accessed March 2017).

Girard, J.-P., and Barnes, D.A., 1995, Illitization and Paleothermal Regimes in the Middle Ordovician St. Peter Sandstone, Central Michigan Basin: K-Ar, Oxygen Isotope, and Fluid Inclusion Data: American Association of Petroleum Geologists Bulletin, v. 79, p. 49–69.

Granger, H.C., McKay, E.J., Mattick, R.E., Patten, L.L., and McIlroy, P., 1971, Mineral resources of the Glacier Primitive Area, Wyoming: U.S. Govt. Print. Off., Bulletin U.S. Geological Survey Numbered Series 1319–F, http://pubs.er.usgs.gov/publication/b1319F (accessed July 2017).

Hamblin, W.K., 1958, The Cambrian sandstones of northern Michigan. [Ph.D. Dissertation]: University of Michigan, 55 p. Michigan Geological Survey Publication #51.

Harrison, R.W., Hoffman, D., Vaughn, J.D., Palmer, J.R., Wiscombe, C.L., McGeehin, J.P., Stephenson, W.J., Odum, J.K., Williams, R.A., and Forman, S.L., 1999, An example of neotectonism in a continental interior - Thebes Gap, Midcontinent, United States: Tectonophysics, v. 305, p. 399-417, doi: 10.1016/S0040-1951(99)00010-4.

Heinrich, E.W., 2001, Economic Geology of the Sand and Sandstone Resources of Michigan. Report of Investigation. Michigan Department of Environmental Quality. http://www.michigan.gov/documents/deq/GIMDL-RI21_216264_7.pdf.

Hesseltine, G., Evans, J.P., Kerner, K., and Mozley, P.S., 2016, Structural diagenesis and micro- to macro-scale structural architecture of basal nonconformities, in Denver, CO, doi: 10.1130/abs/2016AM-284922.

Kawano, S., I. Katayama, and K. Okazaki, 2011, "Permeability Anisotropy of Serpentinite and Fluid Pathways in a Subduction Zone." Geology 39: 939–42. doi:10.1130/G32173.1.

Keranen, K.M., Weingarten, M., Abers, G.A., Bekins, B.A., and Ge, S., 2014, Sharp increase in central Oklahoma seismicity since 2008 induced by massive wastewater injection: Science, v. 345, p. 448–451, doi: http://dx.doi.org.dist.lib.usu.edu/10.1126/science.1255802.

Kerner, K.R., 2015, Permeability architecture of faulted nonconformities: Implications for induced seismicity [M.S.]: New Mexico Institute of Mining and Technology, 162 p., https://search.proquest.com/docview/1749295549/abstract/774D131EA2FF4426PQ/1 (accessed July 2017).

Kerner, K., Mozley, P., Evans, J., and Person, M., 2015, Geologic Controls on Injection Related Reactivation of Basement Faults, in Denver, CO, http://www.searchanddiscovery.com/abstracts/html/2015/90216ace/abstracts/2096068.html (accessed June 2017).

Kerr, P.F., 1955, Hydrothermal Alteration and Weathering: Geological Society of America Special Paper 62, p. 525–546.

Kharaka, Y.K., Ambats, G., Thordsen, J.J., and Davis, R.A., 1997, Deep well injection of brine from Paradox Valley, Colorado: Potential major precipitation problems remediated by nanofiltration: Water Resources Research, v. 33, p. 1013–1020, doi: 10.1029/97WR00573.

Kim, W.-Y., 2013, Induced seismicity associated with fluid injection into a deep well in Youngstown, Ohio: Journal of Geophysical Research: Solid Earth, v. 118, p. 3506–3518, doi: 10.1002/jgrb.50247.

Kim, S.-T., Coplen, T.B., and Horita, J., 2015, Normalization of stable isotope data for carbonate minerals: Implementation of IUPAC guidelines: Geochimica et Cosmochimica Acta, v. 158, p. 276–289, doi: 10.1016/j.gca.2015.02.011.

Kolata, D.R., 2005, Bedrock geology of Illinois: Illinois State Geological Survey Illinois Map 14 Bedrock Geologic Map, https://ngmdb.usgs.gov/Prodesc/proddesc_87181.htm (accessed May 2017).

Lewan, M.D., 1972, Metasomatism and weathering of the Presque Isle serpentinized peridotite, Marquette, Michigan [MSc. thesis]: Michigan Technological University, Houghton, MI, United States (USA), 48 p.

Ma, L., Castro, M.C., and Hall, C.M., 2009, Atmospheric noble gas signatures in deep Michigan Basin brines as indicators of a past thermal event: Earth and Planetary Science Letters, v. 277, p. 137–147, doi: http://dx.doi.org.dist.lib.usu.edu/10.1016/j.epsl.2008.10.015.

Marshak, S., Domrois, S., Abert, C., Larson, T., Pavlis, G., Hamburger, M., Yang, X., Gilbert, H., and Chen, C., 2017, The basement revealed: Tectonic insight from a digital elevation model of the Great Unconformity, USA cratonic platform: Geology, v. 45, p. 391-394.

Marshak, S., and Paulsen, T., 1996, Midcontinent U.S. fault and fold zones: A legacy of Proterozoic intracratonic extensional tectonism? Geology, v. 24, p. 151–154, doi: 10.1130/0091-7613(1996)024<0151:MUSFAF>2.3.CO;2.

Migon, P., and Thomas, M.F., 2002, Grus weathering mantles; problems of interpretation (B. J. Smith, Ed.): Catena, v. 49, p. 5–24.

Milstein, R., 1987, Bedrock Geology of Southern Michigan: Michigan Department of Natural Resources Geological Publication BG-01 Bedrock Geologic Map, https://ngmdb.usgs.gov/Prodesc/proddesc_71887.htm (accessed May 2017).

Murray, K.E., 2015, Class II Saltwater Disposal for 2009-2014 at the Annual-, State-, and County- Scales by Geologic Zones of Completion, Oklahoma: Oklahoma Geological Survey Open-File Report OF5-2015, 18 p., http://ogs.ou.edu/docs/openfile/OF5-2015.pdf (accessed June 2017).

Murray, K., 2016, Fluid Production and Injection Budget for the Arbuckle: Oklahoma, Final Report, Feb 2015–May 2016:, https://scits.stanford.edu/murray-kyle-fluid-production-and-injection-budget-arbuckle-oklahoma-final-report-feb-2015-may-2016 (accessed June 2017).

National Research Council et. al., 2013, Induced Seismicity Potential in Energy Technologies: National Academies Press, Washington, D.C., 238 p.

National Technical Workgroup, and Underground Injection Control, 2014, Minimizing and Managing Potential Impacts of Injection-Induced Seismicity from Class II Disposal Wells: Practical Approaches: U.S. Environmental Protection Agency, https://www.epa.gov/sites/production/files/2015-08/documents/induced-seismicity-201502.pdf (accessed July 2017).

O'Hanley, D.S., 1992, Solution to the Volume Problem in Serpentinization. Geology 20, (August 1, 1992): 705–8. doi:10.1130/0091-7613(1992)020<0705:STTVPI>2.3.CO;2.

Ortiz, J., 2017, The Role of Fault-Zone Architectural Elements and Basal Regolith on Downward Pore Pressure Propagation and Induced Seismicity [MSc. thesis]: New Mexico Tech, Socorro, New Mexico, 45p.

Pain, C.F., 1991, Field Guide for Describing Regolith and Landforms: Australia, CRC LEME, c/o CSIRO Exploration and Mining, 108 p.

Peters, S.E., and Gaines, R.R., 2012, Formation of the “Great Unconformity” as a trigger for the Cambrian explosion: Nature (London), v. 484, p. 363–366, doi: http://dx.doi.org.dist.lib.usu.edu/10.1038/nature10969.

Pettijohn, F.J., Potter, P.E., and Siever, R., 2012, Sand and Sandstone: Springer Science & Business Media, 560 p.

Ramsay, John G. “The Crack–seal Mechanism of Rock Deformation.” Nature 284, no. 5752 (March 13, 1980): 135–39. doi:10.1038/284135a0.

Sen, G., 2013, Petrology: Principles and Practice: Springer Science & Business Media, 371 p.

Sharp, Z., 2007, Principles of Stable Isotope Geochemistry: Upper Saddle River, NJ, Prentice Hall, 360 p.

Sloss, L. L., 1963, Sequences in the Cratonic Interior of North America: Geological Society of America Bulletin, v. 74, p. 93–114.

Sorbie, K.S., and Mackay, E.J., 2000, Mixing of injected, connate and aquifer brines in waterflooding and its relevance to oilfield scaling: Journal of Petroleum Science and Engineering, v. 27, p. 85–106, doi: 10.1016/S0920-4105(00)00050-4.

Stuckless, J.S., 1989, Petrogenesis of Two Contrasting, Late Archean Granitoids, Wind River Range, Wyoming: Professional Paper 1491, https://pubs.usgs.gov/pp/1491/report.pdf (accessed January 2017).

Tyrrell, J.P., Samuels, R.M., Low, P.C., and Anonymous, 2013, Management of produced water from oil and gas wells in California; past trends and future suggestions: Abstracts with Programs - Geological Society of America, v. 45, p. 595.

Urey, H.C., 1947, The thermodynamic properties of isotopic substances: Journal of the Chemical Society (Resumed), p. 562–581, doi: 10.1039/JR9470000562.

U.S. Geological Survey, 2017, Induced Earthquakes: Earthquake Hazards Program, https://earthquake.usgs.gov/research/induced/overview.php.

Vasconcelos, C., McKenzie, J.A., Warthmann, R., and Bernasconi, S.M., 2005, Calibration of the $\delta^{18}O$ paleothermometer for dolomite precipitated in microbial cultures and natural environments: Geology, v. 33, p. 317–320.

Vitaliano, C.J., McCormick, G.R., Dahl, P.S., and Eckstein, Y., 1986, Granitic Rocks from Three Deep Drill-Holes, Illinois: The Journal of Geology, v. 94, p. 594–599.

Walsh, F.R., and Zoback, M.D., 2015, Oklahoma’s recent earthquakes and saltwater disposal: Science Advances, v. 1, 9 p., doi: 10.1126/sciadv.1500195.

Weingarten, M., Ge, S., Godt, J.W., Bekins, B.A., and Rubinstein, J.L., 2015, High-rate injection is associated with the increase in U.S. mid-continent seismicity: Science, v. 348, p. 1336–1340, doi: 10.1126/science.aab1345.

Wilson, T.P., and Long, D.T., 1993, Geochemistry and isotope chemistry of Michigan Basin brines; Devonian formations: Applied Geochemistry, v. 8, p. 81–100, doi: http://dx.doi.org.dist.lib.usu.edu/10.1016/0883-2927(93)90058-O.

Yeck, W.L., Weingarten, M., Benz, H.M., McNamara, D.E., Bergman, E.A., Herrmann, R.B., Rubinstein, J.L., and Earle, P.S., 2016, Far-field pressurization likely caused one of the largest injection induced earthquakes by reactivating a large preexisting basement fault structure: Geophysical Research Letters, v. 43, p. 198-207, doi: 10.1002/2016GL070861

Zhang, Y., Edel, S.S., Pepin, J., Person, M., Broadhead, R., Ortiz, J.P., Bilek, S.L., Mozley, P., and Evans, J.P., 2016, Exploring the potential linkages between oil-field brine reinjection, crystalline basement permeability, and triggered seismicity for the Dagger Draw Oil field, southeastern New Mexico, USA, using hydrologic modeling: Geofluids, v. 16, p. 971–987, doi: 10.1111/gfl.12199.

Zhang, Y., Person, M., Rupp, J., Ellett, K., Celia, M.A., Gable, C.W., Bowen, B., Evans, J., Bandilla, K., Mozley, P., Dewers, T., and Elliot, T., 2013, Hydrogeologic Controls on Induced Seismicity in Crystalline Basement Rocks Due to Fluid Injection into Basal Reservoirs: Groundwater, v. 51, p. 525–538, doi: 10.1111/gwat.12071.